Evaluation of Carbon Emissions from Forest Fires in Southeast Asia during the Period 2001-2010

（2001年から2010年の東南アジアにおける森林火災による炭素放出量の評価）

Yusheng SHI

Evaluation of Carbon Emissions from Forest Fires in Southeast Asia during the Period 2001-2010

（2001年から2010年の東南アジアにおける森林火災による炭素放出量の評価）

SHI, Yusheng

（石 玉勝）

A dissertation for the degree of Doctor of Science

Department of Earth and Environmental Sciences,

Graduate School of Environmental Studies, Nagoya University

（名古屋大学大学院環境学研究科地球環境科学専攻学位論文　博士（理学））

2014

Table of Contents

Acknowledgments iii

Abstract v

List of Tables viii

List of Figures ix

Chapter 1

Introduction 1

1.1 General introduction 1

1.2 Burned area data 2

1.3 Active fire products 4

1.4 Biomass burning emissions 7

1.5 Research objectives 8

1.6 Outline of the dissertation 10

Chapter 2

Fundamentals of Southeast Asia 17

2.1 Southeast Asia geography 17

2.2 Biological geography 19

2.3 Biomass burning emissions in SEA 20

2.4 Effects of biomass burning emissions 24

Chapter 3

Spatio-temporal evaluation of carbon emissions from biomass burning in Southeast Asia during the period 2001-2010 29

3.1 Introduction 30

3.2 Data and methods 34

3.2.1 Data 34

3.2.2 Methods 38

3.2.3 Calibration 44

3.3 Results and discussion 45

3.3.1 The comparison among burned area data 45
3.3.2 Spatial characteristics of fuel load and consumption 51
3.3.3 Spatiotemporal characteristics of fire CE 53
3.3.4 Fire CE in NSEA 65
3.3.5 Fire CE in Indonesia 68
3.4 Conclusions 72

Chapter 4

A high-resolution emissions inventory for open biomass burning in Southeast Asia during 2001-2010 and their global warming potential **81**
4.1 Introduction 82
4.2 Method and data source 85
4.2.1 Burned area and fire counts 85
4.2.2 Available fuels 87
4.2.3 Combustion factor 91
4.2.4 Emission factor 92
4.3 Results and discussions 93
4.3.1 Spatial distributions and variations 93
4.3.2 Temporal variations 101
4.3.3 Comparison with other studies 104
4.3.4 Emission uncertainties 105
4.3.5 Global Warming Potential (GWP) 106
4.4 Conclusions 108
Supporting Information 115

Chapter 5

Conclusions and recommendations **118**
5.1 Summary of the research 118
5.2 Conclusions 119
5.3 Suggestions for future research 121
Appendix 124

Acknowledgments

It is a pleasure to thank the many people who made this dissertation possible.

First of all, I would like to acknowledge my dissertation committee, Professor Sei-ichiro Watanabe, Associate Professor Tomo'omi Kumagai, Professor Yasushi Yamaguchi, for their guidance and valuable advices in improving the manuscript. I extremely appreciate the suggestions and contributions from the committee members.

I would like to express my sincere gratitude and appreciation to my Ph.D. supervisor, Professor Yasushi Yamaguchi, for his consistent guidance, insight, attention, and support during the past three years' research and the preparation of this dissertation. With his enthusiasm, his inspiration, and his great efforts to explain questions clearly and simply, he helped to make remote sensing science desired for me. Throughout my dissertation-writing period, he provided encouragement, sound advice, good teaching, and lots of good ideas. I would also like to express my thanks to the Associate Professors Masao Takano and Yasuhiro Hirano in our lab for their constructive comments, support and guidance during the three years' study.

Special thanks go to the Assistant Professor Takahiro Sasai for sharing the BEAMS model and his help in model study, data processing and analysis. His guidance and valuable advices help me a lot in improving the manuscript. I also gratefully acknowledge Dr. Xuehong Chen from Beijing Normal University for his constant help and idea inspiring over the past days. Besides, I greatly appreciated the time and help from the previous members of Kazuki Aiba, Saori Nakai, Yuko Setoyama, Tatsumi Uezato, Anna Kato of our lab in C Language programming, Linux system operation, and Shell code study. I would like to acknowledge Ho Loan Thi Kim, Xiaoqiang Zhang, Makoto Shimomura, Nao Ishidoshiro, Daisuke Sugiyama, Yukari Mizuta, Daisuke Yamada, for their meaningful suggestions and comments in Seminar.

Also, I thank all the members form GCOE (Global Center of Excellence) program of Nagoya University, including Tetsuzo Yasunari, Yoshitsugu Hayashi, Takeshi

Nakatsuka, Masao Takano, Quanpeng Li, Xin Tian, Wanxin Hou, for their kindness and corporation. Special thanks were given to Associate Professor Chen Liu for her constructive ideas and constant encouragement. I am also grateful to the International Student Advisor Christina Lim for her consistent help and care.

I also gratefully acknowledge Ministry of Education, Culture, Sports, Science and Technology (MEXT), Japan, for awarding me Government Scholarship, under which my study and research in Japan has been implemented.

My deepest and most sincere gratitude go to my beloved parents for their life-long love, support, encouragement and understanding in every moment of my life. Whatever I achieved is only to make them happy and proud. This thesis is dedicated to my parents for their cherished wishes and dreams.

Yusheng Shi

Nagoya University
March 2014

Abstract

Fire and biomass burning are unique disturbances on ecosystem processes and dynamics. They can lead to the direct release of ecosystem carbon that is stored in large terrestrial pools (live vegetation, dead vegetation, litter, organic soil), which have deep implication to the ecosystem productivity and stability. At the same time, they can result in elevated concentrations of trace gases (e.g., carbon monoxide, methane) and aerosol particles in the atmosphere, which have significant effects on global atmospheric chemistry and climate change in various regions of the world, and are causing serious air pollutions as well.

Carbon emissions induced by biomass burning are commonly calculated as a product of burned area, fuel loads, and combustion completeness, integrated over the time and space scales of interest. With the help of the recently released satellite products, and terrestrial biosphere model, this study developed a new high-resolution and multi-year inventory of carbon emissions by open biomass burning in Southeast Asia (SEA) during the period of 2001-2010, and evaluated their global warming potentials. The high resolution emission grid showed its advantage in quantifying small sized fire emissions, which were frequently misinterpreted by the coarse grid data due to their smoothed large pixels.

Using the recently developed MODerate resolution Imaging Spectroradiometer (MODIS) burned area products and the improved biosphere model integrating fire carbon processes at a spatial resolution of 5 km, our results showed that burned areas were predominantly concentrated in Myanmar, north Thailand, eastern Cambodia, and northern Laos, with marked differences in Sumatra and Kalimantan of Indonesia, where peatland is extensively distributed. Through comparison among different burned area products, we found that the burned area datasets from MCD64A1, MCD45A1 and GFED3 (Global Fire Emission Database) showed consistent temporal variation from 2001 to 2010 with average annual burned areas of 68104, 50933 and 61263 km^2 $year^{-1}$, respectively. Fire carbon emissions estimated in the three simulations (BEAMS/MCD64A1, BEAMS/MCD45A1-Peat and

BEAMS/GFED) by using the three burned area products exhibited similar spatial patterns with respect to the burned areas, with average annual fire carbon emissions of 232.6, 214.1 and 228.8 TgC, respectively. The best result among the three estimations was BEAMS/MCD45A1-Peat, which was close to that obtained by GFED3 with 210.7 TgC. Aerosol Optical Depth (AOD) values showed good consistency with both fire CE and Multivariate ENSO (El Niño Southern Oscillation) Index values from 2001 to 2010, likely because of the deep peat soil burning under the influence of the El Niño phenomenon and Indian Ocean Dipole pattern in combination with anthropogenic disturbance through deforestation for palm oil plantation.

Besides, by using the biomass density and spatio-temporal variable combustion factors derived from the satellite observation data, our study also developed a new high-resolution and multi-year emissions inventory for open biomass burning on SO_2, NO_x, CO, Non-Methane Volatile Organic Compounds (NMVOC), NH_3, Black Carbon (BC), Organic Carbon (OC), CH_4, CO_2, and N_2O in SEA during the period of 2001-2010, and evaluated their global warming potentials. The average annual biomass burning emissions were 261.8 Gg year^{-1} SO_2, 1013.2 Gg year^{-1} NO_x, 51838.2 Gg year^{-1} CO, 3529.0 Gg year^{-1} NMVOV, 437.3 Gg year^{-1} NH_3, 302.0 Gg year^{-1} BC, 2278.0 Gg year^{-1} OC, 3525.6 Gg year^{-1} CH_4, 761948.6 Gg year^{-1} CO_2, 96.0 Gg year^{-1} N_2O, respectively. The result showed that high emissions by biomass burning were mainly concentrated in Myanmar, Cambodia, and Indonesia, and were accounted for approximately 60% of the total biomass burning emissions. And forest burning emissions were found to be the dominant contributor to the total emissions among all land types. In addition, we found that the biomass burning emissions exhibited similar trends from 2001 to 2010 with strong interannual and intraannual variability. Three high emission years were 2004, 2007, and 2010, which were attributed to the three peaks of corresponding burned areas in 2003, 2007, and 2010, respectively. The intraannual trend showed that biomass burning emissions in January-March were the highest all year around, with another small peak in Oct. The total net global warming potential estimated from the SEA biomass burning

emissions during 2001-2010 was around 792 (20 year horizon) and 775 (100 year horizon) Tg CO_2 equivalent, which contributed to 8.6% and 10.5% for both time horizons to the globe, respectively.

List of Tables

1.1. A summary of active fire products 6

3.1. Input data used for the BEAMS simulation 35

3.2. Minimum and maximum combustion factors for fuel types in different types of land cover 42

3.3. Average annual burned areas and fire carbon emissions of each country from different results and datasets during 2001-2010, and their spatial correlation coefficient with statistical test 60

4.1. Moisture category factor (mcf) (From Anderson et al., 2004) 92

4.2. Selected emission factors for each kind of land type in g species per kg dry matter burned 93

4.3. Summary of average annual biomass burning emissions during 2001-2010 for each land type in SEA. (Unit: Gg = 10^9 g) 97

4.4. Averaged annual biomass burning emissions of SEA during 2001-2010 (Unit: Gg = 10^9g) 105

4.5. Forest biomass burning emissions of SEA in 2005 (Unit: Gg = 10^9g) 105

4.6. Contribution of SEA biomass open burning to the global biomass open burning GWP 107

S1. GWP of different forcing agents 115

List of Figures

1.1. Annual burned area (as percentage of the area of the grid cell), averaged over 1997-2009. For November 2000 onwards it is for 90% based on mapped MODIS burned area using the direct broadcast algorithm, aggregated from the native 500-meter resolution to 0.5 degree. The remaining 10% and burned area for 1997 - October 2000 are based on relations between active fires (ATSR, TRMM-VIRS, and MODIS) and mapped burned area for periods they overlap. From Global Fire Emission Database 3 (GFED3) 3

1.2. Global 10-day fire maps generated using the MODIS fire locations to represent the current fire activity around the world. (a).04/21/2013 - 04/30/2013; (b). 08/19/2013 - 08/28/2013. From NASA Earth Data Global Fire Maps 4

1.3. Fire counts (#/0.5^{o} grid year^{-1}). (a). MODIS/Terra MOD14CMH (2001-2008), (b). MODIS/Aqua MYD14CMH (2003-2008). Data source: University of Maryland ftp server 5

1.4. Annual carbon emissions (as gC m^{-2} year^{-1}), averaged over 1997-2009. These emissions estimates are build combining burned area data from above with a biogeochemical model (CASA-GFED) that estimates fuel loads and combustion completeness for each monthly time step. These fuel loads are based on satellite derived information on vegetation characteristics and productivity to estimate carbon input, and carbon outputs through heterotrophic respiration, herbivore, and fires 8

2.1. Maps of key physical features of Southeast Asia (SEA) ranging from longitude 90°-160°E and latitude 30°N-10°S. (a) Elevation. (b) Annual mean precipitation (mm). (c) Annual mean temperature (K). (d) Mean radiation (W/m^{2}). (e) Land cover classifications. (f) Gridded Population of the World (GPW), v3. (g) Peatland distribution. All data sources were listed in Chapter 3 19

2.2. Monthly variations in mean air temperature, burned area and mean precipitation in SEA from 2001 to 2010 21

2.3. (a)-(f) Bi-monthly MODIS fire prevalence for 2003-2009 based on Giglio et al. (2006) and Reid et al. (2012). (g) Fire count time series for Indochina and the Maritime Continent for 2003-2009 derived from Reid et al. (2012) 23

2.4. $PM_{2.5}$ emission properties (2003-2009) from GFED3 in SEA 24

3.1. Elevation of Southeast Asia (SEA),1-China; 2-India; 3-Myanmar; 4-Bangladesh; 5-Thailand; 6-Laos; 7-Vietnam; 8-Cambodia; 9-Philippines; 10-Malaysia; 11-Indonesia; 12-Papua New Guinea; 13-Singapore; 14-Brunei. SEA was divided into the Northern SEA (NSEA) and Equatorial SEA (ESEA). The spatial distribution of peat forest (blue area) in SEA was extracted from World Wildlife Fund terrestrial ecoregions map (1999-2000; Tosca et al., 2011) 31

3.2. Flow chart of the fire-induced biomass burning carbon emission process in BEAMS 39

3.3. Percentage of burned area from (a) MCD64A1 with 5 km grid, (b) MCD45A1 with 5 km grid and (c) GFED3 with a 0.5° grid. (d) Comparison of burned area estimated from statistics, MCD64A1, MCD45A1 and GFED3 in Thailand during the period of October 2007 - June 2008. Statistics data were collected from Forest Fire Control Division (FFCD), Thailand, available at: http://www.dnp.go.th/ForestFire/Eng/fire%20statistic.htm 47

3.4. Interannual variations in burned area estimated by MCD64A1, MCD45A1 and GFED3 in SEA and each country during 2001-2010. A Multivariate ENSO Index (MEI) is shown in grey scale, with darker shades indicating higher MEI values (MEI, http://www.esrl.noaa.gov/psd/enso/mei/mei.html) 50

3.5. (a) Spatial variation in biomass carbon distribution in SEA estimated from BEAMS in 2001 (Unit: gC m^{-2}). (b) Scatter plots of BEAMS predicted biomass carbon data using estimates from Saatchi et al. (2011). Data are based on georeferenced in situ forest measurements and remote sensing metrics for Asia around 2000 (Unit: gC m^{-2}), Y = 0.87 X - 140.1 (R^2 = 0.88). 52

3.6. Average annual fire carbon emissions in SEA derived from (a) BEAMS/

MCD64A1, (b) BEAMS/MCD45A1-Peat, (c) BEAMS/GFED from 2001-2010 in SEA with 5 km spatial resolution (Unit: gC m^{-2} $year^{-1}$) 55

3.7. Comparison of fire carbon emissions from (a) BEAMS/MCD64A1 with 5 km grid and (b) GFED3 with 0.5° grid in Kalimantan of Indonesia ranging from 8°N-4S° and 109°E-119°E 56

3.8. Average annual fire carbon emissions estimated by (a) BEAMS/MCD64A1, (b) BEAMS/MCD45A1-Peat, (c) BEAMS/GFED during 2001-2010 in SEA at a spatial resolution of 0.5° resampled to 5 km for consistent comparisons with (d) GFED3 (gC m^{-2} $year^{-1}$) 58

3.9. Interannual variations in fire carbon emissions from BEAMS/MCD64A1, BEAMS/MCD45A1-Peat and BEAMS/GFED and its corresponding average AOD in SEA and each country during 2001-2010. A Multivariate ENSO Index (MEI) is shown in grey scale, with darker shades indicating higher MEI values 61

3.10. (a) Monthly variations in fire carbon emissions estimated by BEAMS/ MCD64A1, BEAMS/MCD45A1-Peat and BEAMS/GFED and its corresponding average AOD in SEA during 2001-2010. (b) Monthly variations in burned area estimated by MCD64A1, MCD45A1-Peat, GFED3, MCD45 in SEA during 2001-2010. (c) Monthly variations in fire carbon emissions in SEA and synchronous variations of DMI (Dipole Mode Index) and Niño3.4 Index. DMI is defined as the difference in SST anomalies between the western equatorial Indian Ocean (50°E-70°E and 10°S to 10°N) and the southeastern equatorial Indian Ocean (90°E-110°E and 10°S to 0°N). The Niño3.4 index was calculated from the Smith and Reynolds global gridded Sea Surface Temperature analysis (Smith and Reynolds, 2003). A Multivariate ENSO Index (MEI) is shown in grey scale, with darker shades indicating higher MEI values 64

3.11. (a) Monthly variations in NSEA fire carbon emissions. (b) Monthly variations in NSEA burned area products estimated by MCD64A1, MCD45A1 and GFED3 during 2001-2010. (c). Spatial distributions of the burned area anomaly during

the drought period of Jan-Mar in 2004, 2007 and 2010 derived from the average burned area estimates from MCD64A1, MCD45A1 and GFED3. (d). Spatial distributions of vapor pressure anomaly during the drought period of Jan-Mar in 2004, 2007 and 2010. A Multivariate ENSO Index (MEI) is shown in grey scale, with darker shades indicating higher MEI values 67

3.12. (a) Monthly variations in Indonesia fire carbon emissions and the corresponding average AOD during 2001-2010. (b) Monthly variations in annual precipitation and vapor pressure in Indonesia during 2001-2010. (c) Indonesia palm oil plantation production growth rate anomaly by year (From United States Department of Agriculture). A multivariate ENSO index (MEI) is shown in grey scale, with darker shades indicating higher MEI values 69

4.1. Land cover maps of Southeast Asia (SEA),1-China; 2-India; 3-Myanmar; 4-Bangladesh; 5-Thailand; 6-Laos; 7-Vietnam; 8-Cambodia; 9-Philippines; 10-Malaysia; 11-Indonesia; 12-Papua New Guinea; 13-Singapore; 14-Brunei. SEA was divided into the Northern SEA (NSEA) and Equatorial SEA (ESEA). The spatial distribution of peat forest in SEA was extracted from World Wildlife Fund terrestrial ecoregions map (1999-2000; Tosca et al., 2011) 87

4.2. Percentage of the average annual burned area with 1 km grid in SEA during 2001-2010 94

4.3. Averaged annual CO_2 emissions from biomass burning with 1 km grid in SEA during 2001-2010 95

4.4. Comparison of CO_2 emissions from biomass burning between (a) this study with 1 km grid and (b) GFED3 with 0.5° grid in Kalimantan of Indonesia ranging from 8° N to 4° S and 109-119° E during the period of 2001-2010 96

4.5. Percentage of average annual emission species from biomass burning for each land in SEA during the period of 2001-2010 97

4.6. Percentage of average annual emission species from biomass burning for each country in SEA during the period of 2001-2010 99

4.7. Interannual variations of (a) burned area, (b) burned biomass and (c) CO_2 emissions from biomass burning in SEA and the amounts from each land type 102

4.8. Intraannual variations of (a) burned area, (b) burned biomass and (c) CO_2 emissions from biomass burning in SEA and the amounts from each land type 103

S1. Overall framework of estimation methodology 124

S2. Steps for estimation of burned area of forest fire (Permadi and Kim Oanh, 2013). Note: HDF (hierarchical data format) 125

Chapter 1

Introduction

1.1 General introduction

Fire and biomass burning are unique disturbances on ecosystem processes and dynamics (Carlson et al., 2012). They can lead to the direct release of ecosystem carbon that are stored in large terrestrial pools (live vegetation, dead vegetation, litter, organic soil), which have deep implication to the ecosystem productivity and stability. At the same time, they can result in elevated concentrations of trace gases (e.g., carbon monoxide, methane) and aerosol particles in the atmosphere, which have significant effects on global atmospheric chemistry and climate change in various regions of the world (Andreae and Merlet, 2001; Zhang et al., 2013).

Since the late 1970s, biomass burning has been known to be a major source of trace gases and aerosols pollutants in local, regional and global atmospheric environment (Seiler and Crutzen, 1980; Streets et al., 2003; Zhang et al., 2008). The emitted pollutants from biomass burning, e.g., organic carbon (OC) and black carbon (BC), may have significantly influenced the light absorption and altered the climate system (IPCC, 2011). The active trace gases released from biomass burning, e.g., NO_x and volatile organic compounds (VOCs), can act as precursors of tropospheric ozone (O_3) and secondary organic aerosols (Langmann et al., 2009), which can alter the atmospheric composition, deteriorate local or regional air quality, and then have significant impacts on human health and the environment (Bo et al., 2008).

Globally, biomass burning contributes today to about 50% of the total direct carbon monoxide (CO) emissions (Petron et al., 2004) and about 15% of surface NO_x emissions (IPCC, 2001). During the period of 1997-2004, biomass burning resulted in approximately 2.5 PgC $year^{-1}$ being emitted globally, and considerable interannual and intraannual variability were observed (van der Werf et al., 2006). During the

period 2000-2010, fires associated with deforestation emitted approximately 1.0 PgC $year^{-1}$ worldwide (Baccini et al., 2012). The recently most severe and devastating 1997/98 El Niño event caused a total range of emissions at between 0.8 and 2.6 PgC (Page et al., 2002), which is equivalent to approximately 40% of global fossil fuel emissions during that time (van der Werf et al., 2008).

Many efforts have been made during the past few decades worldwide to improve biomass burning emission estimates, such as conducting laboratory or field measurements (Reid et al., 2005; Akagi et al., 2011; Zhang et al., 2013) and employing satellite remote sensing information to capture fire events (Duncan et al., 2003). However, little progress has been made on biomass burning emissions in developing countries and regions due to the poor coverage of fire products (Yan et al., 2006; Zhao et al., 2011). Meanwhile, biomass burning estimates have much uncertainty due to the input data, primarily by newly developed satellite information on burned area, improved biogeochemical models for fuel loads estimates, and time variable combustion factors and emission factors.

1.2 Burned area data

Biomass burning emissions are usually estimated by using the product of burned area, fuel loads, combustion factors and emission factors, integrated over the time and space scale of interest. Among all inputs, burned area is usually considered to be the most important and also uncertain parameter because of the potentially high spatial and temporal variability at continental to global scales (Giglio et al., 2006). Burned area identification makes full use of change detection techniques based on classification and threshold techniques that strongly depend on the relationship between the actual signal and the change of features compared to the previous scene (Roy et al., 2002). Burn scars are captured by identifying the areas that were previously related with active fires and have a spectral signature that corresponds with that of a burn scar (Chu et al., 2002; Joy, 2010). The satellite burned area products such as Global Burnt Area - 2000 (GBA2000) (Tansey et al., 2004), European Space Agency's monthly Global Burn Scar satellite product (GLOBSCAR)

(Simon et al., 2004) and MODIS burned area product (Roy et al., 2002) have been developed, which have been widely used due to their broad spatial and long-term temporal coverage.

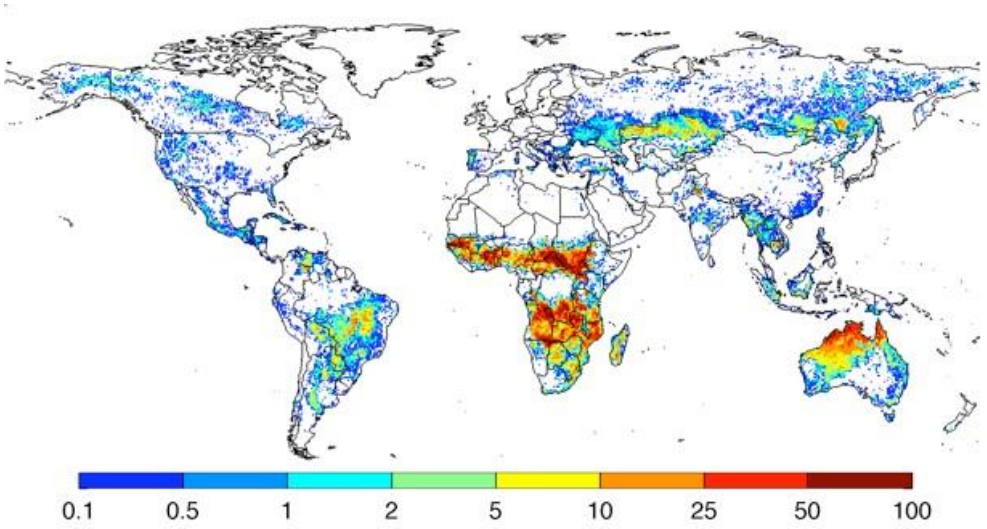

Fig. 1.1 Annual burned area (as percentage of the area of the grid cell), averaged over 1997-2009. For November 2000 onwards it is for 90% based on mapped MODIS burned area using the direct broadcast algorithm, aggregated from the native 500-meter resolution to 0.5 degree. The remaining 10% and burned area for 1997 - October 2000 are based on relations between active fires (ATSR, TRMM-VIRS, and MODIS) and mapped burned area for periods they overlap. From Global Fire Emission Database 3 (GFED3).

The MODIS burned area product integrates a bi-directional reflectance model with inverted multi-temporal 500 m land surface reflection observations, identifying the location of a fire and approximate day of burning (Justice et al., 2002). Due to the failure in accounting for the difference between old and new burns from the spectrally similar unburned features and burned features, MODIS burned area product may overlook small and spatially fragmented fires or burns with low combustion completeness (Roy et al., 2005). Besides, the exact day of burning cannot always be accurately reflected because of cloudy or missing data (Korontzi et al., 2004). The MODIS burned area has a spatial resolution of 500 m and monthly temporal resolution since 2001, and the day of burning and a temporal uncertainty range of the burn date are recorded for every pixel (Fig. 1.1). For the years 1998-

2008, global estimates of the total annual burned area ranged between 3.3 and 4.3 million km^2, with the maximum occurring in 1998 (Giglio et al., 2010).

1.3 Active fire products

The active fire algorithm identifies thermal anomalies in separate pixels which indicate fires, as well as other high temperature sources, such as gas flares and power plants (Justice et al., 2002). Fire detection is performed using a contextual algorithm that exploits the strong emission of mid-infrared radiation from fires

(a)

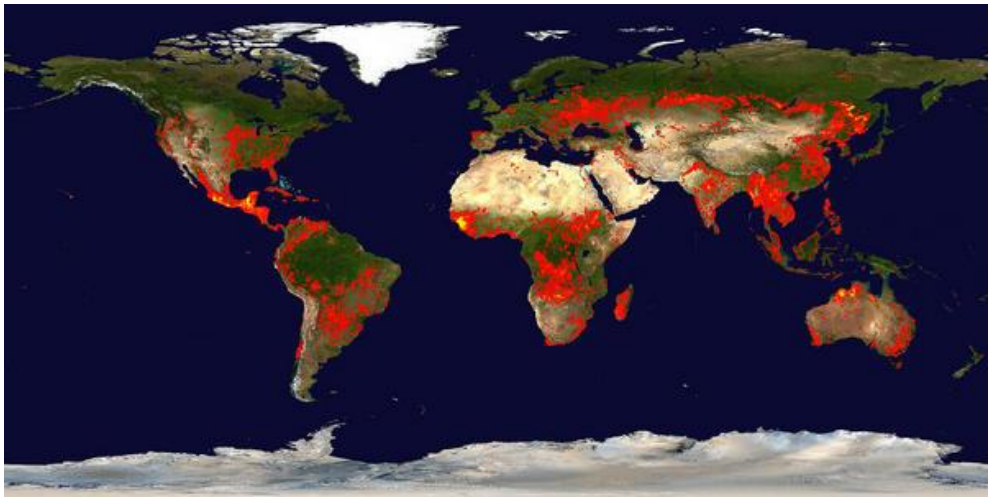

(b)

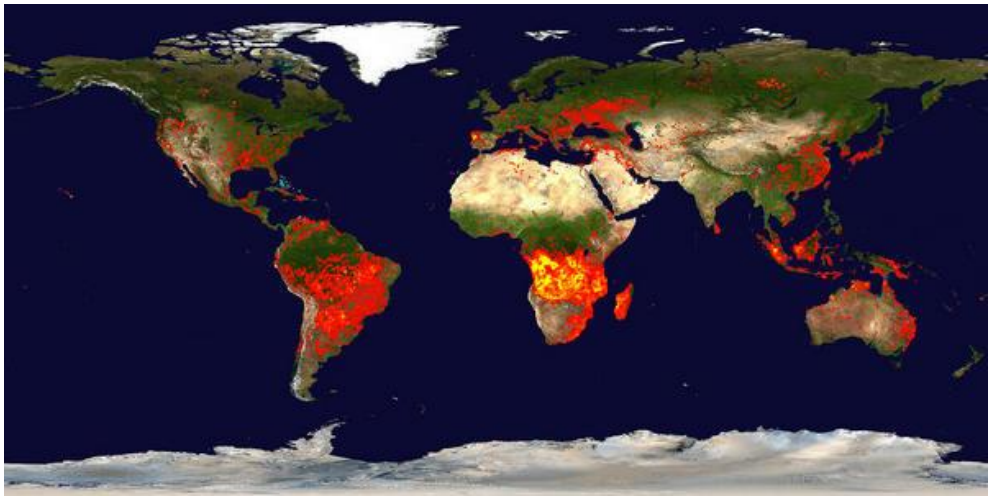

Fig. 1.2 Global 10-day fire maps generated using the MODIS fire locations to represent the current fire activity around the world. (a).04/21/2013 - 04/30/2013; (b). 08/19/2013 - 08/28/2013. From NASA Earth Data Global Fire Maps.

(Giglio et al., 2003) (Fig. 1.2). The algorithm ultimately classified the whole image into 6 classes (missing data, cloud, water, non-fire, fire, or unknown) after examining each pixel of the MODIS swath. Active fire detection algorithms are used to determine the location of hotspots using satellite data, emphasizing the practicality of using satellite remote sensing as a method to monitor biomass burning over an extensive area (Roy et al., 2005). Active fire data can provide us the fire location and counts, even though, it cannot be directly converted into the amount of burned area and emissions released (Schultz, 2002; Korontzi et al., 2004). As a crucial interim

(a)

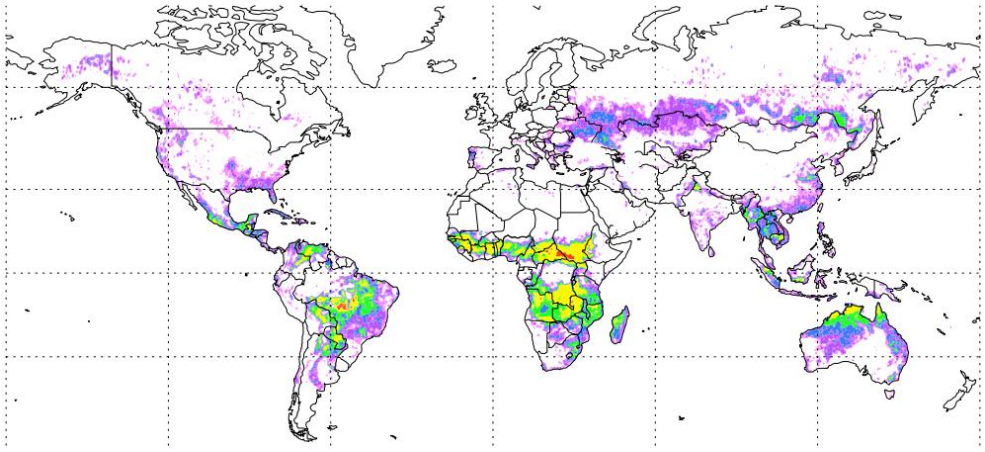

(b)

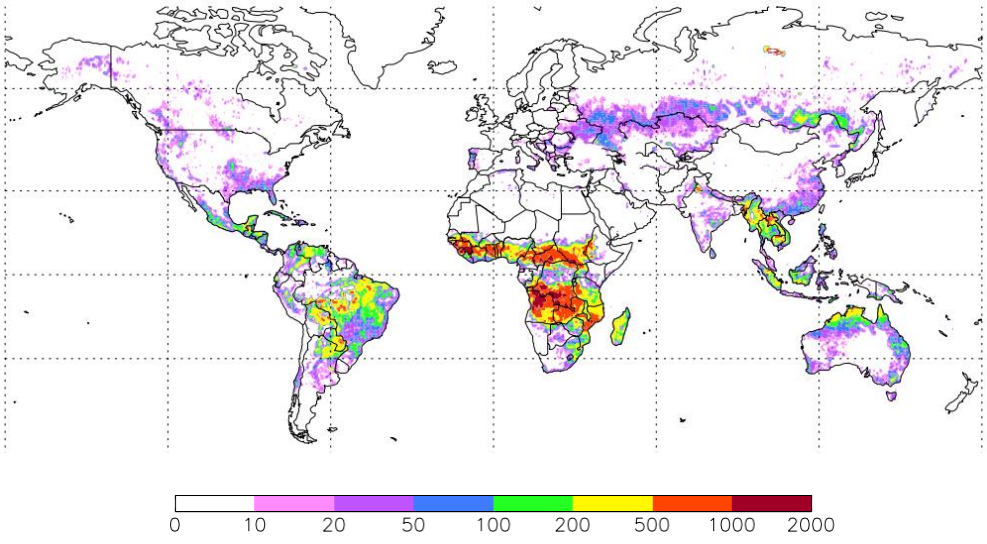

Fig. 1.3 Fire counts (#/0.5° grid year^{-1}). (a). MODIS/Terra MOD14CMH (2001-2008), (b). MODIS/Aqua MYD14CMH (2003-2008). Data source: University of Maryland ftp server.

product, satellite observations are capable of detecting the location of a fire, but cannot provide information regarding the fire intensity, amount and type of biomass burned without additional data (Joy, 2010) (Fig. 1.2).

The MODIS daily Level 3 fire product is tile-based, with each product file spanning one of the 460 MODIS tiles, of which 326 contain land pixels. The product is a 1-km gridded composite of fire pixels detected in each grid cell over each daily (24-hour) compositing period (Roy, 2010). Validation of the product took place using data that has a reliable and known level of accuracy, such as other fire products, ground validation and a global sample of Advanced Spaceborne Thermal Emission and Reflection Radiometer (ASTER) data, due to its high resolution of fire detection (Justice et al., 2002). The Global 10-day fire maps from MODIS showed conspicuous spatial and temporal variations in fire activity across the globe. Of which, extensive fires can be found in Amazon, South of Africa, Siberia, Southeast Asia and Australia with strong seasonality (Fig. 1.2, 1.3). Currently, there are a number of fire products available at the moment (Table 1.1).

Table 1.1 A summary of active fire products.

Product name	Resolution	Frequency	Agency	Products available at
NOAA/AVHRR	1 km	Global active fire day & 10 day	JRC	http://www-gvm.jrc.it/tem/
ERS-ATSR-AATSR ENVISATAATSR	1 km	Global active fire day & 10 day	ESA	http://shark1esrin.esa.it/ionia/FIRE/AF/ATSR/
TRMM-VIRS	2.2 km	+/-40º from Equator active fire day & night	NASA	http://earthobservatory.nasa.gov/Observatory/Datasets/fires.trmm.html
	0.5º	Monthly		
GOES WF_ABBA	1 km	Western hemisphere active fire day & night	CIMMS	http://www.nrlmry.navy.mil/flambe/
MODIS-AQUA, TERRA	500 m Lat lon	Global active fire day and night	MODIS team	http://rapidfire.sci.gsfc.nasa.gov/
MSG FIR	3 km	MSG coverage Active day & night	EUMETSAT	http://eumetsat.int

Note: from Joy (2010).

1.4 Biomass burning emissions

Biomass burning contributes a significant amount of trace gas and aerosols into the atmosphere. Presently, there are some biomass burning emissions database available, which combine satellite information on fire activity and vegetation productivity to estimate gridded monthly burned area and fire emissions, as well as scalars that can be used to calculate higher spatial and temporal resolution emissions of all trace gases.

Till now, there have been many attempts to estimate the emissions of trace gases and particle matters from fire induced biomass burning. At the global scale, there are several bottom-up biomass burning emissions inventories. By using emission factors and estimated burned biomass from published literature, earlier studies estimated the total global emissions of a variety of trace gaseous and particulate species in some specific year (Andreae and Merlet, 2001) and multi-years (1996-2000) (Duncan et al., 2003) with focus on spatial patterns and variations. More recently, Ito and Penner (2004) developed fire emissions inventory at a high spatial resolution of 1 km with monthly time step for the year 2000 by using the satellite burned area data. Hoelzemann et al. (2004) estimated monthly biomass burning emissions of trace gases and particles for 2000 as well with 0.5° × 0.5° grid globally, through employing the Global Wildland Fire Emission Model (GWEM), which was developed by using European Space Agency's monthly Global Burn Scar satellite product (GLOBSCAR) and results from the Lund-Potsdam-Jena Dynamic Global Vegetation Model (LPJ-DGVM). In addition, some other studies have evaluated the carbon monoxide (CO) emissions from biomass burning and other sources by using observations from space and an inverse model (Arellano et al., 2006; Kopacz et al., 2010; Wiedinmyer et al., 2011).

The Global Fire Emissions Database version 3 (GFED3, Randerson et al., 2005; van der Werf et al., 2004, 2006, 2010) is a widely used global biomass burning emissions dataset. GFED3 includes 8-day and monthly emissions of selected trace gas and particulate emissions from burning globally with spatial resolution of 0.5°

since 1997 till now (van der Werf et al., 2006; Giglio et al., 2010; van der Werf et al., 2010) (Fig. 1.4). The available data source of GFED3 is used by global atmospheric chemical transport and climate modelers in efforts to understand the chemical composition of the atmosphere and the potential effects on climate change (e.g., Magi et al., 2009; Nassar et al., 2009; Stavrakou et al., 2009). Currently, there are many other global inventories on biomass burning emissions available (e.g., MACCity, ACCMIP, RCPs, EDGARv4.2, PEGASOS_PBL, EDGARv3.2FT2000, RETRO, GFASv1.0, GFED3, GFED2, GICC, AMMABB, GEIAv1, POET), more specific information on the description of each inventory can be found at the following website: http://eccad.sedoo.fr/eccad_extract_interface/JSF/page_login.jsf.

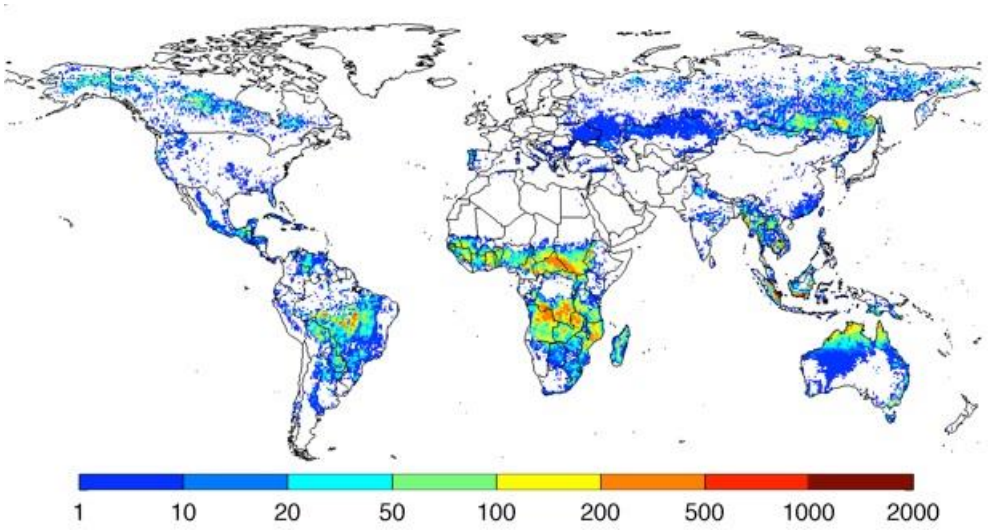

Fig. 1.4 Annual carbon emissions (as gC m^{-2} $year^{-1}$) from GFED3, averaged over 1997-2009. These emissions estimates are build combining burned area data from above with a biogeochemical model (CASA-GFED) that estimates fuel loads and combustion completeness for each monthly time step. These fuel loads are based on satellite derived information on vegetation characteristics and productivity to estimate carbon input, and carbon outputs through heterotrophic respiration, herbivore, and fires.

1.5 Research objectives

Based on the above analysis, we realized that most inventories on biomass burning emissions have a coarse spatial resolution of 0.5°. Since the overwhelming majority of fires in Southeast Asia are set by humans in very small plot scale with

the aim of perfecting their own lands or deforestation for lands, e.g., crop residue burning. Fires at scales as large as 0.5° are rarely observed. And such coarse grid data with 0.5° usually misses the small sized fires in SEA and misinterprets the spatial variations in biomass burning emissions due to its large smoothed pixels. Consequently, the data at a spatial resolution of 0.5° are not considered to be well suited to representing fire-induced biomass burning emissions at regional or continental scales. The combination of a varied topography and the nonlinearity inherent in ecophysiological processes can limit the ability of raster-based information to accurately capture or represent the spatiotemporal variations in fire occurrence and biomass burning in specific or small areas (Randerson et al., 2012). Such limitations routinely lead to misunderstandings of spatial observations in biomass burning emissions and their interactions with climate systems and carbon cycles. Consequently, in order to accurately estimate the carbon budgets of terrestrial ecosystems in SEA, detailed examinations of the spatiotemporal variations in biomass burning emissions from fires at fine level of resolution are urgently required. Therefore, a high resolution and multi-year emissions inventory for biomass burning in Southeast Asia terrestrial ecosystem during recently is more preferred, which will provide an overall assessment of the potential effects and the relevant information for formulation of appropriate mitigation measures for these Southeast Asian developing countries.

The primary objective of this study were:

(1). To quantitatively estimate the spatial variation and temporal dynamics of biomass burning emissions for the period 2001-2010 at a fine spatial resolution to increase our understanding of the contribution of fire-induced carbon emissions to the regional carbon cycle and budget.

We used MODIS burned area products and an improved Biosphere model integrating Eco-physiological And Mechanistic approaches using Satellite data (BEAMS) with fire carbon emissions process embedded to estimate carbon stocks and fire carbon emissions at a spatial resolution of 5 km in SEA between 90° and 160° east, 30° north and 10° south. In addition, by using different burned area

products as model inputs, we also examined the effects of varying burned area products on the fire carbon emissions across the entire SEA, both spatially and temporally, and evaluated the relationship between different burned areas and their corresponding fire carbon emissions.

(2). To develop a high resolution biomass burning emissions inventory covering all land types in Southeast Asia during the period of 2001-2010, and evaluates the global warming potentials.

We employed the newly released burned area product MCD64A1, satellite and observation data based biomass density, and spatio-temporal variable combustion factors to estimate the biomass burning emissions at high spatial resolution of 1 km. Besides, we also evaluated the effects of all the trace gases emissions to the global warming potentials. The trace gases emissions included carbon dioxide (CO_2), carbon monoxide (CO), methane (CH_4), Non-Methane Volatile Organic Compounds (NMVOC), black carbon (BC), organic carbon (OC), nitrogen oxides (NO_x), ammonia (NH_3), nitrous oxide (N_2O), and sulfur dioxide (SO_2).

1.6 Outline of the dissertation

Chapter 1 introduces the significance of fire and biomass burning emissions on ecosystem productivity and atmospheric composition, and lists some products of burned area and active fires, biomass burning emissions inventories.

Chapter 2 presents the peculiar physical and social characteristics of Southeast Asia, and reviews the confronted ecological problems and environmental issues that are related to fire and biomass burning emissions, and also elaborates the effects of biomass burning to trace gases, hazes, cloud and smokes, and evaluates their impacts on ecosystem productivity, atmospheric composition and air pollution.

Chapter 3 gives a full description of the improved biosphere model integrating fire carbon emissions process with high spatial resolution to quantitatively evaluate the spatial variation and temporal dynamics of biomass burning emissions in Southeast Asia for the period 2001-2010.

Chapter 4 develops a new high spatial resolution and multi-year inventory of

biomass burning emissions covering all land types in Southeast Asia during 2001-2010, and evaluates the global warming potentials.

Chapter 5 summarizes the entire research with findings and conclusions. Suggestions for future research are given in broad perspectives of integrating remote sensing products and terrestrial biosphere model for the connections with oceans, atmospheres, biosphere and geosphere.

References:

Akagi, S.K., Yokelson, R.J., Wiedinmyer, C., Alvarado, M.J., Reid, J.S., Karl, T., Crounse, J.D., Wennberg, P.O., 2011. Emission factors for open and domestic biomass burning for use in atmospheric models. Atmos. Chem. Phys., 11, 4039-4072.

Andreae, M.O., Merlet, P., 2001. Emission of trace gases and aerosols from biomass burning. Global Biogeochem. Cycles, 15(4), 955-966.

Arellano Jr., A.F., Kasibhatla, P.S., Giglio, L., van der Werf, G.R., Randerson, J.T., Collatz, G.J., 2006. Time-dependent inversion estimates of global biomass-burning CO emissions using Measurement of Pollution in the Troposphere (MOPITT) measurements. J. Geophys. Res., 111, D09303, doi:10.1029/2005JD006613.

Baccini, A., Goetz, S.J., Walker, W.S., Laporte, N.T., Sun, M., Sulla-Menashe, D., Hackler, J., Beck, P.S.A., Dubayah, R., Friedl, M.A., Samanta, S., Houghton, R.A., 2012. Estimated carbon dioxide emissions from tropical deforestation improved by carbon-density maps. Nature Clim. Change, 2, 182-185.

Bo, Y., Cai, H., Xie, S.D., 2008. Spatial and temporal variation of historical anthropogenic NMVOCs emission inventories in China. Atmos. Chem. Phys., 8, 7297-7316.

Carlson, K.M., Curran, L.M., Ratnasari, D., Pittman, A.M., Soares-Filho, B.S., Asner, G.P., Trigg, S.N., Gaveau, D.A., Lawrence, D., Rodrigues, H.O., 2012. Committed carbon emissions, deforestation, and community land conversion from oil palm plantation expansion in West Kalimantan, Indonesia. PNAS, 109, 7559-7564.

Chu, D.A., Kaufman, Y.J., Ichoku, C., Remer, L.A., Tanre, D., Holben, B.N., 2002. Validation of MODIS aerosol optical depth retrieval over land. Geophys. Res. Lett., 29, DOI: 10.1029/2001GL013205.

Duncan, B.N., Martin, R.V., Staudt, A.C., Yevich, R., Logan, J.A., 2003. Interannual and seasonal variability of biomass burning emissions constrained by satellite observations. J. Geophys. Res., 108 (D2), 4100, doi:10.1029/2002JD002378.

Giglio, L., Csiszar, I., Justice, C.O., 2006. Global distribution and seasonality of active fires as observed with the Terra and Aqua Moderate Resolution Imaging Spectroradiometer (MODIS) sensors. J. Geophys. Res., 111, G02016, doi:10.1029/2005JG000142, 2006.

Giglio, L., Randerson, J.T., van der Werf, G.R., Kasibhatla, P.S., Collatz, G.J., Morton, D.C., DeFries, R.S., 2010. Assessing variability and long-term trends in burned area by merging multiple satellite fire products. Biogeosciences, 7, 1171-1186.

Hoelzemann, J.J., Schultz, M.G., Brasseur, G.P., Granier, C., Simon, M., 2004. Global Wildland Fire Emission Model (GWEM): Evaluating the use of global area burnt satellite data. J. Geophys. Res., 109, D14S04, doi:10.1029/2003JD003666.

IPCC, Climate Change, 2001. Synthesis report. In: Watson, R.T., the Core Writing Team (Eds.), A Contribution of Working Groups I, II, and III to the Third Assessment Report of the Intergovernmental Panel on Climate Change. Cambridge University Press, Cambridge, United Kingdom/New York, NY, USA, p. 398.

Ito, A., Penner, J.E., 2004. Global estimates of biomass burning emissions based on satellite imagery for the year 2000. J. Geophys. Res., 109, D14S05, doi:10.1029/2003JD004423.

Justice, C.O., Giglio, L., Korontzi, S., Owens, J., Morisette, J.T., Roy, D., Descloitres, J., Alleaume, S., Petitcolin, F., Kaufman, Y.J., 2002. The MODIS fire products. Remote Sens. Environ., 83, 244-262.

Kopacz, M., Jacob, D.J., Fisher, J.A., Logan, J.A., Zhang, L., Megretskaia, I.A., Yantosca, R.M., Singh, K., Henze, D.K., Burrows, J.P., Buchwitz, M., Khlystova, I., McMillan,

W.W., Gille, J.C., Edwards, D.P., Eldering, A., Thouret, V., Nedelec, P., 2010. Global estimates of CO sources with high resolution by adjoint inversion of multiple satellite datasets (MOPITT, AIRS, SCIAMACHY, TES). Atmos. Chem. Phys., 10, 855-876.

Korontzi, S., Roy, D.P., Justice, C.O., Ward, D.E., 2004. Modeling and sensitivity analysis of fire emissions in southern Africa during SAFARI 2000. Remote Sens. Environ., 92, 255-275.

Langmann, B., Duncan, B., Textor, C., Trentmann, J., van der Werf, G.R., 2009. Vegetation fire emissions and their impact on air pollution and climate. Atmos. Environ., 43, 107-116.

Magi, B.I., Ginoux, P., Ming, Y., Ramaswamy, V., 2009. Evaluation of tropical and extratropical Southern Hemisphere African aerosol properties simulated by a climate model. J. Geophys. Res., 114, D14204, doi:10.1029/2008JD011128.

Mieville, A., Granier, C., Liousse, C., Guillaume, B., Mouillot, F., Lamarque, J.F., Gregoire, J.M., Petron, G., 2010. Emissions of gases and particles from biomass burning during the 20th century using satellite data and an historical reconstruction. Atmos. Environ., 44, 1469-1477.

Mouillot, F., Field, C.B., 2005. Fire history and the global carbon budget: a 1° × 1° fire history reconstruction for the 20th century. Glob. Chang. Biol., 11, 398-420.

Nassar, R., Logan, J.A., Megretskaia, I.A., Murray, L.T., Zhang, L., Jones, D.B.A., 2009. Analysis of tropical tropospheric ozone, carbon monoxide, and water vapor during the 2006 El Niño using TES observations and the GEOS-Chem model. J. Geophys. Res., 114, D17304, doi:10.1029/2009JD011760.

Page, S.E., Siegert, F., Rieley, J.O., Boehm, H-D.V., Jaya, A., Limin, S., 2002. The amount of carbon released from peat and forest fires in Indonesia in 1997. Nature, 420, 61-65.

Permadi, D.A., Kim Oanh, N.T., 2013. Assessment of biomass open burning emissions in Indonesia and potential climate forcing impact. Atmos. Environ., 78, 250-258.

Petron, G., Granier, C., Khattatov, B., Yudin, V., Lamarque, J.F., Emmons, L., Gille, J., Edwards, D.P., 2004. Monthly CO surface sources inventory based on the 2000-2001 MOPITT satellite data. Geophys. Res. Lett. 31, 21107.

Real, E., Law, K.S., Wienzierl, B., Fiebig, M., Petzold, A., Wild, O., Methven, J., Arnold, S.R., Stohl, A., Huntrieser, H., Roiger, A., Schlager, H., Stewart, D., Avery, M., Sachse, G., Browell, E., Ferrare, R., Blake, D., 2007. Processes influencing ozone levels in Alaskan forest fire plumes during long-range transport over the North Atlantic. J. Geophys. Res., 112, D10S41, doi:10.1029/2006JD007576.

Randerson, J.T., van der Werf, G.R., Collatz, G.J., Giglio, L., Still, C.J., Kasibhatla, P., Miller, J.B., White, J.W.C., DeFries, R.S., Kasischke, E.S., 2005. Fire emissions from C3 and C4 vegetation and their influence on interannual variability of atmospheric CO_2 and $d^{13}CO_2$. Global Biogeochem. Cycle, 19, GB2019, doi:10.1029/2004GB002366.

Reid, J.S., Eck, T.F., Christopher, S.A., Koppmann, R., Dubovik, O., Eleuterio, D.P., Holben, B.N., Reid, E.A., Zhang, J., 2005. A review of biomass burning emissions part III: intensive optical properties of biomass burning particles. Atmos. Chem. Phys., 5, 827-849.

Roy, M., 2010. Monitoring biomass burning emissions using satellite imagery for Southern Africa. University of the Witwatersrand, Ph.D Dissertation. 27-28.

Roy, D.P., Jin, Y., Lewis, P.E., Justice, C.O., 2005. Prototyping a global algorithm for systematic fire-affected area mapping using MODIS time series data. Remote Sens. Environ., 97, 137-162.

Roy, D.P., Lewis, P., Justice, C., 2002. Burned area mapping using multi-temporal moderate spatial resolution data-a bi-directional reflectance model-based expectation approach. Remote Sens. Environ., 83, 263-286.

Schulz, M., Textor, C., Kinne, S., Balkanski, Y., Bauer, S., Berntsen, T., Berglen, T., Boucher, O., Dentener, F., Guibert, S., Isaksen, I.S.A., Iversen, T., Koch, D., Kirkevåg, A., Liu, X., Montanaro, V., Myhre, G., Penner, J.E., Pitari, G., Reddy, S., Seland, Ø., Stier, P., Takemura, T., 2006. Radiative forcing by aerosols as derived

from the AeroCom present-day and pre-industrial simulations. Atmos. Chem. Phys., 6, 5225-5246.

Schultz, M.G., 2002. On the use of ATSR fire count data to estimate the seasonal and interannual variability in vegetation fire emissions. Atmos. Chem. Phys., 2, 387-395.

Seiler, W., Crutzen, P.J., 1980. Estimates of the gross and net fluxes of carbon between the biosphere and the atmosphere from biomass burning. Clim. Change, 2, 207-247.

Simon, M., Plummer, S., Fierens, F., Hoelzemann, J.J., Arino, O., 2004. Burnt area detection at global scale using ATSR-2: The GLOBSCAR products and their qualification. J. Geophys. Res., 109, doi:10.1029/2003JD003622

Singh, H.B., Herlth, D., Kolyer, R., Chatfield, R., Viezee, W., Salas, L.J., Chen, Y., Bradshaw, J.D., Sandholm, S.T., Talbot, R., Gregory, G.L., Anderson, B., Sachse, G.W., Browell, E., Bachmeier, A.S., Blake, D.R., Heikes, B., Jacob, D., Fuelberg, H.E., 1996. Impact of biomass burning emissions on the composition of the South Atlantic troposphere: reactive nitrogen and ozone. J. Geophys. Res. 101 (D19), 24203-24219.

Stavrakou, T., Muller, J.F., DeSmedt, I., van Roozendael, M., van der Werf, G.R., Giglio, L., Guenther, A., 2009. Evaluating the performance of pyrogenic and biogenic emission inventories against one decade of space-based formaldehyde columns. Atmos. Chem. Phys., 9, 1037-1060.

Streets, D.G., Yarber, K.F., Woo, J.H., Carmichael, G.R., 2003. Biomass burning in Asia: Annual and seasonal estimates and atmospheric emissions. Global Biogeochem. Cycles, 17, 1099. doi: 10.1029/2003GB002040.

Tansey, K., Grégoire, J.M., Stroppiana, D., Sousa, A., Silva, J.M.N., Pereira, J.M.C., Boschetti, L., Maggi, M., Brivio, P.A., Fraser, R., Flasse, S., Ershov, D., Binaghi, E., Graetz, D., Peduzzi, P., 2004. Vegetation burning in the year 2000: Global burned area estimates from SPOT VEGETATION data. J. Geophys. Res., 109, D14S03, DOI:10.1029/2003JD003598.

van der Werf, G.R., Dempewolf, J.T., Trigg, S.N., Randerson, J.T., Kasibhatla, P.S., Giglio, L., Murdiyarso, D., Peters, W., Morton, D.C., Collatz, G.J., Dolman, A.J., DeFries,

R.S., 2008. Climate regulation of fire emissions and deforestation in equatorial Asia. PNAS, 105, 20350-20355.

van der Werf, G.R., Randerson, J.T., Collatz, G.J., Giglio, L., Kasibhatla, P.S., Avelino, A., Olsen, S.C., Kasischke, E.S., 2004. Continental-scale partitioning of fire emissions during the 1997-2001 El Niño/La Nina period. Science, 303, 73-76.

van der Werf, G.R., Randerson, J.T., Giglio, L., Collatz, G.J., Kasibhatla, P.S., Arellano Jr., A.F., 2006. Interannual variability in global biomass burning emissions from 1997 to 2004. Atmos. Chem. Phys., 6, 3423-3441.

van derWerf, G.R., Randerson, J.T., Giglio, L., Collatz, G.J., Mu, M., Kasibhatla, P.S., Morton, D.C., DeFries, R.S., Jin, Y., van Leeuwen, T.T., 2010. Global fire emissions and the contribution of deforestation, savanna, forest, agricultural, and peat fires (1997-2009). Atmos. Chem. Phys., 10, 11707-11735.

Wiedinmyer, C., Akagi, S.K., Yokelson, R.J., Emmons, L.K., Al-Saadi, J.A., Orlando, J.J., Soja, A.J., 2011. The Fire INventory from NCAR (FINN): a high resolution global model to estimate the emissions from open burning. Geosci. Model Dev., 4, 625-641.

Wild, O., Prather, M.J., Akimoto, H., 2001. Indirect long-term global radiative cooling from NOx emissions. Geophys. Res. Lett., 28, 1719-1722.

Yan, X., Ohara, T., Akimoto, H., 2006. Bottom-up estimate of biomass burning in mainland China. Atmos. Environ., 40, 5262-5273.

Zhao, Y., Nielsen, C.P., Lei, Y., McElroy, M.B., Hao, J., 2011. Quantifying the uncertainties of a bottom-up emissions inventory of anthropogenic atmospheric pollutants in China. Atmos. Chem. Phys., 11, 2295-2308.

Zhang, X., Kondragunta, S., Schmidt, C., Kogan, F., 2008. Near real time monitoring of biomass burning particulate emissions ($PM_{2.5}$) across contiguous United States using multiple satellite instruments. Atmos. Environ., 42, 6959-6972.

Zhang, Y., Shao, M., Lin, Y., Luan, S., Mao, N., Chen, W., Wang, M., 2013. Emission inventory of carbonaceous pollutants from biomass burning in the Pearl River Delta Region, China. Atmos. Environ., 76, 189-199.

Chapter 2

Fundamentals of Southeast Asia

The 2007 IPCC Report on Impacts, Adaptation and Vulnerability lists Southeast Asia (SEA) as one of the most vulnerable regions of the world to climate change (IPCC, 2007). Over the last several decades, SEA experienced significant growth on economic and population, which enlarged the domestic and international demand for agricultural products such as palm oil, sugar, and rice, which lead to the fast deforestation and biomass burning. In addition, under the influence of Asian Monsoon and El Niño event, the frequency of extreme weather events of SEA increased dramatically (Reid et al., 2013). Given the SEA's variability and complexity in geography, meteorology, and hydrology, establishing the quantitative linkages of terrestrial ecosystem productivity and climate systems become more complicated. The interactions between influential human factors and varying natural phenomena pose potential impacts on regional earth-climate systems, and therefore, made the SEA to be the one of the most vulnerable region.

2.1 Southeast Asia geography

For the different natural and human characteristics, SEA was divided into two distinct parts: 1) the Peninsular SEA, sometimes referred to as Asian continental SEA or Indochina, here we call it Northern SEA (NSEA) and 2) the insular SEA, also often referred to Equatorial SEA (ESEA). The domain of this review is presented in Fig. 2.1, including key physical, climatic, and biological features. The NSEA includes Myanmar, Thailand, Laos, Cambodia, Vietnam, South China, and North Philippines. And ESEA includes Indonesia, Singapore, Brunei, South Philippines and Timor-Leste and Papua New Guinea. The topographic geography of SEA is complex and variable, which includes a series of high and tough mountain ranges and large areas of lowlands. An elevation map is provided in Fig. 2.1. The SEA possesses a series of

(a)

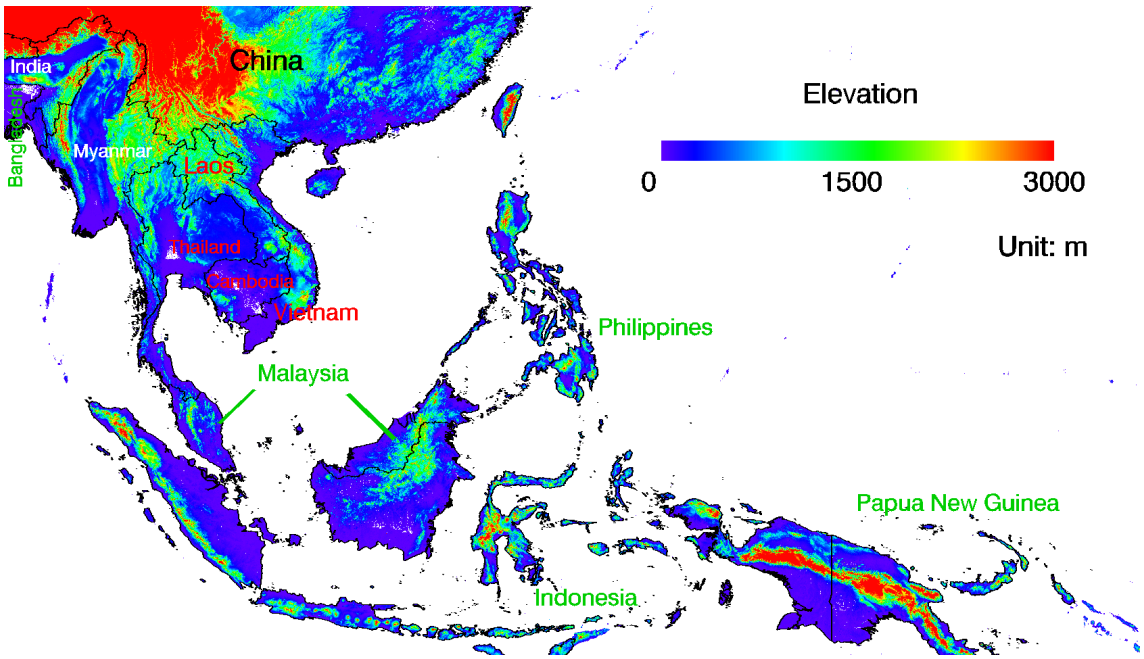
India
China
Myanmar
Laos
Thailand
Cambodia
Vietnam
Philippines
Malaysia
Papua New Guinea
Indonesia
Elevation
0
1500
3000
Unit: m

(b)

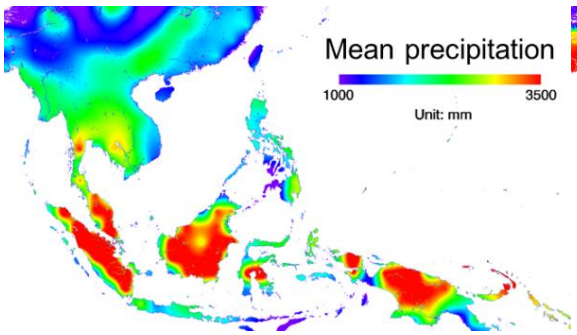
Mean precipitation
1000
3500
Unit: mm

(c)

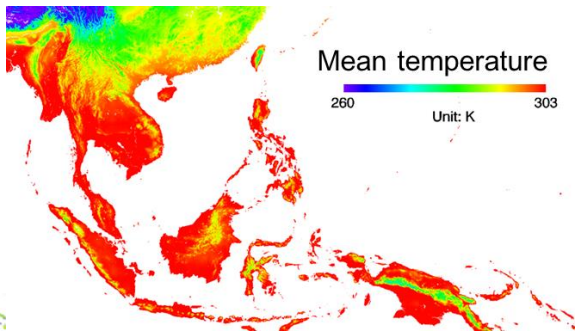
Mean temperature
260
303
Unit: K

(d)

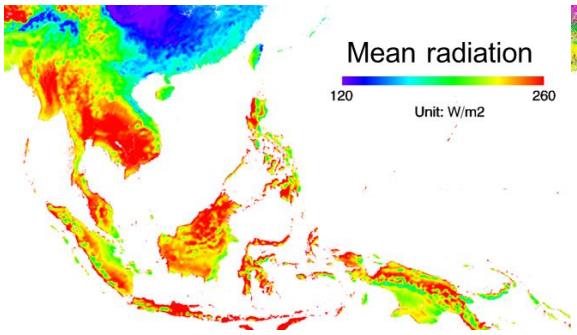
Mean radiation
120
260
Unit: W/m2

(e)

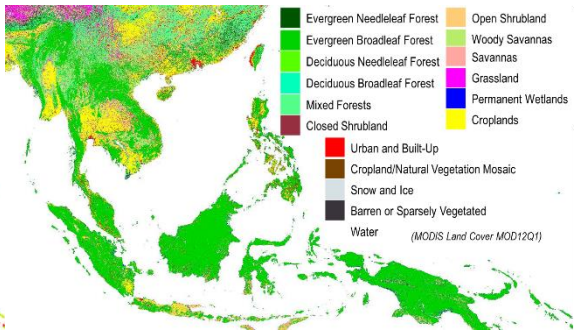
Evergreen Needleleaf Forest
Evergreen Broadleaf Forest
Deciduous Needleleaf Forest
Deciduous Broadleaf Forest
Mixed Forests
Closed Shrubland
Open Shrubland
Woody Savannas
Savannas
Grassland
Permanent Wetlands
Croplands
Urban and Built-Up
Cropland/Natural Vegetation Mosaic
Snow and Ice
Barren or Sparsely Vegetated
Water
(MODIS Land Cover MOD12Q1)

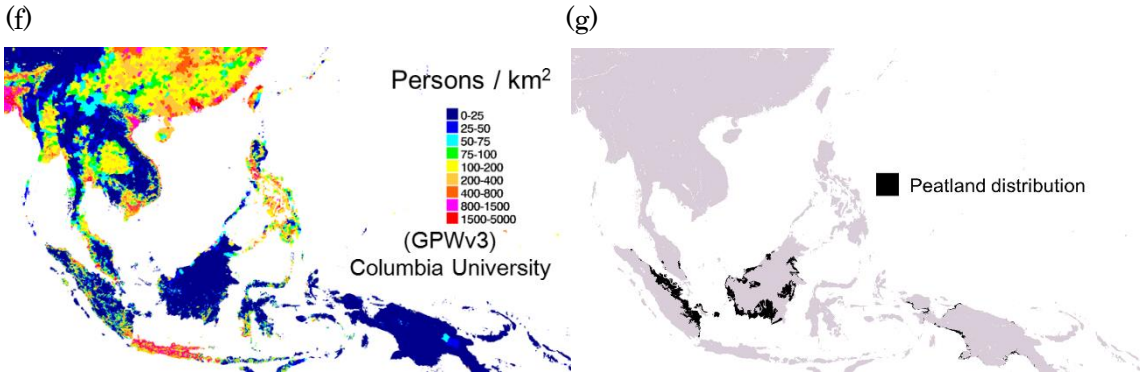

Fig. 2.1 Maps of key physical features of Southeast Asia (SEA) ranging from longitude 90°-160°E and latitude 30°N-10°S. (a) Elevation. (b) Annual mean precipitation (mm). (c) Annual mean temperature (K). (d) Mean radiation (W/m^2). (e) Land cover classifications. (f) Gridded Population of the World (GPW), v3. (g) Peatland distribution. All data sources were listed in Chapter 3.

mountain at the southeast corner of the Tibetan Plateau, separated by plateaus and river drainage basins (Reid et al., 2013). Population densities are one of the highest worldwide, with numerous mega cities in most SEA countries. The island of Indonesia Java and China Pearl River delta stand out as a massive population center. Low population density is found in Cambodia and Laos between Thailand and Vietnam (CIESIN, 2004). Land cover and land use are dynamic, with great numbers of conversions from forest to mosaic to agriculture and urban land users. Vegetation dynamics and land use issues are critically important to climate change as a whole, and in regard to fire emissions.

2.2 Biological geography

The most northern part of ESEA typically witnesses some rain year-around, allowing the humid tropical forests which prevail in the lowland vegetation (Fig. 2.1). The humid tropical part of SEA is considered to be one of the highest biodiversity of all regions across the world (Corlett, 2009). NSEA sees seasonal drought and rain under the influence of Asian Monsoon with dry period lasting from January to April annually. The major land type is the tropical broadleaf and needleleaf forests. In ESEA, the most distinctive feature is the broad distribution and vast extent of tropical peatlands with thickness up to 20 m, which are mainly distributed in the

lowland of South Sumatra, South Kalimantan and Some of Papua New Guinea (Fig. 2.1). These peatlands with high carbon density around 250,000 km^2 (~ 56% of total tropical peatland) (Page et al., 2002) contain up to 70 Gt of carbon (~ 77% of tropical peat carbon), approximately 11% of total carbon peat pool of the earth, which have numerous hydrological, ecological and societal functions in the region (Corlett, 2009).

The monsoonal climate of SEA has a profound effect on the vegetation (Corlett, 2009; Reid et al., 2013). In NSEA, tropical seasonal forests and tropical deciduous forests. The tropical seasonal forest and tropical deciduous forest are the original vegetation types. Of which, the tropical seasonal forest have been deforested for agricultural use, with considerable decrease in this forest types. The periodic slash-and-burn shifting agriculture and land clearing process accelerate the deforestation of tropical seasonal forests. Simultaneously, in drier areas, anthropogenic fire activity has resulted in noticeable degradation of the deciduous tropical forests into other kind of land covers (e.g., savanna, grasslands). In ESEA, currently, due to severe human impact and periodic drought season, large fractions of natural forest have been degraded and converted into managed land cover types or reduced to savannas, grassland, and "unnatural" grasslands. At the same time, great amounts of peatland have been drained and burned for the transformation into palm oil plantation. Indeed, rapid environmental degradation and land cover changes continue to take place in this region, especially in ESEA during the past decade (Miettinen et al., 2011). Such conversion intensifies the biomass burning and can arouse negative effect in SEA (e.g. haze, carbon emissions, ecosystem destruction, etc.).

2.3 Biomass burning emissions in SEA

It is believed that biomass burning emission in SEA is a major source of atmospheric aerosols and trace gases. The released emissions usually include carbon dioxide (CO_2), carbon monoxide (CO), nitrogen oxides (NO_x), methane (CH_4), formaldehyde (HCHO), nonmethane hydrocarbon (NMHC), and methyl chloride (CH_3Cl)) (Andreae and Merlet, 2001). The direct released emission into the air have

significant impacts on atmospheric composition, climate change, causing serious air pollutions as well. Therefore, the biomass burning over the SEA continent has gained more and more attentions in the recent years. Burning related with agriculture residues, including sugar cane, rice, and pasture, savanna as well as deforestation burning, have strong seasonal features throughout SEA.

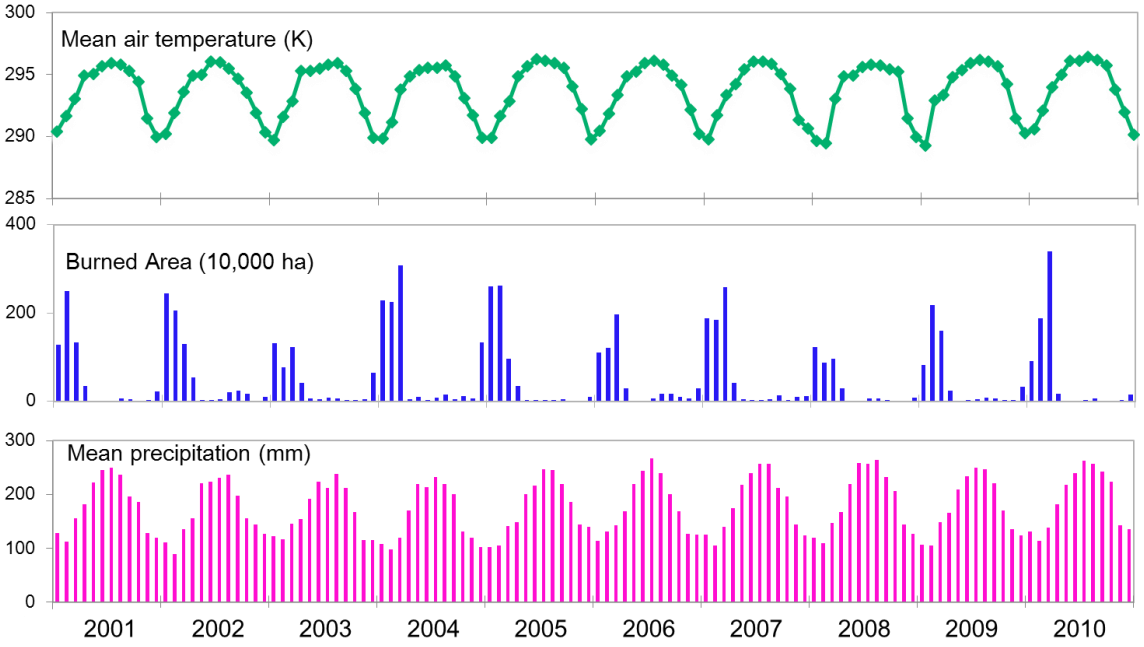

Fig. 2.2 Monthly variations in mean air temperature, burned area and mean precipitation in SEA from 2001 to 2010.

Throughout SEA nearly all fires can be considered to be of human induced, and fire is closely associated to land use activities in the region. But such fire burning extensively occurs in annual dry season with little precipitation, relative low temperature. The burned area showed large peaks in January-April annually with another small one in August-October for peatland burning in the ESEA (Fig. 2.2). Open burning is used for disposal of crop residue, preparation of agricultural fields, forest clearing and conversion to cultivated lands.

Biomass burning plumes, not only deteriorate air quality, causing serious smoke pollution and transboundary haze episodes, but also have significant impacts on atmospheric chemistry and radiative forcing (Chan et al., 2003; Tang et al., 2003; Wang et al., 2007). Earlier study reported that the SEA biomass burning activities result in the enhanced O_3 concentrations at 2-4 km altitude during the spring season

(Chan et al., 2003). Still, particle matters from biomass burning in SEA affect the regional air quality greatly, posing large potential to respiratory disease, with highest concentration in South Sumatra and South Kalimantan (Marlier et al., 2013). Therefore, it is known that SEA is one of the most intensive biomass burning areas in the world.

The seasonality of biomass burning emissions in SEA is still very apparent. Satellite observations data show that the biomass burning hot spots in the SEA are mainly observed during the period of January-April and reach a maximum in March annually (Shi et al., 2014). For the purpose of demonstration, Fig. 2.3 shows bi-monthly maps of average fire hot spot counts from the sum of the MOD/MYD14 product between 2003 and 2009 of MODIS Terra (~ 10:30 LST)/Aqua (~ 13:30 LST) (Justice et al., 2002; Giglio et al., 2003). The fire activity in SEA presents a very clear spatial and temporal pattern. Over the whole SEA, the fires events generally corresponded well with the drought season within the year, and end with the start of the rainy season even though the fire occurrences are strongly depend on human impacts, because in dry seasons humans set fires to burn it more fully (Reid et al., 2013). The winter monsoon is at its southernmost extent in January-February when, generally, NSEA burning starts from Cambodia. Fire induced biomass burning activity progresses through Thailand, Laos, and Myanmar, peaking in March and April and ending in early May, when the monsoonal transition from winter to summer take places (Reid et al., 2013). In NSEA, significant open burning effectively reduces when it comes to May-June with the start of rainy season. Rains have stopped burning in NSEA during July-August, while in the ESEA, the local farmers are harvesting and cutting forests and draining peatland to allow drying. Extensive burning associated with agriculture and peatland begins in central Sumatra in July, with peak in September-October. Peak fire activity then spread eastward across the ESEA, with a maximum in Papua in November, and the alternation goes back to Cambodia of NSEA in January-February.

Totally, NSEA covers more land than ESEA and the fire prevalence in NSEA are significantly larger than that of ESEA. Different regions have different peak fire

month under different dry season and driving forces. In NSEA, the drought period lasts from January-April annually, while the dry season of ESEA persists from August to October. Drought is just a trigger of biomass burning, it is human that is the fundamental forces of biomass burning emissions. During dry season, people in NSEA make full use of the weather condition to deforest and burn agricultural waste for land clearing. In ESEA, land holders drained the peatland and combust it for palm oil plantations, leading to large amounts of smoke and haze in the air.

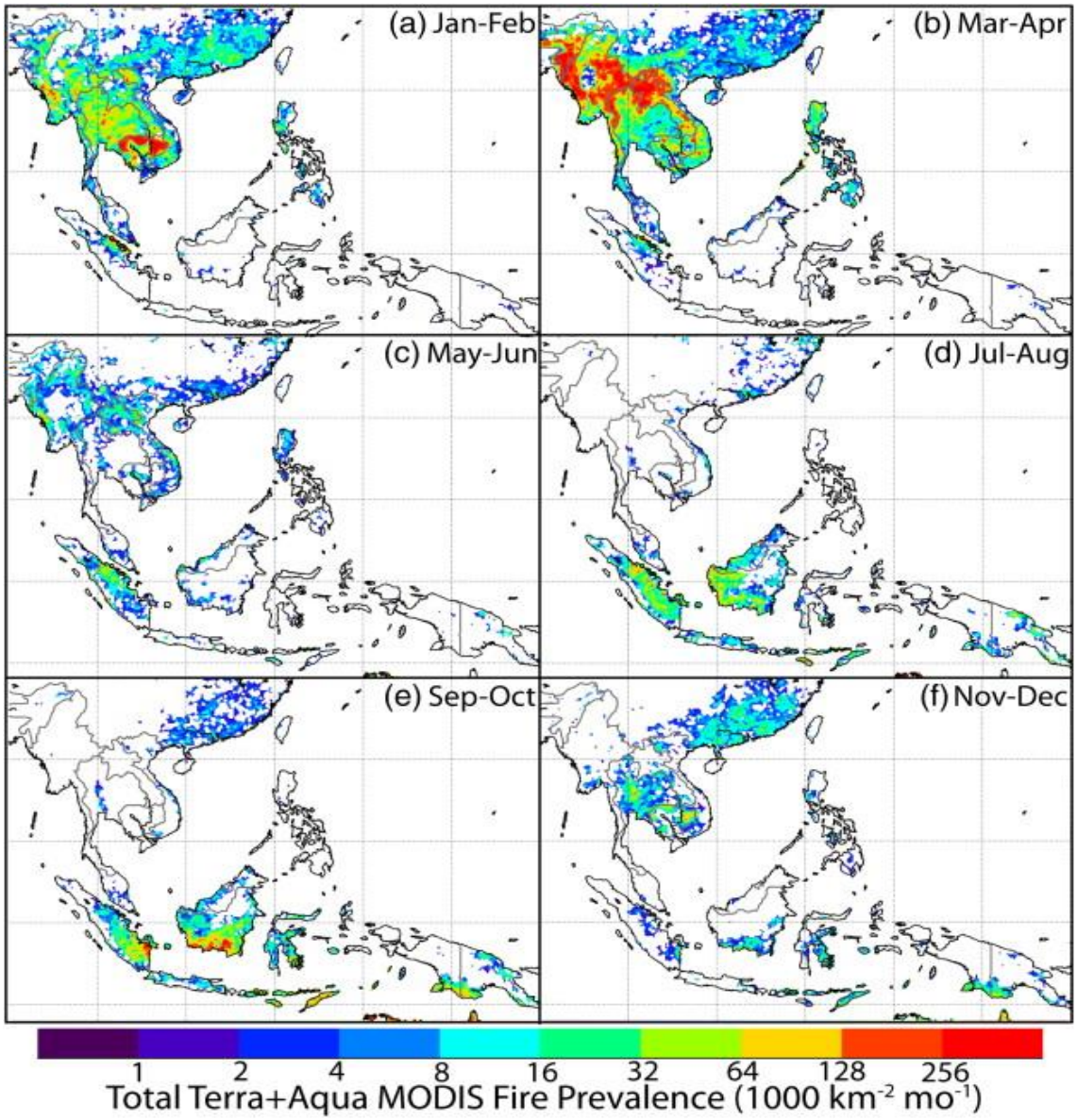

Fig. 2.3 (a)-(f) Bi-monthly MODIS fire prevalence for 2003-2009 based on Giglio et al. (2006) and Reid et al. (2012).

2.4 Effects of biomass burning emissions

Biomass burning releases large amounts of trace gases (e.g., carbon dioxide (CO_2), carbon monoxide (CO), and methane (CH_4)), which play a significant role in atmospheric composition and climate change. Not only the trace gases, the emissions also release great numbers of particle matters, which degrade visibility and affect both regional and global air quality, and then has strong impacts on human health and environmental pollution. Very recently great efforts have been made to estimate particle emissions from remote sensing data and biogeochemical model. The emissions are estimated by a number of assumptions, including burned area, fuel load, combustion factors, and emission factors (Crutzen and Andreae, 1990; Streets et al., 2003; Reid et al., 2005; Reid et al., 2009; van der Werf et al., 2010; Akagi et al., 2011). The currently available data source of Global Fire Emission Database v3 (GFED3) estimates the trace gases and aerosols emissions from biomass burning at a spatial resolution of 0.5 degree with monthly time step globally. Here, we presents the distributions of $PM_{2.5}$ emission properties from GFED3 (Fig. 2.4).

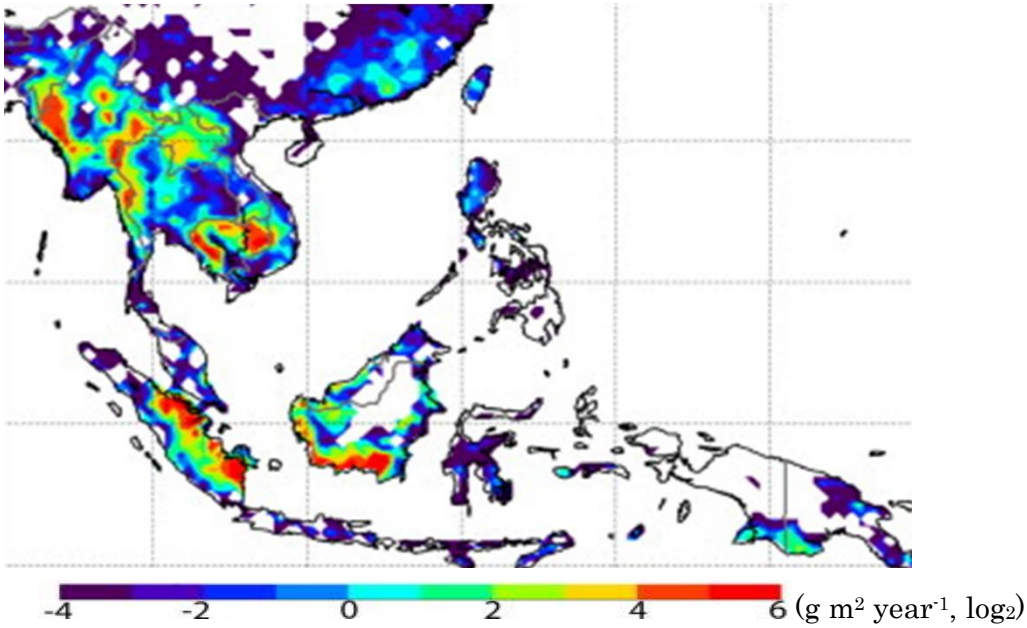

Fig. 2.4 $PM_{2.5}$ emission properties (2003-2009) from GFED3 in SEA.

In general, the spatial distribution of $PM_{2.5}$ emissions (Fig. 2.4) showed good correspondence with the MODIS fire prevalence (Fig. 2.3). $PM_{2.5}$ emissions product displayed high values in west Myanmar, north Thailand, Cambodia, south Sumatra

and south Kalimantan of Indonesia, respectively. While, in south China, small emissions can be observed. Extensive fire combusted great numbers of biomass, leading to high emissions of aerosols and haze in the air.

References:

Akagi, S.K., Yokelson, R.J., Weidinmyer, C., Alvarado, M.J., Reid, J.S., Karl, T., Crounse, J.D., Wennberg, P.O., 2011. Emission factors for open and domestic biomass burning for use in atmospheric models. Atmos. Chem. Phys., 11, 4039-4072.

Center for International Earth Science Information Network (CIESIN), 2004. Gridded Population of the World (GPW). Version 3 Columbia University, Palisades, NY. http://beta.sedac.ciesin.columbia.edu/gpw.

Chan, C.Y., Chan, L.Y., Harris, J.M., Oltmans, S.J., Blake, D.R., Qin, Y., Zheng, Y.G., Zheng, X.D., 2003. Characteristics of biomass burning emission sources, transport, and chemical speciation in enhanced springtime tropospheric ozone profile over Hong Kong. J. Geophys. Res., 108, D1, 4015.

Cochrane, M.A., 2003. Fire science for rainforests. Nature, 421, 913-919.

Crutzen, P.J., Andreae, M.O., 1990. Biomass burning in the tropics: impacts on atmospheric chemistry and biogeochemical cycles. Science, 250, 1669-1678.

Giglio, L., Csiszar, I., Justice, C.O., 2006. Global distribution and seasonality of active fires as observed with the Terra and Aqua MODIS sensors. J. Geophys. Res., 111, G02016. http://dx.doi.org/10.1029/2005JG000142.

Giglio, L., Descloitres, J., Justice, C.O., Kaufman, Y.J., 2003. An enhanced contextual fire detection algorithm for MODIS. Remote Sens. Environ., 87, 273-282.

Goldammer, J.G., 2006. History of equatorial vegetation fires and fire research in Southeast Asia before the 1997-98 episode: a reconstruction of creeping environmental changes. Mitig. Adapt. Strateg. Glob. Chang., 12, 13-32.

IPCC, 2007. Impacts, adaptation, and vulnerability. In: Parry, M.L., Canziani, O.F., Palutikof, J.P., van der Linden, P.J., Hanson, C.E. (Eds.), Climate Change 2007. Cambridge University Press, United Kingdom.

Justice, C.O., Giglio, L., Korontzi, S., Owens, J., Morisette, J.T., Roy, D., Descloitres, J., Alleaume, S., Petitcolin, F., Kaufman, Y.J., 2002. The MODIS fire products. Remote Sens. Environ., 83, 244-262.

Marlier, M.E., DeFries, R.S., Voulgarakis, A., Kinney, P.L., Randerson, J.T., Shindell, D.T., Chen, Y., Faluvegi, G., 2013. El Niño and health risks from landscape fire emissions in Southeast Asia. Nature Clim. Change, 3, 131-136.

Miettinen, J., Liew, S.C., 2009. Burn-scar patterns and their effect on regional burnt-area mapping in insular South-east Asia. Int. J. Wildland Fire, 18, 837-847.

Miettinen, J., Shi, C.H., Liew, S.C., 2011. Deforestation rates in insular Southeast Asia between 2000 and 2010. Glob. Chang. Biol., 17, 2261-2270.

Pochanart, P., Akimoto, H., Kajii, Y., Sukasem, P., 2003. Carbon monoxide, regional-scale transport, and biomass burning in tropical continental Southeast Asia: Observations in rural Thailand. J. Geophys. Res., 108, D17. DOI: 10.1029/2002JD003360.

Reid, J.S., Eck, T.F., Christopher, S.A., Koppmann, R., Dubovik, O., Eleuterio, D.P., Holben, B.N., Reid, E.A., Zhang, J., 2005. A review of biomass burning emissions part III: intensive optical properties of biomass burning particles. Atmos. Chem. Phys., 5, 827-849.

Reid, J., Hyer, E., Johnson, R., Holben, B., Yokelson, R., Zhang, J., Campbell, J., Christopher, S., Girolamo, L., Giglio, L., Holz, R., Kearney, C., Miettinen, J., Reid, E., Turk, F., Wang, J., Xian, P., Zhao, G., Balasubramanian, R., Chew, B., Janai, S., Lagrosas, N., Lestari, P., Lin, N., Mahmud, M., Nguyen, A., Norris, B., Oahn, N., Oo, M., Salinas, S., Welton, E., Liew, S., 2013. Observing and understanding the Southeast Asian aerosol system by remote sensing: An initial review and analysis for the Seven Southeast Asian Studies (7SEAS) program. Atmos. Res., 122, 403-468.

Reid, J.S., Hyer, E.J., Prins, E.M., Westphal, D.L., Zhang, J.L., Wang, J., Christopher, S.A., Curtis, C.A., Schmidt, C.C., Eleuterio, D.P., Richardson, K.A., Hoffman, J.P., 2009. Global monitoring and forecasting of biomass burning smoke: description and lessons from the Fire Locating and Modeling of Burning Emissions (FLAMBE) program. IEEE J. Sel. Top. Appl. Remote Sens., 2, 144-162.

Reid, J.S., Xian, P., Hyer, E.J., Flatau, M.K., Ramirez, E.M., Turk, F.J., Sampson, C.R., Zhang, C., Fukada, E.M., Maloney, E.D., 2012. Multi-scale meteorological conceptual analysis of observed active fire hotspot activity and smoke optical depth in the Maritime Continent. Atmos. Chem. Phys., 12, 2117-2147.

Reid, J.S.,Westphal, D.L., Livingston, J.M., Savoie, D.L., Maring,H.B., Jonsson,H.H., Eleuterio, D.P., Kinney, J.E., Reid, E.A., 2002. Dust vertical distribution in the Caribbean during the Puerto Rico Dust Experiment. Geophys. Res. Lett., 29(7), 1151. http://dx.doi.org/10.1029/2001GL014092.

Shi, Y., Sasai, T., Yamaguchi, Y., 2014. Spatio-temporal evaluation of carbon emissions from biomass burning in Southeast Asia during the period 2001-2010. Ecol. Model., 272, 98-115.

Streets, D.G., Yarber, K.F.,Woo, J.H., Carmichael, G.R., 2003. Biomass burning in Asia: annual and seasonal estimates and atmospheric emissions. Global Biogeochem. Cycles, 17, 1099. http://dx.doi.org/10.1029/2003 GB002040.

Tang, Y., Carmichael, G.R., Uno, I., Woo, J.H., Kurata, G., Lefer, B., Shetter, R.E., Huang, H., Anderson, B.E., Avery, M.A., Clarke, A.D., Blake, D.R., 2003. Impacts of aerosols and clouds on photolysis frequencies and photochemistry during TRACE-P: 2. Three-dimensional study using a regional chemical transport model. J. Geophys. Res., 108, 8822. http://dx.doi.org/10.1029/2002JD003100.

van der Werf, G.R., Randerson, J.T., Giglio, L., Collatz, G.J., Mu, M., Kasibhatla, P.S., Morton, D.C., DeFries, R.S., Jin, Y., van Leeuwen, T.T., 2010. Global fire emissions and the contribution of deforestation, savanna, forest, agricultural, and peat fires (1997-2009). Atmos. Chem. Phys., 10, 11707-11735.

Wang, S.H., Lin, N.H., Chou, M.D., Woo, J.H., 2007. Estimate of radiative forcing of Asian biomass-burning aerosols during the period of TRACE-P. J. Geophys. Res., 112, D10222. http://dx.doi.org/10.1029/2006JD007564.

Chapter 3

Spatio-temporal evaluation of carbon emissions from biomass burning in Southeast Asia during the period 2001-2010

Abstract: Carbon emissions (CE) from fire-induced biomass burning have a marked effect on interannual fluctuations in global atmospheric carbon dioxide concentrations. Biomass burning in Southeast Asia (SEA) is a dominant contributor towards these emissions, primarily through the effects of El Niño-induced droughts and deforestation. Nonetheless, our understanding of the spatiotemporal patterns and variability in fire CE of SEA is limited. In this study, fire CE in SEA were estimated at a spatial resolution of 5 km during 2001-2010 using the recently developed MODerate resolution Imaging Spectroradiometer (MODIS) burned area products and the Biosphere model integrating Eco-physiological And Mechanistic approaches using Satellite data (BEAMS) with fire CE embedded. Three series of burned area data from MCD64A1, MCD45A1 and Global Fire Emissions Database version 3 (GFED3) in SEA were employed to estimate fire CE. In general, the three burned area datasets showed consistent temporal variation from 2001 to 2010 with average annual burned areas measuring 68,104, 50,933 and 61,263 km^2 $year^{-1}$, respectively. Burned areas were predominantly concentrated in Myanmar, northern Thailand, eastern Cambodia, and northern Laos, with marked differences in Sumatra and Kalimantan of Indonesia where peatland is extensively distributed. Fire CE estimated in the three simulations (BEAMS/MCD64A1, BEAMS/ MCD45A1-Peat and BEAMS/GFED) exhibited similar spatial patterns with respect to burned area, with average annual fire CE of 232.6, 214.1 and 228.8 TgC, respectively, of which, in our current study the best result among the three

estimations was BEAMS/MCD45A1-Peat, which was close to that obtained by GFED3 with 210.7 TgC. Aerosol Optical Depth (AOD) values showed good consistency with both fire CE and Multivariate ENSO (El Niño Southern Oscillation) Index values during 2001 to 2010, likely because of the deep peat soil burning under the influence of the El Niño phenomenon and Indian Ocean Dipole pattern in combination with anthropogenic disturbance through deforestation for palm oil plantation production.

Key words: Burned area, fire carbon emissions, peatland, finer resolution, Southeast Asia

3.1 Introduction

Fires and biomass burning are important factors affecting ecosystem processes and dynamics and a major cause of disturbance and change in a wide range of biomes at regional and global scales (Carlson et al., 2012; Kasischke and Hoy, 2012). They can result in an instantaneous loss of carbon stored in large terrestrial pools (live vegetation, dead vegetation, litter, organic soil) and lead to the direct release of large quantities of carbon-containing greenhouse gases and aerosols into the atmosphere (van der Werf et al., 2003; Kasischke and Hoy, 2012). Although the duration of release is typically very short, the amounts of fire-induced biomass-burning emissions that are produced are very high. During the period of 1997-2004, biomass burning resulted in approximately 2.5 PgC $year^{-1}$ being emitted globally, and considerable inter- and intraannual variability was observed (van der Werf et al., 2006). During the period 2000-2010, fires associated with deforestation emitted approximately 1.0 PgC $year^{-1}$ worldwide (Baccini et al., 2012).

Of all global forests, the tropical rainforests in Southeast Asia (SEA) are currently being deforested at the highest rate worldwide (Langner and Siegert, 2009). Major drivers of deforestation are frequently linked to anthropogenic activities, such as slash-and-burn agriculture and shifting cultivation, logging of natural forests in

Northern SEA (NSEA), and the establishment of oil palm plantations and industrial timber estates in Equatorial SEA (ESEA) (Harris et al., 2012; Carlson et al., 2013). Most of these activities employ fire, which is one of the most important drivers of forest loss and subsequent carbon dioxide emissions (Page et al., 2002).

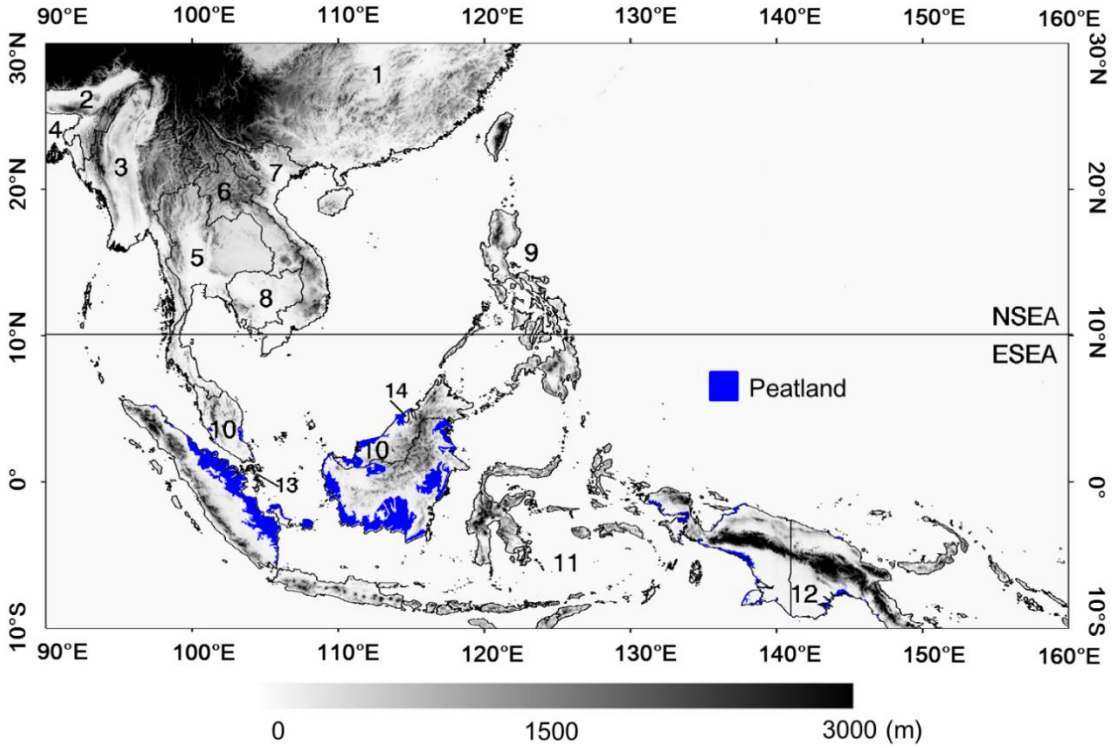

Fig. 3.1 Elevation of Southeast Asia (SEA),1-China; 2-India; 3-Myanmar; 4-Bangladesh; 5-Thailand; 6-Laos; 7-Vietnam; 8-Cambodia; 9-Philippines; 10-Malaysia; 11-Indonesia; 12-Papua New Guinea; 13-Singapore; 14-Brunei. SEA was divided into the Northern SEA (NSEA) and Equatorial SEA (ESEA). The spatial distribution of peat forest (blue area) in SEA was extracted from World Wildlife Fund terrestrial ecoregions map (1999-2000; Tosca et al., 2011).

The large areas burned in Laos, Cambodia, Thailand and Vietnam (Fig. 3.1) are usually attributed to slash-and-burn agricultural practices and land clearing activities, especially during dry weather conditions (Chang and Song, 2010). The extent of fires in NSEA is comparatively small (Field et al., 2009; Giglio et al., 2010; Randerson et al., 2012), compared to other large regions (e.g., the Amazon basin, Africa, Siberia and continental areas of Australia). In Indonesia, Malaysia and Papua New Guinea (Fig. 3.1), fires have received considerable attention for a variety

of reasons, particularly habitat loss associated with forest conversion (Miettinen et al., 2011), and the large amounts of carbon released by combustion of drained peatland (Page et al., 2002; van der Werf et al., 2010; Fenner and Freeman, 2011) (Fig. 3.1). These emissions vary markedly from year to year, resulting in interannual variability of atmospheric CO_2 and concentrations of trace gases (Langenfelds et al., 2002; van der Werf et al., 2004).

In addition, under the influence of the East Asia Monsoon, the NSEA region (Myanmar, Thailand, Laos, Cambodia, Vietnam, Philippines and southern China) experiences a warm, rainy summer monsoon season and a cold, dry winter monsoon season. The monsoon intensively affects rainfall variability and the changes of moisture conditions and hence the terrestrial productivity of ecosystems and the biosphere, which have a marked effect on the regional carbon cycles and stocks (Tian et al., 2003). While, the Australian-Indonesian Summer Monsoon mainly impacts the countries in ESEA with much rainfall during summer monsoon season; however, during drought season, the reduced rainfall and persisting drought across Indonesia usually lead to high possibility of fire occurrence, especially the less rainfall in eastern Indonesia (Griffiths et al., 2010). Nonetheless, El Niño-induced droughts do strike the SEA periodically, causing extensive interannual variability in fire activity through a coupling of El Niño and anthropogenic land-use changes which cause large-scale droughts and fire-induced biomass combustion. The 1997/98 El Niño event was the most severe and devastating such event in recent years; the total carbon emissions attributable to these fires were estimated at between 0.8 and 2.6 PgC (Page et al., 2002), which is equivalent to approximately 40% of global fossil fuel emissions during that time (van der Werf et al., 2008).

Several approaches for estimating emissions from fires have been developed over the last two decades (van der Werf et al., 2006; Chang and Song, 2010). At present, satellite data and integrated biogeochemical models have been used to estimate the spatial extent of burned areas and the biomass available for burning, respectively. By combining these methods, emissions from fire-induced biomass burning can be compared interannually on a continental or global scale (van der Werf et al., 2006).

The Global Fire Emissions Database version 3 (GFED3), currently the best source of global fire emissions data available (Field and Shen, 2008), was compiled using a MODerate resolution Imaging Spectroradiometer (MODIS) burned area product, other satellite data, and the Carnegie-Ames-Stanford Approach (CASA) biogeochemical model. GFED3 has been used to estimate the spatiotemporal variations in global fire-induced biomass burning emissions at monthly intervals from 1997 to the present (Field and Shen, 2008). However, GFED3 has a coarse spatial resolution of 0.5°. Since the majority of fires started by humans in SEA occur at the scale of small plots, fires at scales as large as 0.5° are rarely observed. Consequently, the data at a spatial resolution of 0.5° are not considered to be well suited to representing fire-induced biomass burning emissions at regional or continental scales. The combination of a varied topography and the nonlinearity inherent in ecophysiological processes can limit the ability of raster-based information to accurately capture or represent the spatiotemporal variations in fire occurrence and biomass burning in specific or small areas (Randerson et al., 2012). Such limitations routinely lead to misunderstandings of spatial observations in biomass burning emissions and their interactions with climate systems and carbon cycles. Consequently, in order to accurately estimate the carbon budgets of terrestrial ecosystems in SEA, detailed examinations of the spatiotemporal variations in biomass burning emissions from fires at fine level of resolution are urgently required.

Our primary objective was to quantitatively estimate the spatial variation and temporal dynamics of biomass burning emissions for the period 2001-2010 at a fine spatial resolution to increase our understanding of the contribution of fire-induced carbon emissions (CE) to the regional carbon cycle and budget. We used MODIS burned area products and an improved Biosphere model integrating Eco-physiological And Mechanistic approaches using Satellite data (BEAMS) with fire CE process embedded to estimate carbon stocks and fire CE at a spatial resolution of 5 km in SEA between 90° and 160° east, 30° north and 10° south (Fig. 3.1). In addition, by using different burned area products as model inputs, we also examined

the effects of varying burned area products on the fire CE across the entire SEA, both spatially and temporally, and evaluated the relationship between different burned areas and their corresponding fire CE.

3.2 Data and methods

3.2.1 Data

3.2.1.1 Climate and satellite-derived data

BEAMS requires ten temporally variable and four temporally fixed parameters as model inputs. The temporally variable parameters are solar radiation, fraction of absorbed photosynthetically active radiation (fPAR), leaf area index (LAI), precipitation, vapor pressure, air temperature, atmospheric CO_2 concentration, land surface temperature (LST), albedo, and wind speed. The temporally fixed parameters are plant function type, elevation, soil texture, and soil depth value. Table 3.1 lists the required input data in primary BEAMS model. All inputs were converted to a spatial resolution of 5 km × 5 km and a monthly temporal resolution according to the data preprocessing method of Sasai et al. (2011).

We employed MODIS products, the Global Precipitation Climatology Project (GPCP) data set, and a reanalyzed data set obtained from the National Center for Environmental Prediction and National Center for Atmospheric Research (NCEP/NCAR) for the nine time variable and four time-fixed model inputs (Table 3.1). First, the MODIS products were preprocessed by choosing pixels flagged with only the best quality control (QC) level (clear-sky conditions) to remove cloud contamination. Then, to fill in missing (cloud-contaminated) pixels using as much observed data as possible, we combined the 8 day composite Terra and Aqua/MODIS products. When both QC flags represented the best conditions, the average was used to represent the pixel. Moreover, we also converted from the 8 day to monthly composite data. Finally, pixels that were still missing were spatially interpolated, using the weighted Euclidean distance from surrounding pixels having the same land cover type as that of the missing pixels (Setoyama and Sasai, 2013). The land cover map was also mosaicked and resampled with the same approach. The original

Table 3.1 Input data used for the BEAMS simulation.

Parameter	Dataset name
LST	MOD11A2[a], MYD11A2[a]
fPAR, LAI	MOD15A2[b], MYD15A2[b]
Albedo	MOD43B3[c]
Incoming solar radiation	JAXA/MODIS Radiation product[d]
Air temperature	NCEP/NCAR re-analysis dataset[e]
Relative humidity	NCEP/NCAR re-analysis dataset
Wind speed	NCEP/NCAR re-analysis dataset
Precipitation	GPCP version 2.2 dataset[f]
Atmospheric CO_2 concentration	Observation in Mauna Loa[g]
Elevation	SRTM 30[h]
Soil texture	IGBP-DIS[i]
Soil depth	FAO soil texture groups
Land cover map	MOD12Q1[j]

a. Terra and Aqua/MODIS Land Surface Temperature/Emissivity 8-Day L3 Global 1 km (Wan et al., 2002); b. Terra and Aqua/MODIS Leaf Area Index/fPAR 8-Day L4 Global 1 km (Myneni et al., 1997, 2002); c. Terra/MODIS Albedo 16-Day L3 Global 1 km (Liang et al., 2002; Lucht and Lewis, 2000); d. Solar radiation provided by Japan Aerospace Exploration Agency (JAXA) (Frouin and Murakami, 2007); e. National Center for Environmental Prediction and National Center for Atmospheric Research (NCEP/NCAR) re-analysis dataset; f. Global Precipitation Climatology Project (GPCP) version 2.2 dataset (Huffman et al., 2009); g. Atmospheric CO_2 values (ppmv) derived from in situ air samples collected at Mauna Loa, Hawaii, USA provided by the CDIAC Web site (Keeling et al., 1995, 2009); h. Shuttle Radar Topography Mission (SRTM) 30 arc-seconds Digital Elevation Model (DEM) dataset (Farr et al., 2007); i. International Geosphere-Biosphere Programme (IGBP) - Data and Information System (DIS) soil dataset; j. MODIS Land Cover Type 96-Day L3 Global 1 km (Friedl et al., 2010).

data of air temperature, vapor pressure, wind speed, and precipitation have coarse spatial resolution (2.5 by 2.5 NCEP/NCAR grids and 1 by 1 GPCP grids), we converted them into 5 km grid resolution using the ordinary kriging interpolation method, assuming the data indicate the value at the central point of each pixel (Sasai et al., 2011). In addition, we corrected air temperature with altitude based on the moist adiabatic lapse rate (= 0.65°C/100 m) and the vapor pressure from the air temperature and elevation with an assumption-based hydrostatic equation under the polytropic atmosphere (Setoyama and Sasai, 2013). Besides, we assumed a global standard atmospheric CO_2 concentration equal to that measured at Hawaii's Mauna Loa Observatory.

3.2.1.2 Burned area data

Burned area data were derived from the MODIS 500-m direct broadcast burned area product (MCD64A1), which was used to estimate the entire area that was burned in SEA for the ten fire years from 2001-2010. MCD64A1 is a MODIS satellite-derived product that uses surface reflectance, daily active fire, and land cover products to delineate burned areas and burn cells are tagged with approximate burn data (Giglio et al., 2009). And MCD64A1 has a spatial resolution of 500 m and temporal resolution of a month, and the day of burning and a temporal uncertainty range of the burn date are noted for every pixel. MCD64A1 took peatland into consideration and estimated the burned area from human drained peatland into other kind of economic crops with large fires occurrence (Giglio et al., 2010). In addition, another burned area product - MODIS Collection 5 Moderate-Resolution Imaging Spectroradiometer (MCD45A1) - was also selected. MCD45A1 employs a change detection algorithm that based on a bidirectional reflectance distribution function model (Roy et al., 2005). And MCD45A1 has a spatiotemporal resolution of 500 m and one month, and records the approximate day of burning by locating instances of rapid change in daily surface reflectance time series data over an entire year. It should be noted that the large difference of algorithm between the MCD64A1 and MCD45A1 products is whether they use the active fire products as input data or not when interpreting burned area. MCD64A1 makes extensive use of active fire

observations in its algorithm, whereas MCD45A1 uses no active fire information. MCD64A1 and MCD45A1 were resampled from the original 500 m binary grid map into 5 km percentage grid map by counting the burned pixels in every 100 pixels. Moreover, GFED3 data provided a consistent estimate of the area burned globally on a monthly basis. Daily information consisting of a combination of surface reflectance and active fire detection data from several satellites was aggregated to produce monthly burned-area estimates at a resolution of 0.5° (Giglio et al., 2010). Of these data, fire occurrence and burned area were determined from cross-calibrated Along-Track Scanning Radiometer, Tropical Rainfall Measuring Mission, and MODIS hot spot counts data. To integrate the obtained monthly data with other types of input data, GFED3 burned area was resampled into 5 km grids with percentage by using the method of bilinear interpolation.

3.2.1.3 Peatland map

The spatial distribution of peat forest in SEA was derived from the 1999-2000 terrestrial ecoregions map published by the World Wildlife Fund (Fig. 3.1). An aggregate vegetation class was created by combining peat swamp (class numbers 40104, 40145 and 40160), freshwater swamp (class numbers 40153 and 40157), heath forest (class number 40161) and mangrove forest (class number 11401) ecoregions, as these ecoregions had similar peat soil surface layers and plant species. The aggregate vegetation class was primarily located in Peninsular Malaysia, southern Borneo, eastern Sumatra and Papua New Guinea. By using ArcGIS software to regrid the World Wildlife Fund vector data, a 5 km × 5 km spatial resolution raster peatland map was generated.

3.2.1.4 Aerosol Optical Depth

Aerosol Optical Depth (AOD) is the degree to which aerosols prevent the transmission of light in the atmosphere, which is a useful index of air cleanliness, and an indication of fire-induced biomass burning intensity. In SEA, forest fires are the main source of haze and aerosols, and burning peatland in Malaysia and Indonesia constitutes the most serious forest fires. Indeed, more than 90% of the transboundary haze in ESEA is linked to peatland fires (Tosca et al., 2011) and

numerous studies have shown that the haze in these regions was primarily attributable to smoldering peat fires in Sumatra and Kalimantan (Page et al., 2002; Marlier et al., 2013). In order to clarify the occurrence of peat fires and their effect on the entire SEA region, we used MODIS Collection 5.1 Level 3 monthly mean Aerosol Optical Depth at 550 nm from Terra MODIS (MOD08_M3, available at http://disc.sci.gsfc.nasa.gov/giovanni/overview/index.html) over ten years to define burned peatland and to illustrate the relationship between burned peatland and fire CE. The AOD data was resampled from a spatial resolution of 0.5° to 5 km at monthly intervals.

3.2.2 Methods

In order to quantitatively estimate the biomass burning emissions in the SEA, an improved terrestrial biosphere model with a fire CE process embedded was developed (Fig. 3.2). CE processes were embedded into the model as they are closely linked to, and strongly controlled by, soil moisture and biomass (van der Werf et al., 2003, 2006). We conducted three simulations of CE from fires by using different burned area products, constant available fuel loads, and variable combustion factors of each land cover with BEAMS model (Fig. 3.2). The first estimation used the MCD64A1 burned area product coupled with available fuel loads from BEAMS model and combustion factors from Andreae and Merlet (2001), the resulting fire CE data were abbreviated as BEAMS/MCD64A1. Since the limitations of the MCD45A1 burned area product in detecting the burned area of peatland were demonstrated previously by Giglio et al. (2010), we considered the peatland burned area, i.e. areas with monthly AOD > 0.85 (Eck et al., 2009; Vadrevu et al., 2012) and land surface temperatures exceeding 28ºC (Justice et al., 2002; Giglio et al., 2006, 2009; Vadrevu et al., 2012), into the analysis. The second estimation of fire CE (BEAMS/MCD45A1-Peat) consisted of two parts: MCD45A1-based CE and peatland CE. In the third estimation, GFED3 burned area data was applied to the BEAMS model to examine the effects of different fuel loads on fire CE, and the burned area data was resampled from 0.5° into 5 km for consistency (BEAMS/GFED). Finally, we compared the extent to which the spatiotemporal characteristics of the fire CE obtained with the three

models corroborated the fire CE contained within the GFED3.

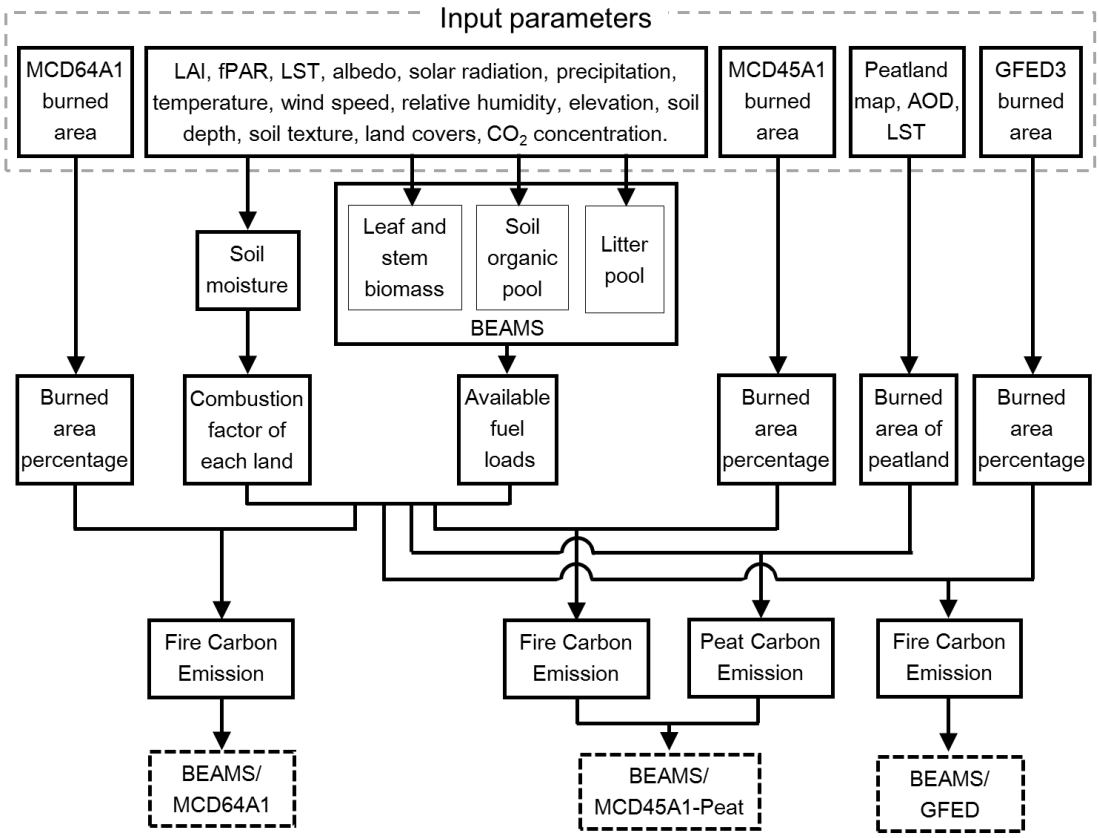

Fig. 3.2 Flow chart of the fire-induced biomass burning carbon emission process in BEAMS.

3.2.2.1 BEAMS model with fire CE embedded

SEA biomass was estimated based on the physical process-based diagnostic model BEAMS (Sasai et al., 2005, 2007, 2011, 2012), which simulates monthly carbon, energy, and water fluxes based on satellite observations and climate data. The model consists of heat, water, and carbon submodels. The heat submodel has four heat processes: net radiation and latent, sensible, and ground heat fluxes. Similarly, the water submodel has four water pools and eight water processes comprising canopy-intercepted precipitation and evaporation, ground surface evaporation, transpiration, snowmelt, percolation, run-off, and base flow. The carbon submodel has three vegetation, four litter, and five soil carbon pools, and six carbon processes comprising gross primary production (GPP), autotrophic respiration (Ra), allocation, litter fall (LF), soil decomposition, and carbon leaching.

$$\frac{dCbio(t)}{dt} = GPP(t) - Ra(t) - LF(t) - CE(t), \quad (1)$$

Here, we added another carbon flux process, which we referred to as fire Carbon Emission (CE). And dCbio/dt was the monthly change of biomass. In BEAMS, biomass consists of three parts: leaf biomass, stem biomass and root biomass. The GPP of BEAMS was calculated by introducing an environmental stress factor, which is a function of the three parameters of temperature, relative humidity, and soil water content, which we used to calculate the actual light use efficiency more accurately. The Ra of leaves, stems, and roots consists of maintenance respiration, which is proportional to biomass and it is temperature dependent, and growth respiration, which is proportional to the potential net primary productivity. Leaf LF is calculated from leaf biomass of the previous and the current month; while LF from stems and roots is assumed to be proportional to stem and root biomass, respectively. The water submodel has four water pools and eight water processes comprising canopy-intercepted precipitation and evaporation, ground surface evaporation, transpiration, snowmelt, percolation, run-off, and base flow. The water pools consist of a surface snowpack pool, and two layers at depths of 0-500 mm and >500 mm, defined for each soil type.

3.2.2.2 Fire CE

Fire-induced CE from biomass burning are commonly calculated as the product of burned area, available fuel loads, and a combustion factor, integrated over the time and space scales of interest (Seiler and Crutzen, 1980), which can be represented as follows:

$$CE = \sum_{i=1}^{11} B \times F \times CF, \quad (2)$$

where, B denotes an important parameter of burned area (m^2); F is the available fuel loads, in this study, it represents biomass density and mainly consists of aboveground (leaf and stem) biomass and belowground (root) biomass, surface litter carbon and soil organic carbon ($gC\ m^{-2}$); CF represents the fraction of available fuels exposed to fires that are actually burned during combustion (-); and i means land cover types.

Burned areas were derived from MODIS and GFED3 burned area products, which provided the monthly information of burned area location by locating the occurrence of rapid changes in daily surface reflectance time series data during the whole year. For each grid cell in each month, fuel loads were calculated based on the available fuel loads of the previous month, inputs from GPP and losses due to autotrophic respiration, soil respiration and fire. In the BEAMS model, the respiration (Ra) of leaves, stems, and roots consists of maintenance respiration (Ram) and growth respiration (Rag); Ram is proportional to biomass and it is temperature dependent (Heinsch et al., 2003), and Ram is proportional to the potential net primary productivity (= GPP - Ram), both of which can be represented as follows:

$$Ram_{leaf,stem,root} = kr_{leaf,stem,root} \times Cbio_{leaf,stem,root} \times Q10_{function}, \quad (3)$$

$$Rag_{leaf,stem,root} = fr_g \times \left(GPP_{leaf,stem,root} - Ram_{leaf,stem,root}\right), \quad (4)$$

where $kr_{leaf,stem,root}$ is the specific respiration rate of leaves, stems and roots (Heinsch et al., 2003), and $Cbio_{leaf,stem,root}$ is the carbon mass of leaves, stems and roots. Only $Cbio_{leaf}$ is calculated using LAI and specific leaf area defined for each Plant Function Type (PFT) (Heinsch et al., 2003). The $Q10_{function}$ indicates the relationship between temperature and Ram (=2.0). fr_g is a fraction of growth respiration in the potential net primary productivity (=0.25).

The LF of stems and roots ($LF_{stem,root}$) are considered to be proportional to stem and root biomass, respectively. Leaf LF (LF_{leaf}) can be determined based on the $Cbio_{leaf}$ of the previous and current months. Each litter fall can be calculated as:

$$LF_{stem,root} = kl_{stem,root} \times Cbio_{stem,root}, \quad (5)$$

$$LF_{leaf} = NPP_{leaf} - \left(Cbio_{leaf}(t) - Cbio_{leaf}(t-1)\right), \quad (6)$$

where kl_{stem}, kl_{root} are the specific litter fall rate of stems and roots, respectively. LF is divided into structural and metabolic plant material based on the ratio of lignin to nitrogen, which is defined as a constant for each PFT. LF_{leaf} and LF_{stem} represent metabolic and structural surface litter, respectively, and LF_{root} refers to metabolic

and structural root litter following Parton et al. (1993).

Combustion factor (CF) was defined as the ratio of fuel consumption to the total fuel available. The CF of fine fuels is usually high, up to 1, for dry and inflammable surface litter and twigs, while for coarse fuels, such as stems and woody debris, CF is relatively low as it burns less completely. In BEAMS, we allowed the CF to vary among different fuel types (leaves and stems of the aboveground layer, roots and soil organic matter of the underground layer) in areas of different land cover (forest, grassland, cropland, etc.) in successive months (van der Werf et al., 2006).

Table 3.2 Minimum and maximum combustion factors for fuel types in different types of land cover.

Land cover type	Combustion factor (%)			
	Above ground		Below ground	
	Min.	Max.	Min.	Max.
Broadleaf evergreen forest	20.0	30.0	3.0	90.0
Coniferous evergreen forest	20.0	30.0	3.0	90.0
Mixed forest and woodland	17.0	26.0	3.0	90.0
Boreal forest and woodland	12.0	16.0	3.0	90.0
Shrubs and bare ground	98.0	98.0	50.0	80.0
Wooded grassland	40.0	40.0	60.0	90.0
Grassland	80.0	100.0	20.0	80.0
Cropland	50.0	90.0	40.0	80.0

Source: Andreae and Merlet (2001).

Each fuel type in an area of different land cover has minimum (CF_{min}) and maximum (CF_{max}) values for above- and belowground biomass (Table 3.2), and the actual monthly CF value for each land type was estimated using soil moisture conditions (relative soil moisture) to linearly scale between these values. To consider the effect of moisture content of the aboveground live biomass (leaf, stem), CF was scaled linearly with a BEAMS GPP moisture scalar (w_scalar) as follows:

$$CF_{leaf,stem} = CF_{max} - (CF_{max} - CF_{min}) \times w\_scalar, \quad (7)$$

$$CF_{root} = CF_{max} - (CF_{max} - CF_{min}) \times soil\_moisture, \quad (8)$$

where $CF_{leaf,stem}$ are CF of leaves and stems, and CF_{root} is the CF of roots.

Soil water content (W_1, W_2) can be calculated using the equation below. Only field capacity and wilting point limit the maximum and minimum soil water content, and each can be defined for different soil properties (Saxton et al., 1986) as follows:

$$\frac{dW_1(t)}{dt} = PPT(t) - \beta_1 \times EET(t) - Perc(t) - runoff_1, \quad (9)$$

$$\frac{dW_2(t)}{dt} = Perc(t) - \beta_2 \times EET(t) - runoff_2, \quad (10)$$

where β_1 and β_2 are derived from the soil water content and a root fraction for each soil layer ($\beta_1 + \beta_2 = 1.0$), *Perc* is the percolation determined from the empirical equation based on Darcy's law, and PPT is water flux into the soil, including snowmelt. The estimated evapotranspiration (EET) is based on the bulk method.

Most of the burned area in tropical Asia occurred in areas that had been deforested for agricultural cropland, followed by forest, grassland, and then shrubland (Chang and Song, 2010; Carlson et al., 2013). The large areas of burned cropland can be attributed to numerous fire related slash-and-burn agricultural practices and land clearing in NSEA (Chang and Song, 2010). However, in ESEA, especially in Sumatra and Kalimantan, a large fraction of fire emissions comes from the combustion of soil organic matter in drained peatland (Carlson et al., 2012). Recent research in Indonesia has also highlighted the importance of peatland as the main source of CE in tropical regions of SEA (Carlson et al., 2012). In Indonesia, peat clearing for oil palm plantations goes on practically all year, particularly during the dry season of Aug-Oct in drought years when there is relatively little rainfall. These peatland fires tend to burn continuously for months, particularly in drought years, and large quantities of carbon released into the atmosphere (Page et al., 2002). Recent studies have proposed that the combustion of belowground biomass may be an important source of emissions in tropical regions (Page et al., 2002). Indeed, large

fires that burn for a long time can penetrate the soil to a depth of 30 cm (van der Werf et al., 2006), and can burn even deeper according to Page et al. (2002). However, since relatively little information currently exists on the depth or thickness of burning in SEA, quantifying the emissions resulting from the combustion of soil organic matter of peatland is difficult.

We based burning depths in peatland on the values measured by Batjes (1999) and empirical data of Kasischke et al. (2005) and van der Werf et al. (2006). For BEAMS, we assumed that only the carbon stored in the upper soil layers (represented by the surface litter pool and active soil pool) could burn. Since burning depths vary greatly from place to place and burning is strongly controlled by the relative soil water content, the maximum depth that a fire could penetrate into the organic soil layer of peat was set to 30 cm (van der Werf et al., 2006), even though fires have been reported to penetrate deeper into the soil in some regions (Page et al., 2002). Then, burning depth was assumed to be a linear function of soil moisture scalar; only when the soil water content was sufficiently low would the fire burn to the maximum depth discussed above (van der Werf et al., 2006). In addition, in BEAMS, we assumed that fires in the peatland areas of tropical SEA always burn a minimum of 50% of the soil carbon pools; soil water content determines how much of the remaining 50% of the soil organic matter can be burned (van der Werf et al., 2006). In addition, although some studies have shown that soil carbon density increases gradually with depth (Hooijer et al., 2010), we assumed that soil carbon density changed little with depth.

3.2.3 Calibration

Before conducting any simulations, all carbon and water pools in the model were initialized assuming that the carbon and water cycles in the initial year 2001 were in equilibrium. We performed spin-up for 4000 years so that carbon release matched inputs and reached a steady state, which means that the sum of autotrophic respiration, soil decomposition and fire CE were equal to GPP. Hydrologically, at steady state, precipitation is equal to evapotranspiration plus runoff. Based on the equilibrium status, we ran model simulations from 2001 to 2010. The BEAMS

estimated biomass was a slightly smaller than the results of Saatchi et al. (2011). We then calibrated our carbon submodel for calculating $Ram_{leaf,stem,root}$ by optimizing parameters $kr_{leaf,stem,root}$ for the respiration rates of leaves, stems and roots using above- and belowground biomass from Saatchi et al. (2011). In addition, several small modifications were also made to the litter fall rates of stems and roots so that they would more accurately reflect plant activities in tropical SEA. In addition, forest stand age is a key parameter, which has a large impact on the carbon storage. We adjusted the standing age of each forest type according to some published data (Wang et al., 2011) and statistics depending on the age of trees (from 40 to 150 years) which ranged from very old in some areas of primary forest to relatively young in the artificial forests and plantations of anthropogenically disturbed regions.

3.3 Results and discussion

3.3.1 The comparison among burned area data

Burned area is usually considered to be the potentially variable factor in fire CE estimations, especially at large spatial scales. Fig. 3.3 shows the burned areas derived from MCD64A1, MCD45A1 and GFED3 burned area products over the ten fire years from 2001 to 2010. The average percentage of the burned areas generated by MCD64A1 and MCD45A1 were consistent across SEA, with the burned areas in Myanmar, northern Thailand, eastern Cambodia, and northern Laos being most apparent in NSEA. While generally consistent, several differences between MCD64A1 and MCD45A1 were also observed in ESEA. Specifically, MCD64A1 showed significantly more extensive burning in Sumatra and Kalimantan of Indonesia than MCD45A1, even though the extent was relatively small. Briefly, average annual burned areas determined by MCD64A1, MCD45A1 and GFED3 for the period of 2001-2010 in SEA were 68,104, 50,933, and 61,263 km^2 $year^{-1}$, respectively. The burned area estimated by GFED3 was between that observed by the two MODIS products, higher than MCD45A1 and lower than MCD64A1. The largest difference between the two MODIS products were observed in the Indonesia of ESEA (Fig. 3.3a, b), with MCD45A1 underestimating the extent of the burned area

compared to MCD64A1.

(a)

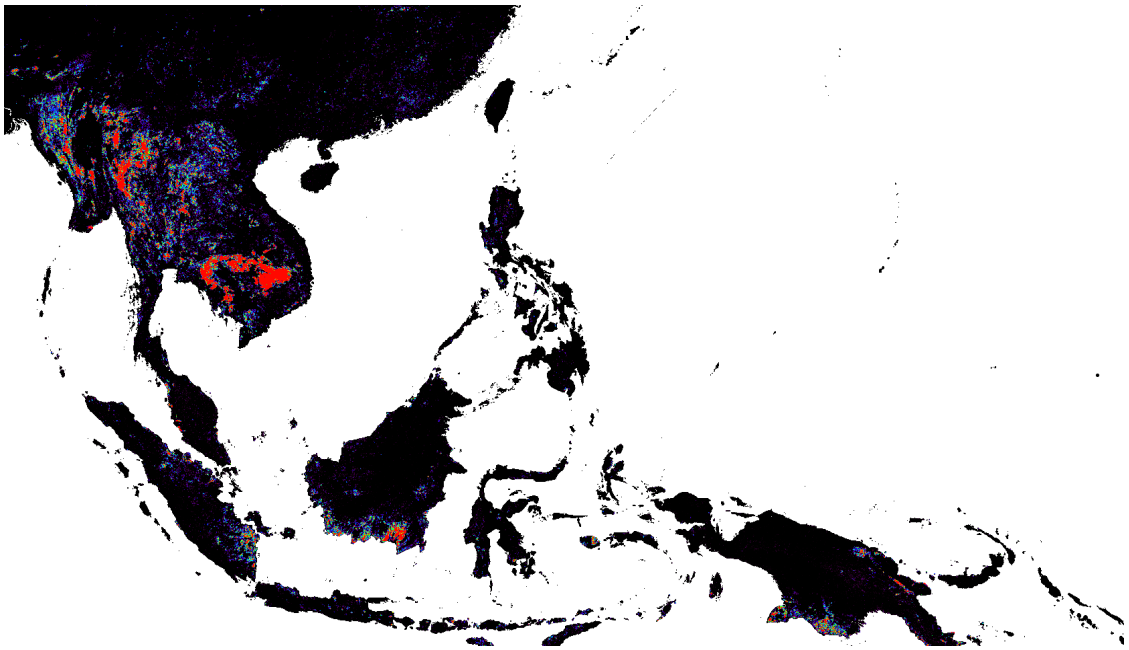

(b)

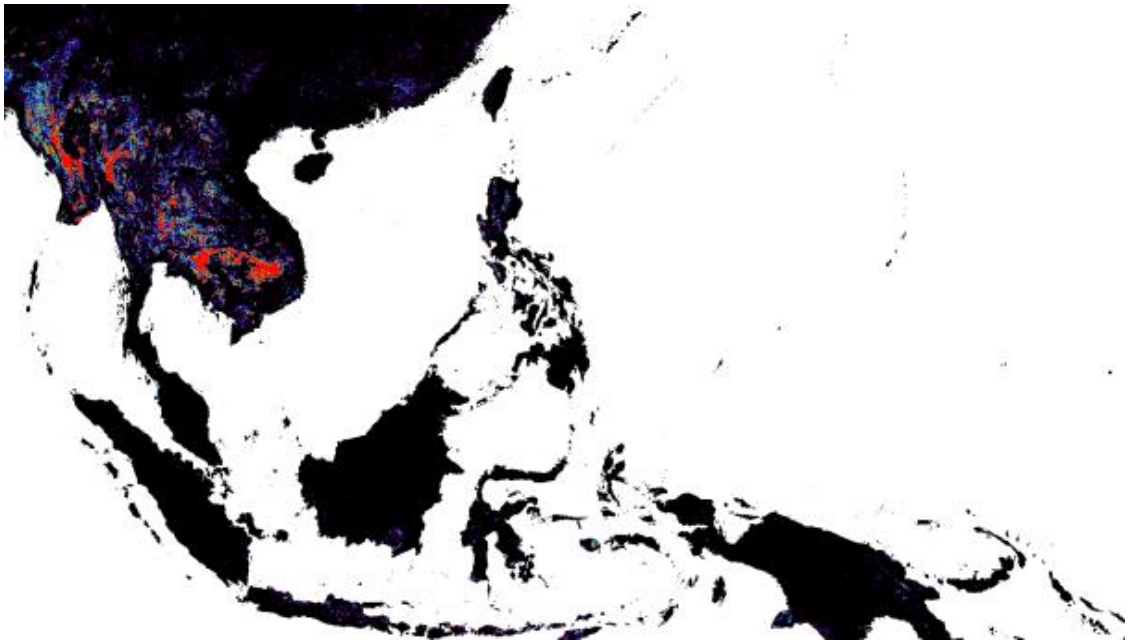

(c)

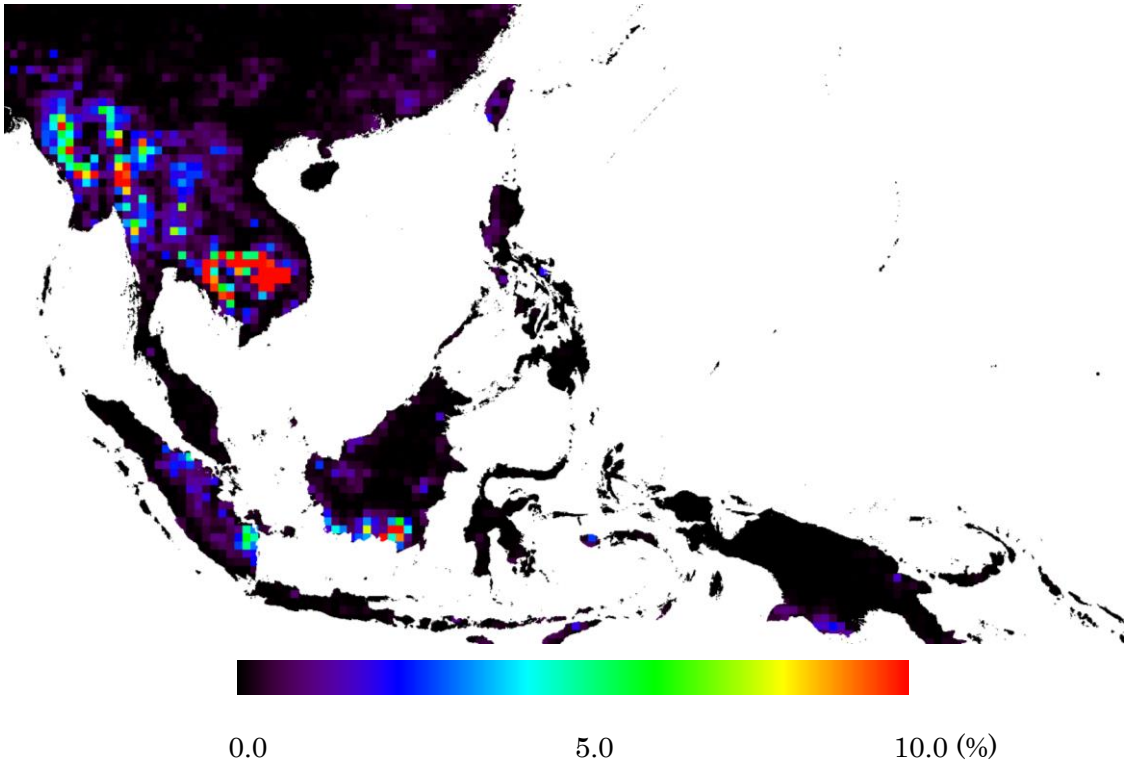

(d)

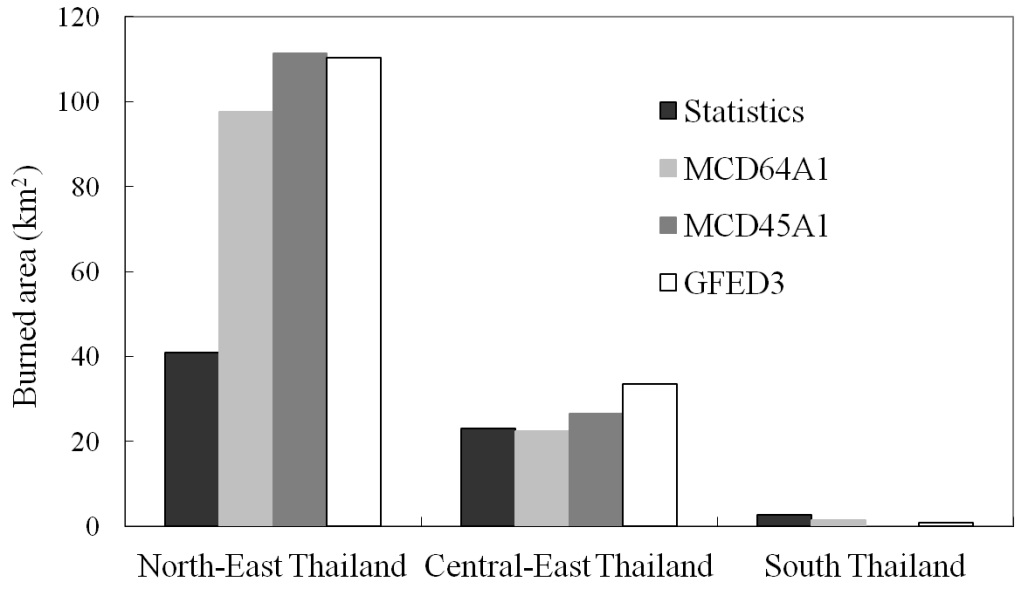

Fig. 3.3 Percentage of burned area from (a) MCD64A1 with 5 km grid, (b) MCD45A1 with 5 km grid and (c) GFED3 with a 0.5° grid. (d) Comparison of burned area estimated from statistics, MCD64A1, MCD45A1 and GFED3 in Thailand during the period of October 2007 - June 2008. Statistics data were collected from Forest Fire Control

Division (FFCD), Thailand, available at: http://www.dnp.go.th/ForestFire/Eng/fire%20 statistic.htm.

Fig. 3.3c shows the average annual percentage of the burned area estimated by GFED3, which was more consistent with MCD64A1 than with MCD45A1, primarily because the primary source of the burned area information for GFED3 was MCD64A1. Overall, the considerable size of the burned area in NSEA can be attributed to numerous fire-related slash-and-burn agricultural and land clearing practices, while in ESEA, peat combustion, especially in Malaysia and Indonesia, accounts for a large proportion of the burned area, especially during El Niño periods (Page et al., 2002; Field et al., 2009). The large differences in the extent of the burned areas identified by MCD64A1 and MCD45A1 were most apparent in ESEA (Fig. 3.3), with MCD45A1 missing a large number of forest fires. In addition to the different algorithms and ancillary data of MCD64A1, the main reason for the inability of MCD45A1 to detect burned areas is considered to be due to the unique characteristics of the peatlands in Malaysia and Indonesia. Fires in such areas (i.e. drained peat fires) usually occur during severe droughts and are associated with considerable amounts of smoke and haze, and very high CE. Haze and smoke are now prevalent in Sumatra and Kalimantan every year, both of which are pushed far into Peninsular Malaysia (Marlier et al., 2013). Extensive haze and smoke decrease visibility and adversely affect the image quality of remote sensors; for example, the ability of MCD45A1 to detect burned areas is markedly decreased when there is dense haze and smoke. In additions, the inability in detecting burned area in ESEA was likely due to the presence of persistent cloud cover during the burning season, which led to insufficient cloud-free data to obtain the data required by burned area algorithms (Roy et al., 2008; Chang and Song, 2010). However, because MCD64A1 uses an active fire-based burned area mapping algorithm it is somewhat more tolerant of cloud and aerosol contamination since such noise is often more likely to be encountered in a direct broadcast data stream. Moreover, comparing the MCD64A1 direct broadcast burned area mapping algorithm with the bi-directional reflectance modeling approach MCD45A1, reveals several important differences.

According to Giglio et al. (2010), such differences include: 1) The MCD64A1 direct broadcast algorithm makes extensive use of active fire observations, whereas the MCD45A1 algorithm uses no active fire information. 2) The MCD64A1 direct broadcast algorithm relies primarily on changes in the vegetation index to identify burns, whereas the MCD45A1 algorithm relies primarily on changes in reflectance.

To validate the robustness of results from MODIS and GFED3, burned area products were compared against statistical test data from Thailand (Fig. 3.3d). Generally, the three satellite-based dataset were comparable to statistical data even though some differences. In central-eastern Thailand and southern Thailand, MCD64A1, MCD45A1, GFED3 and statistical data were almost identical. However, in northeastern Thailand, large difference existed among the three burned areas and statistics. Results showed that the extent of burned areas from MCD64A1, MCD45A1 and GFED3 were 1.2, 1.7 and 1.6 times greater than that shown by the statistical data. This was mainly attributable to the spatial resolution of satellite data, which usually results in overestimation of burned area due to the small fires. As MODIS burned area product has a spatial resolution of 500 m, when small fire happens (less than 500 m × 500 m), the whole pixel will be assigned to be burned, which means the pixel is usually misclassified into the completely burned one. Therefore, in other words, the satellite data usually provides overestimation to some degrees compared with the statistical or ground observation data. In total, compared to the statistical data, MCD64A1 was generally much closer than MCD45A1 and GFED3, showing that MCD64A1 had higher accuracy in this area. But actually the largest difference among MCD64A1, MCD45A1 and GFED3 was the burned peatland in Sumatra and Kalimantan of Indonesia, however, due to the data unavailability of ground observation or statistical data in Indonesia (van der Werf, et al., 2006), we have difficulties in validating the burned area in this region. The correlation coefficient among the three burned areas showed that totally MCD64A1 and GFED3 had highest correlation (R^2=0.90; $p>0.05$). The burned areas in Myanmar, Thailand and Malaysia statistically presented significant difference among MCD64A1, MCD45A1 and GFED3. However, our improved MCD45A1 with

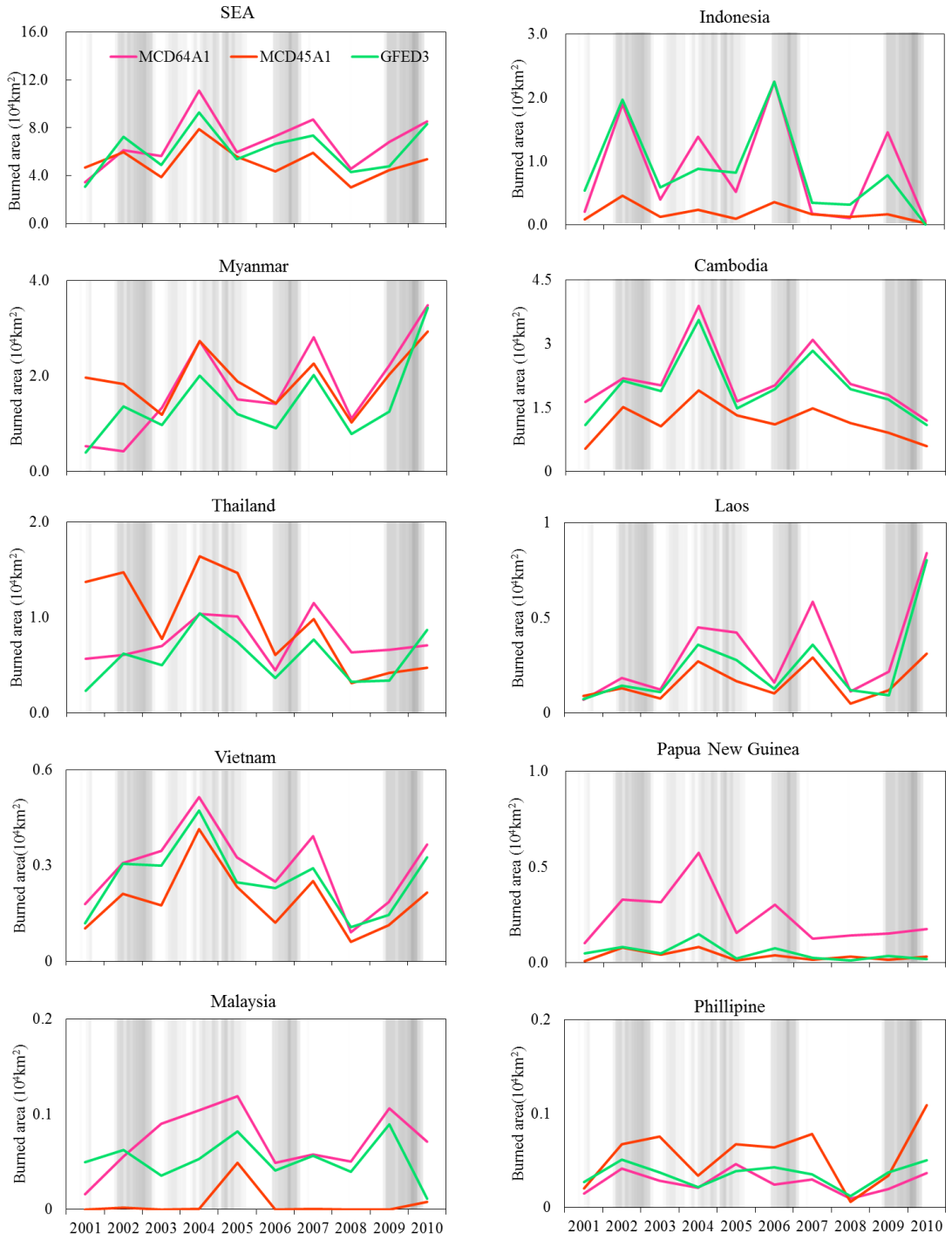

Fig. 3.4 Interannual variations in burned area estimated by MCD64A1, MCD45A1 and GFED3 in SEA and each country during 2001-2010. A Multivariate ENSO Index (MEI) is shown in grey scale, with darker shades indicating higher MEI values (MEI, http://www.esrl.noaa.gov/psd/enso/mei/mei.html).

burned peatland in Indonesia showed closer correlation (R^2=0.79; $p<0.01$) with GFED3 compared with MCD64A1 (R^2=0.62; $p>0.05$) (Table 3.3).

Meanwhile, data from all three datasets showed that temporal variations in burned areas were consistent from 2001 to 2010 with peaks in 2004 (Fig. 3.4). However, we also found that relatively large differences existed between MCD64A1 and MCD45A1 in 2004, 2006, 2007 and 2010, when MCD45A1 considerably underestimated the burned area in comparison with MCD64A1. Although GFED3 burned area data was mainly based on MCD64A1, the obtained values were slightly less than those obtained from MCD64A1 but greater than those obtained from MCD45A1 in SEA. Still, we noticed that MCD45A1 burned area recorded fewer burned area compared with MCD64A1 and GFED3 in most countries with exceptions in Thailand before 2006 and Philippine. The large difference among the three burned area were observed in Indonesia, Thailand and Cambodia. And our improved MCD45A1-Peat in Indonesia noted 1.1×10^4 km^2 burned area, larger than the primary 0.2×10^4 km^2.

3.3.2 Spatial characteristics of fuel load and consumption

Biomass carbon stocks in SEA were estimated using an improved BEAMS with fire CE embedded. The biomass data estimated using BEAMS was plotted against the data of Saatchi et al. (2011) (Fig. 3.5), which employed data from multiple satellites as well as thousands of ground plots to estimate the carbon stored above and below ground and to map the spatial variations of biomass across three tropical continents. In general, our biomass estimates showed a high degree of consistency with the study of Saatchi et al. (2011) across the entire SEA (R^2 = 0.88). The distribution of biomass was highly heterogeneous in SEA, with stored carbon ranging from 80 gC m^{-2} to 24,901 gC m^{-2} (mean: 9,120 gC m^{-2}) and the total biomass carbon was 68.1 PgC. In Saatchi et al. (2011), biomass carbon ranged from 500 gC m^{-2} to 25,000 gC m^{-2} (mean: 10,828 gC m^{-2}) and total biomass carbon was 82.8 PgC; however, their data also showed uncertainties ranging from 25% to 50%.

Both studies presented a broadly consistent spatial distribution data, with only subtle discrepancies in some areas of the NSEA, where BEAMS underestimated

(a)

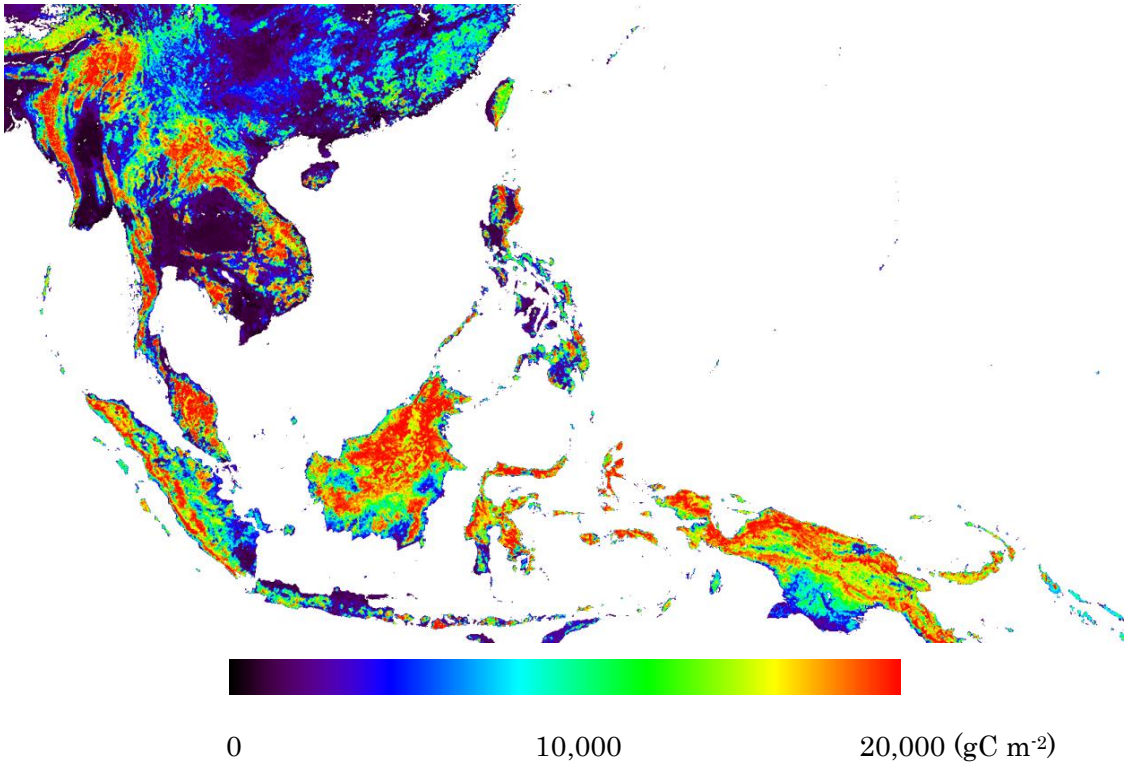

(b)

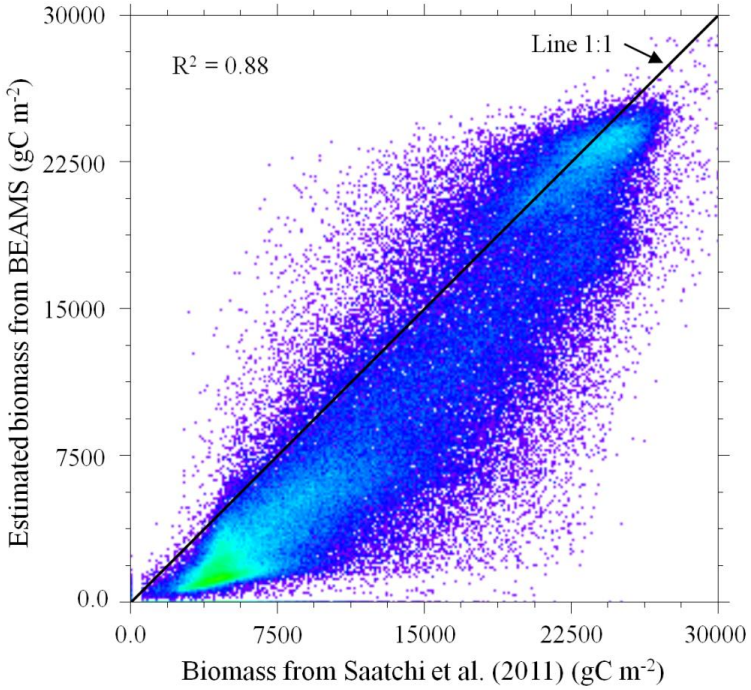

Fig. 3.5 (a) Spatial variation in biomass carbon distribution in SEA estimated from BEAMS in 2001 (Unit: gC m^{-2}). (b) Scatter plots of BEAMS predicted biomass carbon

data using estimates from Saatchi et al. (2011). Data are based on georeferenced *in situ* forest measurements and remote sensing metrics for Asia around 2000 (Unit: gC m^{-2}), Y = 0.87 X – 140.1 (R^2 = 0.88).

the biomass carbon in South China, Cambodia and eastern Thailand. SEA has a complex topography, which affects the geographical extent of carbon stocks (Fig. 3.5). Examination of the high resolution (5 km) biomass map clearly showed the spatial variations and differences in carbon stocks, particularly in steep mountainous areas with their marked differences in elevation (e.g., southwestern Sumatra and central Papua). Generally, biomass tended to decrease away from the equator, with ESEA having an extraordinarily higher carbon storage capacity than the NSEA. Regionally, Malaysia, Indonesia and Papua New Guinea store vast amounts of organic carbon, while areas such as southern China in NSEA have extensive areas of land with considerably less stored carbon. However, some exceptions (i.e. areas of low carbon storage) can also be found in Vietnam, eastern Myanmar, northern Laos and eastern Thailand. We also found that carbon stocks typically increased with elevation, primarily because tropical forests with their high carbon storage capacities are typically at higher altitudes than the flatter, lower-lying areas that have been converted to cropland and which have relatively low carbon storage capacities.

3.3.3 Spatiotemporal characteristics of fire CE

Average annual fire CE in SEA over the ten-year period were quantified by using different burned area products embedded in BEAMS at a resolution of 5 km (Fig. 3.6). Generally, fire CE could be observed throughout SEA. With the exception of several minor disparities, fire CE estimated by BEAMS/MCD64A1, BEAMS/ MCD45A1-Peat, and BEAMS/GFED all had similar spatiotemporal characteristics. Moderate differences were observed in NSEA where large amounts of carbon from fires were emitted from eastern and western Myanmar, northern Thailand, eastern Cambodia, and northern Laos. In ESEA, fire CE were high in Malaysia and Indonesia, and relatively low in Papua New Guinea. The distribution of fire CE throughout the ESEA corresponded closely with peatland distribution in SEA (Fig. 3.1). Of the differences that were observed among the three estimations,

BEAMS/GFED indicated that fire CE were the highest in eastern Cambodia and Kalimantan in Indonesia. SEA fires were primarily caused by humans starting small fires, which produced fire scars with a speckled pattern. The fire CE from MODIS burned area products with fine spatial resolutions were more effective at capturing the effects of small fires in certain plots. For example, the fire CE of GFED3, which

(a)

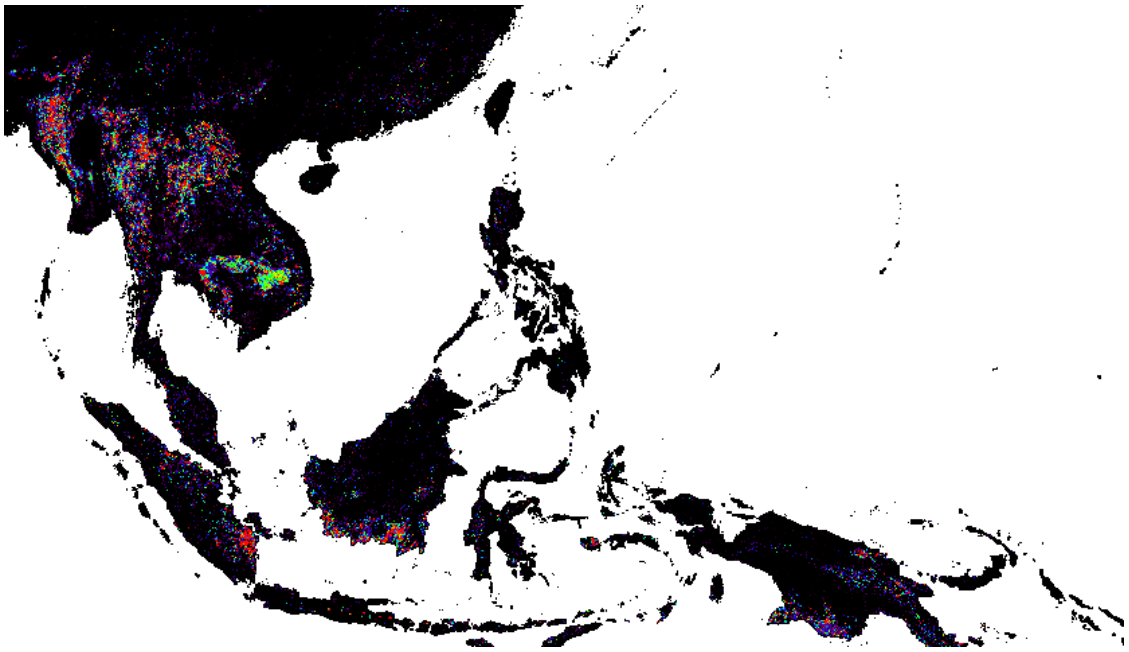

(b)

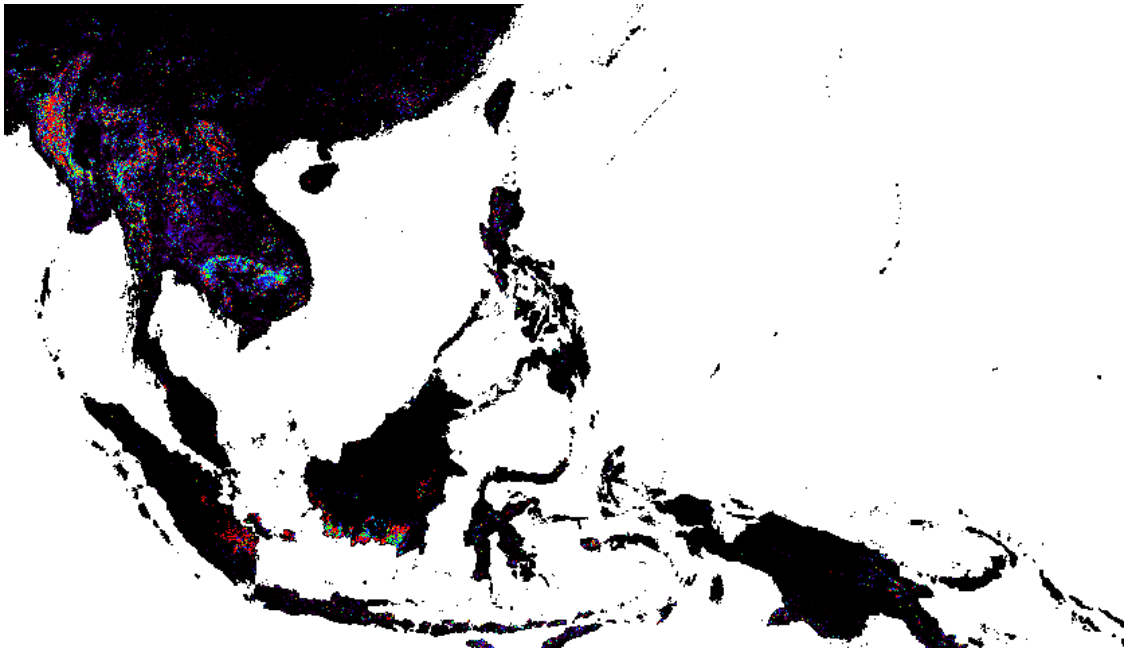

(c)

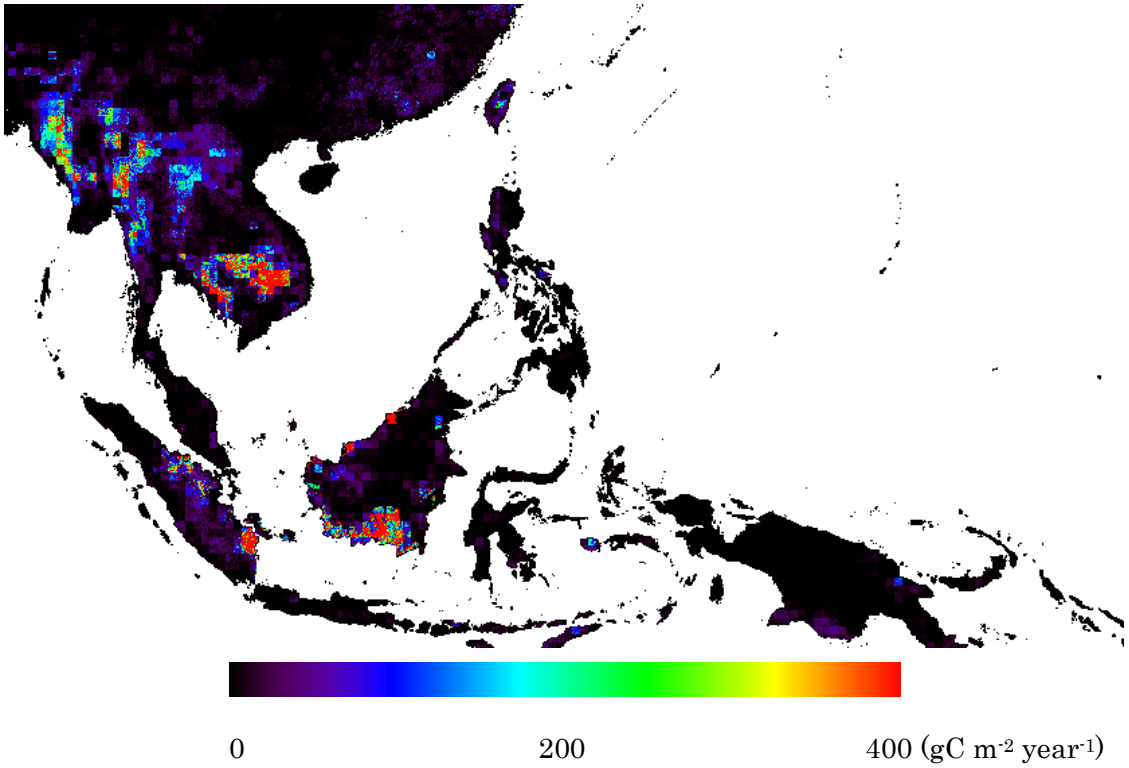

Fig. 3.6 Average annual fire carbon emissions in SEA derived from (a) BEAMS/ MCD64A1, (b) BEAMS/MCD45A1-Peat, (c) BEAMS/GFED from 2001-2010 in SEA with 5 km spatial resolution (Unit: gC m^{-2} $year^{-1}$).

had a relatively low spatial resolution, were frequently misinterpreted in small areas (Fig. 3.7).

To assess the robustness of our estimations, all fire CE data were resampled from 5 km into 0.5° so that they can be compared with GFED3 (Fig. 3.8). The comparisons of fire CE from BEAMS/MCD64A1, BEAMS/MCD45A1-Peat, BEAMS/ GFED and GFED3 all had similar spatial characteristics, even though the magnitudes of the emissions varied in places. In NSEA, large fire CE were observed in eastern and western Myanmar, northern Thailand, northern Laos, and Cambodia. Four results show high levels of spatial consistency in NSEA, although moderate differences can be observed in Sumatra and Kalimantan of Indonesia in ESEA, where GFED3 produced larger emissions than BEAMS/MCD64A1, BEAMS/ MCD45A1-Peat and BEAMS/GFED. Differences among our three estimations are considered to be attributable to the use of different burned area data inputs. In NSEA, compared with

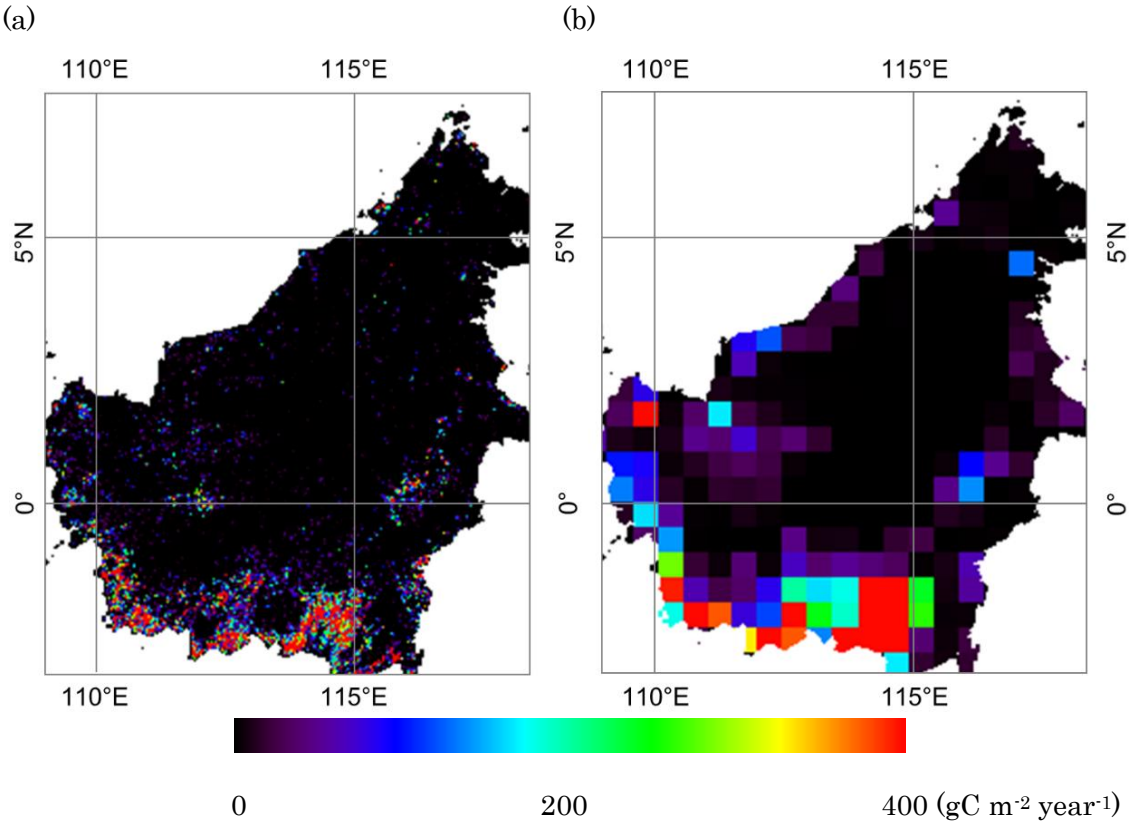

Fig. 3.7 Comparison of fire carbon emissions from (a) BEAMS/MCD64A1 with 5 km grid and (b) GFED3 with 0.5° grid in Kalimantan of Indonesia ranging from 8°N-4S° and 109°E-119°E.

BEAMS/MCD45A1-Peat and BEAMS/GFED, fire CE from BEAMS/MCD64A1 are higher because the latter product is more sensitive to detect burned areas (Fig. 3.3). Conversely, in ESEA, fire CE from our three estimations are lower than GFED3. The discrepancies between BEAMS/GFED and GFED3 are considered to be the use of different biomass estimates obtained from BEAMS and CASA. Although our SEA biomass estimates were slightly lower than those of Saatchi et al. (2011), we were unable to show that CASA estimated biomass in SEA had been validated. Further, GFED3 burned area had never been compared with field observation data or burned-area statistical data in SEA. However, the extent of burned area shown by our improved burned area model, MCD45A1-Peat, was similar to GFED3, indicated that peatland burning in ESEA did contributed markedly to fire CE in SEA even though its small proportion in burned area among the total SEA (Table 3.3).

(a)

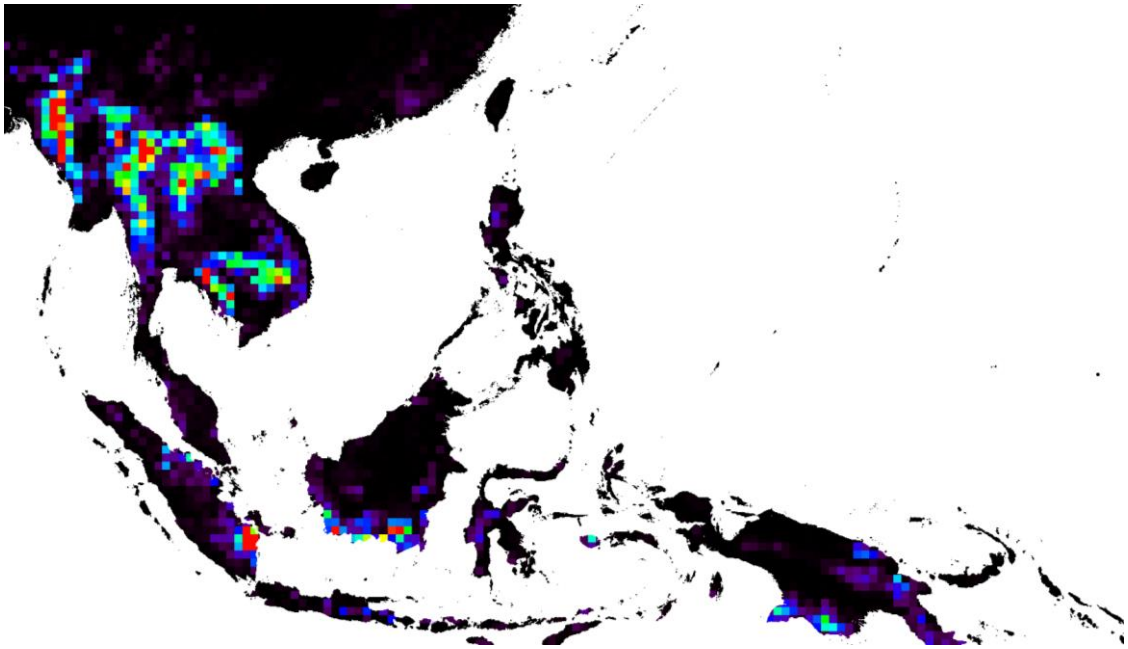

(b)

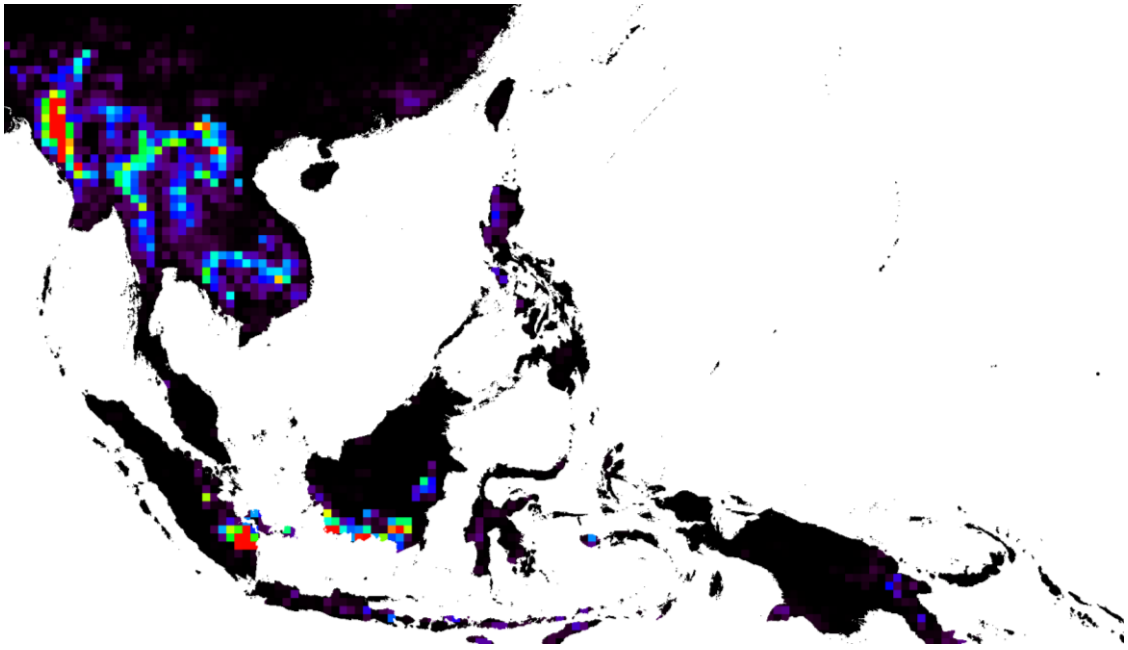

(c)

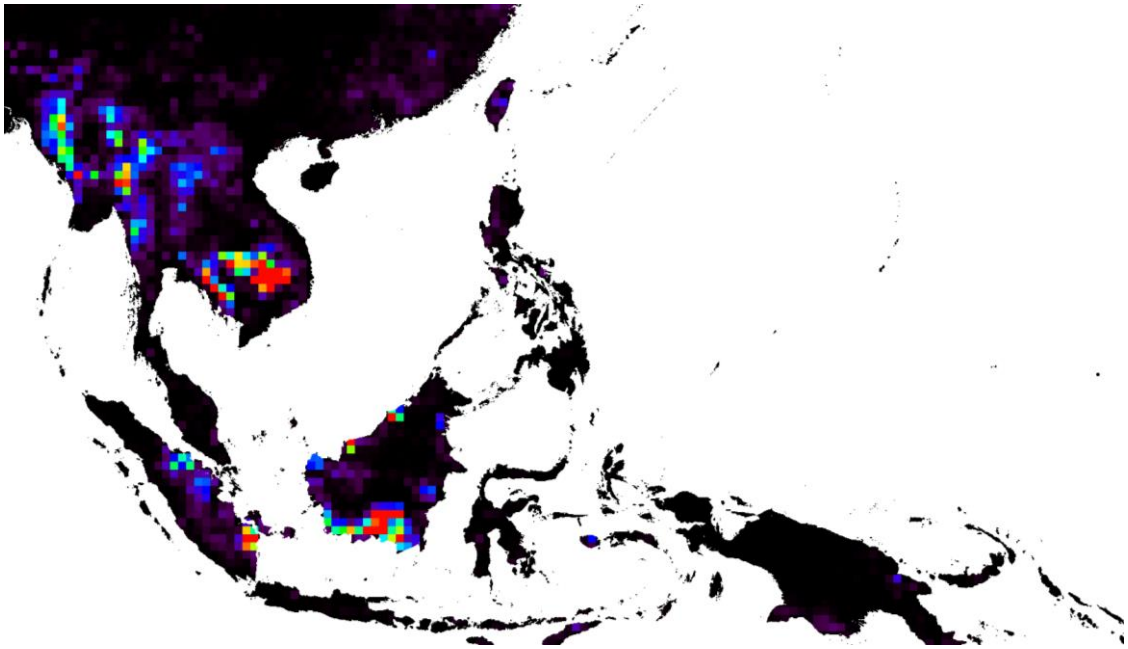

(d)

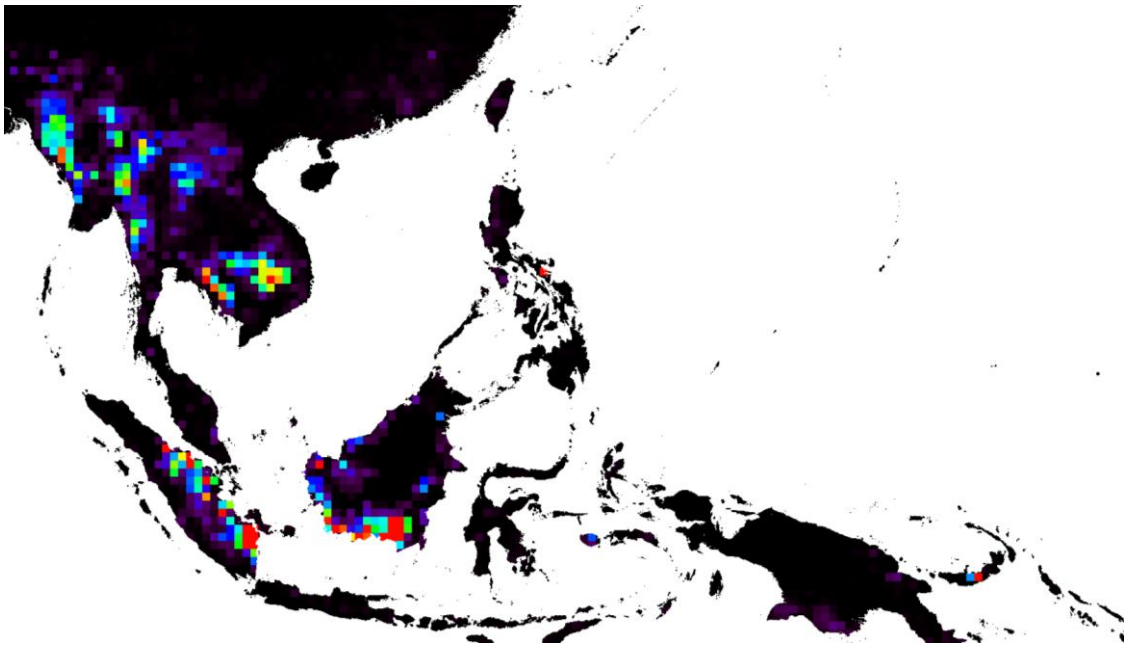

0 200 400 (gC m^{-2} $year^{-1}$)

Fig. 3.8 Average annual fire carbon emissions estimated by (a) BEAMS/MCD64A1, (b) BEAMS/MCD45A1-Peat, (c) BEAMS/GFED during 2001-2010 in SEA at a spatial

resolution of 0.5° resampled to 5 km for consistent comparisons with (d) GFED3 (gC m^{-2} $year^{-1}$).

We quantified the fire CE of each country from the three estimations and GFED3 (Table 3.3). The all four emissions showed similar results with small differences among them. Totally, our 5 km spatial resolution estimates for average annual fire CE from BEAMS/MCD64A1, BEAMS/MCD45A1-Peat, BEAMS/GFED reached as high as 232.6, 214.1 and 228.8 TgC, and all were around GFED3 estimates of 210.7 TgC. The largest dominant contributor to the total fire CE in SEA was Indonesia, followed by Myanmar and Cambodia. The fire CE from the three countries accounted for almost 67% to 78% of the total. Fire CE in Indonesia showed almost nearly half of the total, and our estimations by using MCD64A1, MCD45A1-Peat, and GFED3 burned area presented similar results. And the largest difference was detected in Cambodia between BEAMS/MCD45A1-Peat and BEAMS/GFED with 12.0 and 26.7 TgC $year^{-1}$. To examine the statistically significant differences of fire CE from each country among the four results, we calculated the correlation coefficients by using the four simulation results (120 images: 12 month × 10 years) and statistical *t* test at 5% and 1% significance level. We found that BEAMS/MCD45A1-Peat and GFED3 had no significant differences in most countries (e.g., Myanmar, Laos, Philippine, Malaysia, Indonesia, and Papua New Guinea). In total, compared with BEAMS/MCD64A1 and BEAMS/GFED in the whole SEA, the fire CE from GFED3 showed better correlation with BEAMS/ MCD45A1-Peat (R^2=0.57; $p<0.01<0.05$). It means that BEAMS/MCD45A1-Peat and GFED3 had similar results in fire CE estimation. The fire CE in Indonesia also manifested that BEAMS/MCD45A1-Peat and GFED3 displayed higher correlation. Besides, we can notice that in Cambodia there were statistically significant differences among the four results except the relation between BEAMS/MCD64A1 and GFED3 (R^2=0.88; $p > 0.05$).

Interannual variations in fire CE from biomass burning in SEA during 2001-2010 estimated from the three estimations were compared against AOD dynamics (Fig. 3.9). Changes in AOD in SEA are mainly caused by biomass burning emissions and are regarded as an optimal indicator of fire CE. Although the magnitude of fire

Table 3.3 Average annual burned areas and fire carbon emissions of each country from different results and datasets during 2001-2010, and their spatial correlation coefficient with statistical test.

					Correlation coefficients					
	A	B	C	D	AB	AC	AD	BC	BD	CD
Indonesia	*0.8*	*1.1*	*0.9*		*0.63***	*0.62*		*0.79***		
	87.0	101.1	92.8	97.7	0.66*	0.86**	0.31**	0.41	0.63**	0.46**
Myanmar	*1.8*	*1.9*	*1.4*		*0.68**	*0.81***		*0.67***		
	48.6	43.5	45.8	45.8	0.77	0.82	0.78**	0.66	0.72**	0.87**
Cambodia	*2.2*	*1.2*	*2.0*		*0.78***	*0.97*		*0.75***		
	21.3	12.0	26.7	20.7	0.73**	0.87**	0.88	0.66**	0.63**	0.94**
Thailand	*0.8*	*1.0*	*0.6*		*0.61***	*0.71***		*0.57***		
	17.1	14.9	18.1	12.0	0.72*	0.65	0.59**	0.50**	0.57**	0.77**
Laos	*0.3*	*0.2*	*0.2*		*0.73***	*0.81*		*0.55***		
	19.9	11.0	15.4	12.0	0.71**	0.82**	0.76**	0.49	0.60**	0.89**
Vietnam	*0.3*	*0.2*	*0.3*		*0.77***	*0.94*		*0.75**		
	9.2	7.4	7.9	4.3	0.75*	0.67	0.59**	0.32**	0.40	0.92**
P.N.Guinea	*0.2*	*0.0*	*0.1*		*0.28***	*0.76***		*0.20**		
	9.0	1.8	3.9	3.6	0.21**	0.56**	0.12**	0.03	0.33**	0.22
Malaysia	*0.1*	*0.0*	*0.1*		*0.26***	*0.13***		*0.04***		
	4.3	2.8	4.9	3.7	0.87**	0.53	0.10**	0.10	0.51**	0.39
Philippine	*0.0*	*0.1*	*0.0*		*0.63***	*0.43***		*0.40***		
	1.0	1.9	2.2	5.3	0.55**	0.53**	0.01	0.01	0.56	0.50
Total	*6.8*	*5.9*	*6.1*		*0.69***	*0.90*		*0.67***		
	232.6	214.1	228.8	210.7	0.65*	0.82	0.39	0.41	0.57*	0.52

The italic showed the burned areas (A: MCD64A1, B: MCD45A1-Peat, C: GFED3) (10^4 km^2). AB mean the correlation coefficient between A (MCD64A1) and B (MCD45A1-Peat); the upright indicated fire CE (A: BEAMS/MCD64A1, B: BEAMS/MCD45A1-Peat, C: BEAMS/GFED, D: GFED3) (TgC). AB mean the correlation coefficient between A (BEAMS/MCD64A1) and B (BEAMS/MCD45A1-Peat). The statistically significant difference were displayed with $p < 0.01$ (**), $0.01 < p < 0.05$ (*), and $p > 0.05$ ().

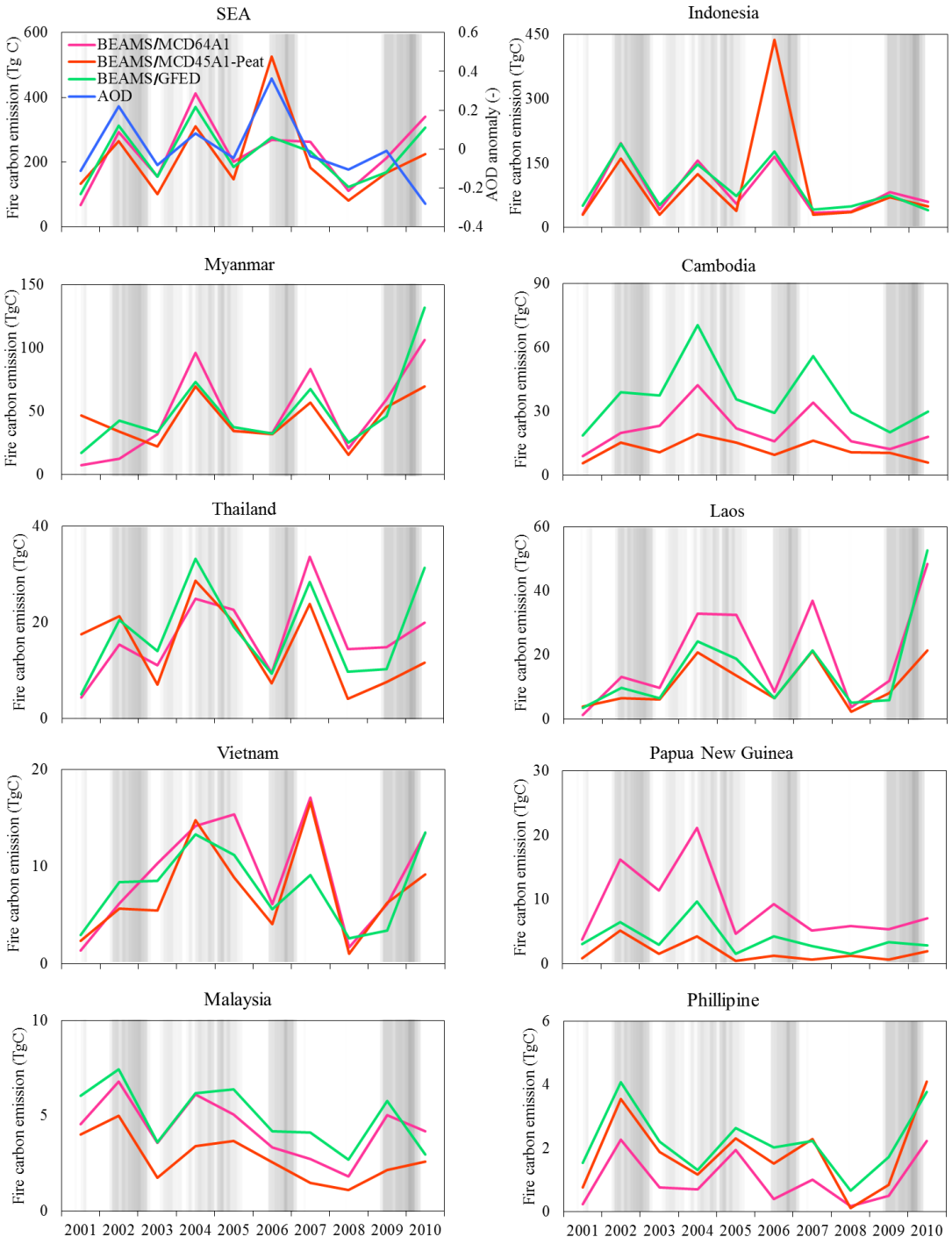

Fig. 3.9 Interannual variations in fire carbon emissions from BEAMS/MCD64A1, BEAMS/MCD45A1-Peat and BEAMS/GFED and its corresponding average AOD in SEA and each country during 2001-2010. A Multivariate ENSO Index (MEI) is shown in grey scale, with darker shades indicating higher MEI values.

CE varied considerably between years, on the whole, the BEAMS-based fire CE were comparable to AOD temporal patterns for the years 2001 to 2010. Interannual variations in AOD peaked in 2002, 2004, 2006 and 2010, when fire CE in SEA also reached higher values. The interannual variation data showed that fire CE derived from BEAMS/MCD64A1 and BEAMS/GFED were consistent for the years 2001-2010, except in 2006 when the most severe fire episode of this decade occurred during an El Niño event (Field et al., 2009). The fire CE from BEAMS/MCD45A1-Peat showed a more consistent interannual trend with AOD showing a large peak in 2006.

In general, the interannual variations in fire CE corresponded with burned areas, but discrepancies between both factors were also observed; for example, burned area reached a maximum in 2004 but the largest fire CE were observed in 2006. Among all the countries in SEA, Indonesia was the largest fire carbon emitter during 2001-2010 period. Still, we found that four obvious peaks of fire CE in 2002, 2004, 2006 and 2009 in Indonesia corresponded well with its four peaks in the burned area (Fig. 3.9). These findings indicate that while burned peatland only accounted for a small proportion of the total area burned in SEA, peatland burning was the dominant source of CE in SEA in certain years. The reason for the marked fluctuation in CE is due to the occurrence of droughts during the period 2001-2010. The other large emitters of fire CE were noticed in NSEA (e.g., Myanmar, Cambodia, Thailand, Laos, Vietnam, etc). The peaks of fire CE in these countries showed different temporal trend, with highest emissions in 2004, 2007 and 2010, respectively (Fig. 3.9). Such temporal variations can be explained by the consistent trend of burned area with corresponding peaks in 2004, 2007 and 2010. By comparing the three estimations in Myanmar, Cambodia, Thailand, Laos, and Vietnam, we found that the three results were also similar and exhibited consistent temporal trends from 2001 to 2010, even though there were small differences in magnitude.

Besides, fire CE estimated using the three different burned area products all produced comparable temporal trends with clear monthly variations (Fig. 3.10). The largest difference in fire CE was captured in October 2006, when the effects of an El

Niño event were at their most intense, releasing considerable amounts of carbon into the air. And our improved MCD45A1-Peat burned area model showed that most of these fire CE were attributable to peatland burning during extreme drought of the El Niño event. The carbon release can also be demonstrated by the extraordinarily high AOD in October of 2006, when our improved MCD45A1-Peat burned area indicated that an extensive area had burned and this was associated with very high fire CE. Several small differences in fire CE were observed during Aug-Oct of 2002 and 2004, primarily due to the underestimation of burned peatland in ESEA.

Interestingly, even though the stringency of MCD45A1-Peat had been improved by introducing AOD to more accurately estimate the peat burning in the peatlands of Sumatra and Kalimantan (Fig. 3.1, Fig. 3.10), the area of burned peatland was also slightly underestimated resulting in relatively small values for CE. In addition, we concluded that the extensive burning that occurred in 2002, 2004, 2006 and 2009 showed excellent correspondence with the large Multivariate ENSO (El Niño Southern Oscillation) Index (MEI) values during these years (Fig. 3.10).

Although fires in SEA are primarily anthropogenic, caused either intentionally or unintentionally through practices such as slash-and-burn agriculture, or draining peatland and deforesting areas to establish oil palm plantations, the strong seasonality and overall activity of fires in SEA is largely correlated with the ENSO. For example, the severity of the 2006 event was exacerbated by the presence of an ENSO, which intensified a seasonal drought in SEA region from July to October (Field et al., 2009). Our results showed that the fire CE were closely correlated with the ENSO, and that large CE were associated with high MEI values (Fig. 3.10). Further, there was strong evidence that the Indian Ocean Dipole (IOD) pattern also contributed to drought over Indonesia (Hong et al., 2008). We specifically examined the influence of the IOD using the dipole mode index (DMI), as the IOD is an important indicator of fire CE in SEA (Field et al., 2009). Fire CE were strongly correlated with DMI during 2001-2010, and Niño3.4 also appeared to be positively correlated with fire CE (Fig. 3.10c).

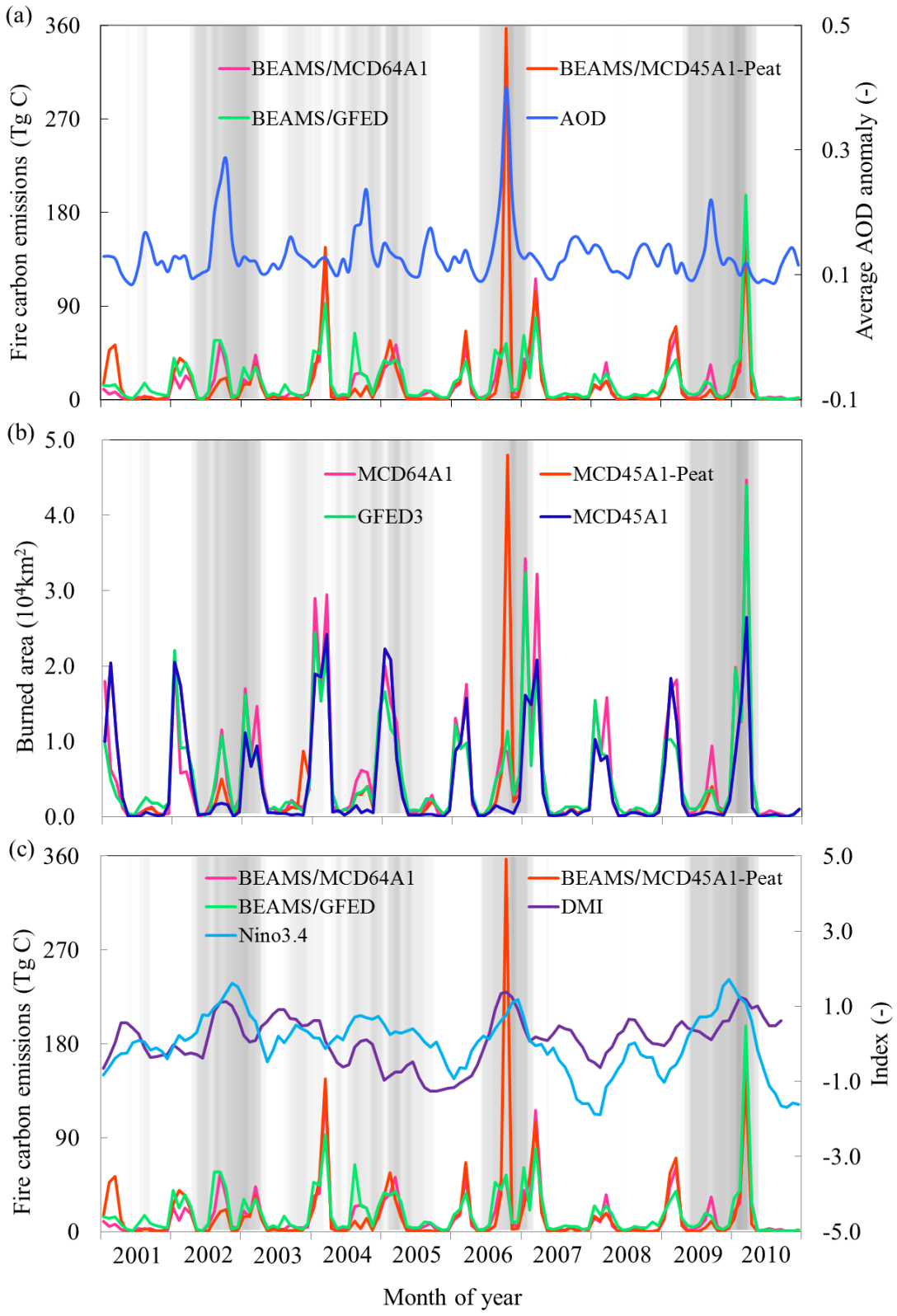

Fig. 3.10 (a) Monthly variations in fire carbon emissions estimated by BEAMS/ MCD64A1, BEAMS/MCD45A1-Peat and BEAMS/GFED and its corresponding average

AOD in SEA during 2001-2010. (b) Monthly variations in burned area estimated by MCD64A1, MCD45A1-Peat, GFED3, MCD45 in SEA during 2001-2010. (c) Monthly variations in fire carbon emissions in SEA and synchronous variations of DMI (Dipole Mode Index) and Niño3.4 Index. DMI is defined as the difference in SST anomalies between the western equatorial Indian Ocean (50°E-70°E and 10°S to 10°N) and the southeastern equatorial Indian Ocean (90°E-110°E and 10°S to 0°N). The Niño3.4 index was calculated from the Smith and Reynolds global gridded Sea Surface Temperature analysis (Smith and Reynolds, 2003). A Multivariate ENSO Index (MEI) is shown in grey scale, with darker shades indicating higher MEI values.

3.3.4 Fire CE in NSEA

Fire CE in NSEA estimated using the three simulations all showed strong and consistent interannual and intraannual variations with few differences between them (Fig. 3.11a). Average annual fire CE derived from BEAMS/MCD64A1, BEAMS/MCD45A1-Peat and BEAMS/GFED were 130.3, 107.0 and 151.5 TgC, which was equivalent to 56.0%, 61.0% and 66.2% of the total estimated fire CE in SEA. However, the burned area showed that NSEA overwhelmingly dominated 82.5%, 81.5% and 82.0% of the SEA with the burned area of 56181, 48403, 50211 km^2, respectively. Intraannual variations in fire CE revealed that they were highest during Jan-Mar when relatively dry weather prevailed (Field et al., 2009). The dry season of the monsoon period generally lasts from Jan through Mar when relatively little precipitation falls (Taylor, 2010) and the potential for burning areas to clear and renew farmland and rangeland before the spring growing season is highest.

People usually prepare fields by cutting down any vegetation, which they then allow to dry until immediately before the rainiest part of the year to ensure an effective burn (Taylor, 2010). Consequently, values for fire CE and burned area are typically high during the dry period (Jan-Mar), and they typically accounted for a large proportion of the burned area values obtained during the year (Fig. 3.11). In addition, the highest fire CE and most extensive burned areas in NSEA were observed in 2004, 2007 and 2010 (Fig. 3.4, Fig. 3.11b). During the Jan-Mar dry seasons in 2004, 2007 and 2010, the areas that were burned appeared to increase

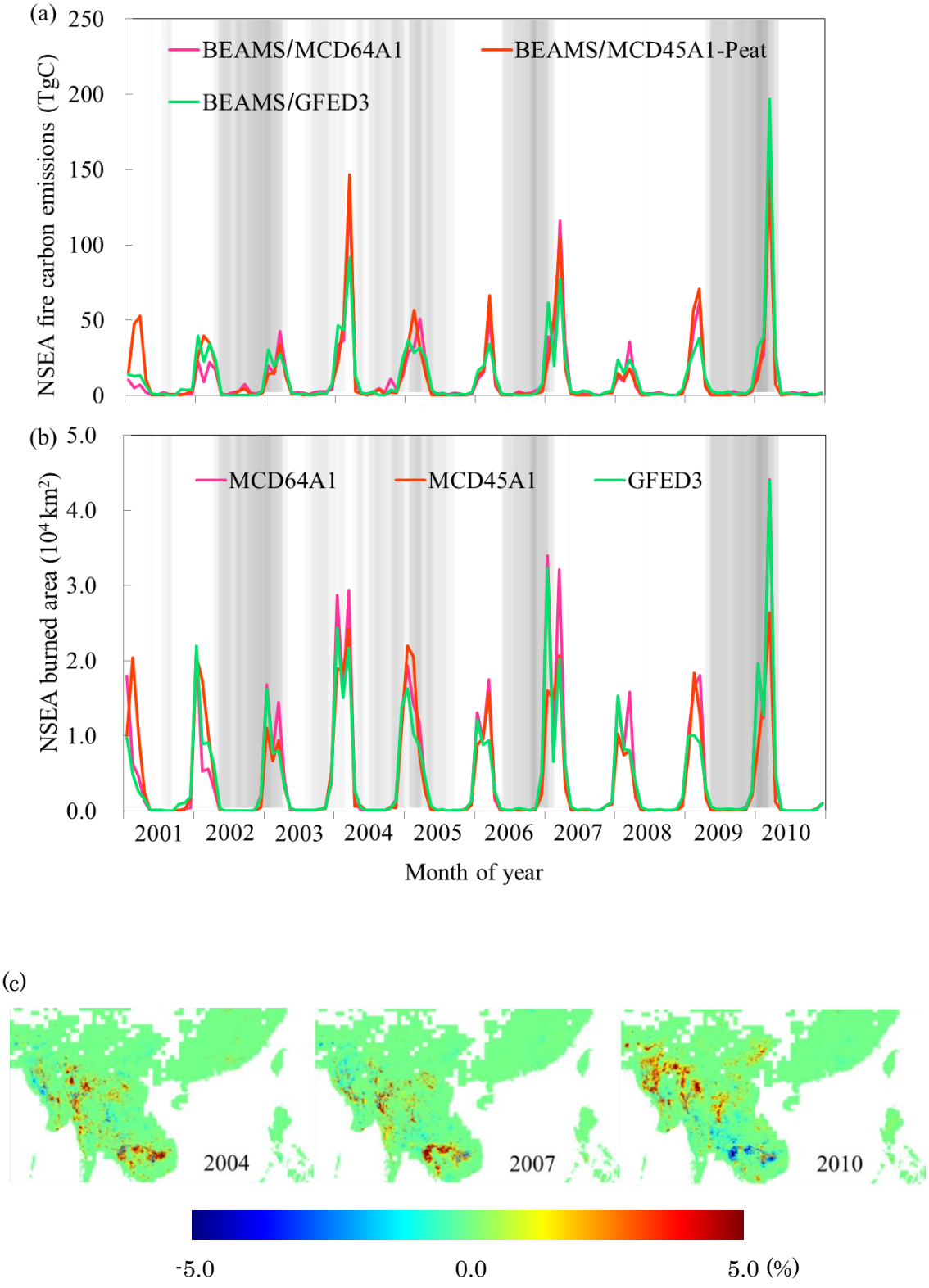
(a)
NSEA fire carbon emissions (TgC)
250
200
150
100
50
0
BEAMS/MCD64A1
BEAMS/MCD45A1-Peat
BEAMS/GFED3
(b)
NSEA burned area (10^4 km^2)
5.0
4.0
3.0
2.0
1.0
0.0
MCD64A1
MCD45A1
GFED3
2001
2002
2003
2004
2005
2006
2007
2008
2009
2010
Month of year

(c)

2004
2007
2010
-5.0
0.0
5.0 (%)

(d)

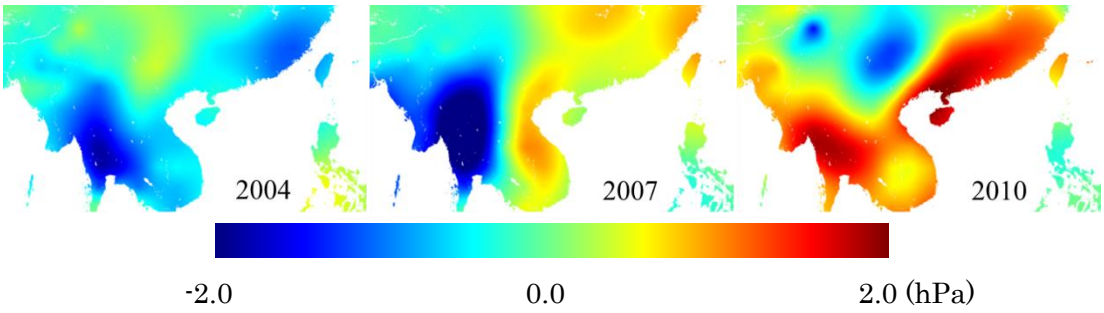

Fig. 3.11 (a) Monthly variations in NSEA fire carbon emissions. (b) Monthly variations in NSEA burned area products estimated by MCD64A1, MCD45A1 and GFED3 during 2001-2010. (c). Spatial distributions of the burned area anomaly during the drought period of Jan-Mar in 2004, 2007 and 2010 derived from the average burned area estimates from MCD64A1, MCD45A1 and GFED3. (d). Spatial distributions of vapor pressure anomaly during the drought period of Jan-Mar in 2004, 2007 and 2010. A Multivariate ENSO Index (MEI) is shown in grey scale, with darker shades indicating higher MEI values.

across the NSEA as land was cleared for agricultural use (Chang and Song, 2010; http://visibleearth.nasa.gov/view/php?id=70170). When we examined the spatial distributions of the burned area anomaly during the Jan-Mar drought period in 2004, 2007 and 2010, we found that burned areas in these three years had a positive anomaly value spatially (Fig. 3.11). In 2004 and 2007, the positive anomaly value of burned area mainly were distributed in eastern Myanmar, northern Thailand, and some areas of northern Laos, however, the burned area in Cambodia and western Myanmar decreased compared to the annual average burned area in NSEA. Comparing burned area data with synchronous vapor pressure anomaly clearly showed that as vapor pressure decreased throughout most of NSEA, the burned area increased in 2004. In 2007, the burned area anomaly in eastern Myanmar and northern Thailand also showed agreement with the decrease in vapor pressure in the dry season (Fig. 3.11c).

However, in 2010, the spatial characteristics of burned areas were markedly different to those observed in 2004 and 2007. The burned areas in Cambodia showed an obvious decrease in 2010, while the burned areas in eastern and western

Myanmar and northern Thailand all increased considerably (Fig. 3.4). In 2010, the extent of the burned area decreased in Cambodia while vapor pressure increased. However, in western Myanmar and northern Thailand, an increase in burned area was associated with an increase in vapor pressure (Fig. 3.11d). The discrepancy between the positive burned area anomaly and vapor pressure around Cambodia in 2007 was actually attributable to the human-induced slash-and-burn cultivation, even though high vapor pressure conditions were prevalent (Fig. 3.11c, d). The positive burned area anomaly could be explained by the high levels of coconut production in Cambodia in 2007 (7.10×10^4 t), compared to the 10 years previously (average: 6.76×10^4 t). Similarly, groundnut production also peaked at 3.00×10^4 t in 2007, which was greater than the average of 2.04×10^4 t produced previously (FAOSTAT, available at faostat3.fao.org/home/index.html #VISUALIZE).

Conversely, in 2010, coconuts production in Cambodia dropped to 6.55×10^4 t, which was less than the average of 6.76×10^4 t, therefore, leading to the negative burned area anomaly (Fig. 3.11c, Fig. 3.4). The abrupt and extensive increase in burned area in western Myanmar and northern Thailand can be explained by the sudden rise in crop production which was produced using slash-and-burn cultivation. Increases were also observed in crops such as cotton (1.33×10^5 t), natural rubber (1.12×10^5 t) and fiber crops (1.47×10^5 t); levels that were considerably higher than the average of 6.82×10^4, 6.30×10^4, and 9.91×10^4 t, respectively, that were produced previously. Rice production in Thailand also reached its peak with 3.6×10^7 t produced in 2010, which was higher than the mean of 3.1×10^7 t (FAOSTAT, available at faostat3.fao.org/home/index.html#VISUALIZE.

3.3.5 Fire CE in Indonesia

In Indonesia, fire CE from the three estimations showed generally corresponded to average monthly AOD values. In 2002, 2004, 2006 and 2009, monthly AOD values peaked during Aug-Oct, with levels being considerably higher than average values. The most obvious peak from the three estimations was observed in Sep-Nov of 2006 with 2.8, 5.6, 2.2 times larger than average monthly AOD during the previous ten years (Fig. 3.12). In Fig. 3.11a, four peaks in fire CE can be seen during Aug-Oct of

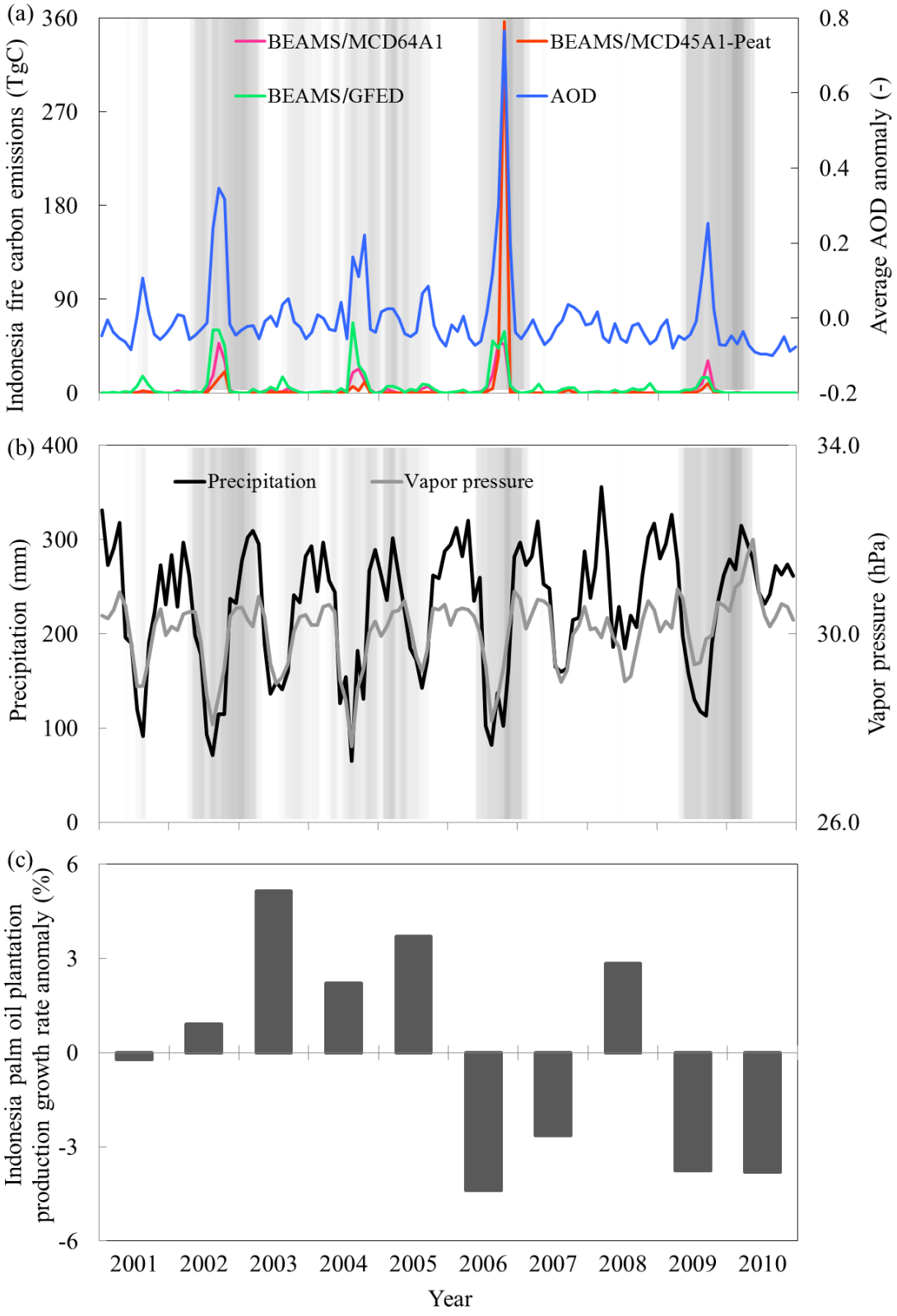

Fig. 3.12 (a) Monthly variations in Indonesia fire carbon emissions and the corresponding average AOD during 2001-2010. (b) Monthly variations in annual

precipitation and vapor pressure in Indonesia during 2001-2010. (c) Indonesia palm oil plantation production growth rate anomaly by year (From United States Department of Agriculture). A multivariate ENSO index (MEI) is shown in grey scale, with darker shades indicating higher MEI values.

2002, 2004, 2006, and 2009 from the three estimations in fire CE even though their magnitudes are different.

The differences in fire CE among the three estimations revealed that different burned area products were either more or less effective at detecting burned areas, which accounted for the observed discrepancies in the fire CE data obtained from these products. The highest CE, which were 77 times the monthly average, were recorded by BEAMS/MCD45A1-Peat in Oct 2006 (Fig. 3.12). Comparisons of burned area data generated by MCD64A1, MCD45A1-Peat and GFED3 revealed that the burned area values generated by MCD45A1-Peat for were identical to those generated by MCD64A1 and GFED3, except in Aug-Oct of 2002, 2004, 2009 when MCD45A1-Peat generated burned area values that were lower than those generated by MCD64A1 and GFED3 and in Oct of 2006 when MCD45A1-Peat generated burned area values that were higher than those of the other two models (Fig. 3.10).

During the past few decades, many Southeast Asian countries have constantly been plagued by recurring episodes of smoke haze resulting from traditional slash-and-burn agricultural practices or uncontrolled forest fires (Marlier et al., 2013). This is particularly serious in Indonesia, where the bulk of emissions are due to the continuous burning of peat soils for up to four consecutive months every year (Page et al., 2002). These Indonesian fires produce vast palls of heavy smoke and high concentrations of aerosols, which significantly reduce the air visibility on an almost annual basis, particularly during dry years when the pollution is exacerbated by El Niño events (Field et al., 2009). In this study, high AOD values were observed in SEA during the dry years of 2002, 2004, 2006 and 2009, with good correspondence also apparent between fire CE and MEI values from 2001 to 2010 (Fig. 3.12). The four peaks in fire CE and the corresponding AOD values in Indonesia in 2002, 2004, 2006 and 2009 can be attributed to the simultaneous action of relatively low precipitation

and low vapor pressures at those times. The five-month rainy season (Jul to Nov) in 2006 was very dry (586 mm) compared with the rainy season in 2002 (630 mm), 2004 (799 mm) and 2009 (784 mm); in 2001-2010, in Indonesia, average rainfall for this five-month period was 901 mm and average annual rainfall was 2739 mm according to GPCP data. During the five-month drought in 2006, which was exacerbated by the intense El Niño event, extensive areas burned and fire penetrated deep inside peat soils resulting in massive emissions and extremely high AOD values in the atmosphere.

The intensity and the scale of fires have increased substantially in Indonesia in recent years due to the rapid expansion of oil palm plantations and industrial logging (Carlson et al., 2013). The dramatic increase in the rate of palm oil plantation development during the past decade decreased slightly in the El Niño years of 2006 and 2009. The decrease observed in the development of these plantations meant that fire CE were markedly affected by the El Niño phenomenon, and that fire CE were more tightly linked to the occurrence of natural drought cycles than to any increase caused by anthropogenic fires in the both years (Fig. 3.12). In 2002 and 2004, a marked increase in the rate of palm oil plantation development was observed and the strong El Niño events also exacerbated fire CE as large areas of forest burned, increasing emissions. The years 2003, 2005 and 2008 were characterized as having low MEI values with more precipitation and higher vapor pressures (Fig. 3.12b). Nonetheless, the minor peaks in fire CE that were observed as palm oil plantations were produced means that, compared to natural factors, human factors were primarily responsible for the observed amounts of fire CE in these years. SEA fire CE exhibit considerable interannual variability due to a coupling between El Niño-induced drought and anthropogenic land use changes (Field et al., 2009). On one hand, SEA forest fires has been particularly intense in years when the weather was noticeably dry due to the effects of the El Niño phenomenon, and there is considerable evidence fire CE in SEA are mainly driven by the drought conditions associated with El Niño or Indian Ocean Dipole events (Field et al., 2009). On the other hand, humans set fire to accessible areas of forest, increasing the occurrence

of fire. Drought acts as a trigger for fire occurrence, but it is humans who ignite the fires. In Indonesia, fire is primarily used to clear vegetation waste and is closely associated with deforestation and agricultural expansion (Siegert et al., 2001). Indeed, the main causes of forest fires are the traditional farmers, small holders, and large scale investors (plantation owners) who clear their land to plant commercial tree crops (palm oil trees) (Jones et al., 2006). Of these, the large timber and palm oil plantation companies have caused the most extensive fires as they develop areas at a considerably greater scale than practitioners of shifting cultivation and land developers (Jones et al., 2006). Importantly, the large amounts of smoke (aerosols) has reduced rainfall further, compounding the effects of El Niño and reducing the sunlight available for photosynthesis in plants.

3.4 Conclusions

In this study, fire CE from biomass burning in SEA were estimated for ten fire years from 2001 to 2010 at spatial resolution of 5 km. The methods used recently released satellite products and a physical process-based biosphere model (BEAMS) with embedded CE. The high spatial resolution was effective for detecting small scale fires and CE that are usually lost in data with a coarser resolution. Briefly, average annual burned areas determined by MCD64A1, MCD45A1 and GFED3 for the period of 2001-2010 in SEA were 68104, 50933, and 61263 km^2 $year^{-1}$, respectively. The largest difference between the two MODIS products was observed in the Indonesia of ESEA. In general, the burned area data obtained using the three products were consistent over the period examined (2001 to 2010), and all showed a peak in burned areas in 2004. Burned areas were predominantly concentrated in Myanmar, northern Thailand, eastern Cambodia, and northern Laos in NSEA. However, several marked differences between the models were observed in ESEA where peatlands are extensively distributed. The improved MCD45A1-Peat burned area data showed that the average annual burned area was 59420 km^2 $year^{-1}$ with a net increase of 8487 km^2 $year^{-1}$ in the peatlands of ESEA.

The spatial characteristics of the fire CE from the BEAMS/MCD64A1,

BEAMS/MCD45A1-Peat and BEAMS/GFED simulations corresponded with the burned areas, even though the magnitude of CE varied markedly from place to place. Average annual fire CE were 232.6, 214.1 and 228.8 TgC, respectively, of which, the best result among the three estimations in our current study was BEAMS/MCD45A1-Peat, which was close to that obtained by GFED3 with 210.7 TgC. And the largest emitter of fire CE was Indonesia, followed by Myanmar, Cambodia and Thailand. Compared with interannual variability in AOD, fire CE presented consistent temporal trends. Marked increases in AOD values were observed during the dry years of 2002, 2004, 2006 and 2009, when BEAMS/MCD45A1-Peat displayed same trend. The temporal variation in fire CE closely corresponded with El Niño occurrence and Indian Ocean Dipole patterns, as well as deforestation for palm oil plantation production. In this study, we evaluated the spatial and temporal variations in fire CE from Southeast Asia during 2001-2010 by using three estimations and our results were only validated in some area of SEA. But actually the largest difference among MCD64A1, MCD45A1 and GFED3 was the burned peatland in Sumatra and Kalimantan of Indonesia, however, due to the data unavailability of ground observation or statistical data in Indonesia (van der Werf et al., 2006), until now we have difficulties in validating the satellite burned area data and fire CE in this area. More ground observation data and experimental flux measurement data are urgently needed for further validation in our following work.

References

Andreae, M.O., Merlet, P., 2001. Emission of trace gases and aerosols from biomass burning. Global Biogeochem. Cycles, 15, 955-966.

Baccini, A., Goetz, S.J., Walker, W.S., Laporte, N.T., Sun, M., Sulla-Menashe, D., Hackler, J., Beck, P.S.A., Dubayah, R., Friedl, M.A., Samanta, S., Houghton, R.A., 2012. Estimated carbon dioxide emissions from tropical deforestation improved by carbon-density maps. Nature Clim. Change, 2, 182-185.

Batjes, N.H., 1999. Management options for reducing CO_2 concentrations in the atmosphere by increasing carbon sequestration in the soil, NRP Report No. 410-200-031. Dutch National Research Programme on Global Air Pollution and Climate Change (NRP).

Carlson, K.M., Curran, L.M., Ratnasari, D., Pittman, A.M., Soares-Filho, B.S., Asner, G.P., Trigg, S.N., Gaveau, D.A., Lawrence, D., Rodrigues, H.O., 2012. Committed carbon emissions, deforestation, and community land conversion from oil palm plantation expansion in West Kalimantan, Indonesia. PNAS, 109, 7559-7564.

Carlson, K.M., Curran, L.M., Asner, G.P., Pittman, A.M., Trigg, S.N., Adeney, J.M., 2013. Carbon emissions from forest conversion by Kalimantan oil palm plantations. Nature Clim. Change, 3, 283-287.

Chang, D., Song, Y., 2010. Estimates of biomass burning emissions in tropical Asia based on satellite-derived data. Atmos. Chem. Phys., 10, 2335-2351.

Eck, T.F., Holben, B.N., Reid, J.S., Sinyuk, A., Hyer, E.J., O'Neill, N.T., Shaw, G.E., Vande Castle, J.R., Chapin, F.S., Dubovik, O., Smirnov, A., Vermote, E., Schafer, J.S., Giles, D., Slutsker, I., Sorokine, M., Newcomb, W.W., 2009. Optical properties of boreal region biomass burning aerosols in central Alaska and seasonal variation of aerosol optical depth at an Arctic coastal site. J. Geophys. Res., 114, D11201, doi:10.1029/2008JD010870.

Farr, T.G., Rosen, P.A., Caro, E., Crippen, R., Duren, R., Hensley, S., Kobrick, M., Paller, M., Rodriguez, E., Roth, L., Seal, D., Shaffer, S., Shimada, J., Umland, J., Werner, M., Oskin, M., Burbank, D., Alsdorf, D., 2007. The shuttle radar topography mission. Rev. Geophys., 45, RG2004, doi:10.1029/2005RG000183.

Fenner, N., Freeman, C., 2011. Drought-induced carbon loss in peatlands. Nature Geosci., 4, 895-900.

Field, R.D., Shen, S.S.P., 2008. Predictability of carbon emissions from biomass burning in Indonesia from 1997 to 2006. J. Geophys. Res., 113, G04024.

Field, R.D., van der Werf, G.R., Shen, S.S.P., 2009. Human amplification of drought-

induced biomass burning in Indonesia since 1960. Nature Geosci., 2, 185-188.

Friedl, M.A., Sulla-Menashe, D., Tan, B., Schneider, A., Ramankutty, N., Sibley, A., Huang, X., 2010. MODIS Collection 5 global land cover: Algorithm refinements and characterization of new datasets. Remote Sens. Environ., 114, 168-182.

Frouin, R., Murakami, H., 2007. Estimating photosynthetically available radiation at the ocean surface from ADEOS-II global imager data. J. Oceanogr., 63, 493-503.

Giglio, L., Csiszar, I., Justice, C.O., 2006. Global distribution and seasonality of active fires as observed with the Terra and Aqua Moderate Resolution Imaging Spectroradiometer (MODIS) sensors. J. Geophys. Res., 111, G02016.

Giglio, L., Randerson, J.T., van der Werf, G.R., Kasibhatla, P.S., Collatz, G.J., Morton, D.C., DeFries, R.S., 2010. Assessing variability and long-term trends in burned area by merging multiple satellite fire products. Biogeosciences 7, 1171-1186.

Giglio, L., Loboda, T., Roy, D.P., Quayle, B., Justice, C.O., 2009. An active-fire based burned area mapping algorithm for the MODIS sensor. Remote Sens. Environ., 113, 408-420.

Griffiths, M.L., Drysdale, R.N., Gagan, M.K., Frisia, S., Zhao, J.X., Ayliffe, L.K., Hantoro, W.S., Hellstrom, J.C., Fischer, M.J., Feng, Y.X., Suwargadi, B.W., 2010. Evidence for Holocene changes in Australian-Indonesian monsoon rainfall from stalagmite trace element and stable isotope ratios. Earth Planet. Sci. Lett., 292, 27-38.

Harris, N.L., Brown, S., Hagen, S.C., Saatchi, S.S., Petrova, S., Salas, W., Hansen, M.C., Potapov, P.V., Lotsch, A., 2012. Baseline Map of Carbon Emissions from Deforestation in Tropical Regions. Science 336, 1573-1576.

Heinsch, F.A., Reeves, M., Votava, P., Kang, S., Milesi, C., Zhao, M., Glassy, J., Jolly, W.M., Loehman, R., Bowker, C.F., Kimball, J.S., Nemani, R.R., Running, S.W., 2003. NTSG MODIS algorithms user's guide GPP and NPP (Mod17A2/A3). http://www.ntsg.umt.edu/modis/.

Hong, C.C., Lu, M.M., Kanamitsu, M., 2008. Temporal and spatial characteristics of positive and negative Indian Ocean dipole with and without ENSO. J. Geophys. Res.,

113, D08107, doi:10.1029/2007/JD009151.

Hooijer, A., Page, S., Canadell, J.G., Silvius, M., Kwadijk, J., Wösten, H., Jauhiainen, J., 2010. Current and future CO_2 emissions from drained peatlands in Southeast Asia. Biogeosciences 7, 1505-1514.

Huffman, G.J., Adler, R.F., Bolvin, D.T., Gu, G., 2009. Improving the global precipitation record: GPCP version 2.1. Geophys. Res. Lett., 36, L17808.

Jones, D.S., 2006. ASEAN and transboundary haze pollution in Southeast Asia. Asia Eur. J., 4, 431-446.

Justice, C.O., Giglio, L., Korontzi, S., Owens, J., Morisette, J.T., Roy, D., Descloitres, J., Alleaume, S., Petitcolin, F., Kaufman, Y., 2002. The MODIS fire products. Remote Sens. Environ., 83, 244-262.

Kasischke, E.S., Hoy, E.E., 2012. Controls on carbon consumption during Alaskan wildland fires. Glob. Change Biol., 18, 685-699.

Kasischke, E.S., Hyer, E.J., Novelli, P.C., Bruhwiler, L.P., French, N.H.F., Sukhinin, A.I., Hewson, J.H., Stocks, B.J., 2005. Influences of boreal fire emissions on Northern Hemisphere atmospheric carbon and carbon monoxide. Global Biogeochem. Cycles, 19, GB1012, doi:10.1029/2004GB002300.

Keeling, C.D., Whorf, T.P., Wahlen, M., van der Plicht, J., 1995. Interannual extremes in the rate of rise of atmospheric carbon dioxide since 1980. Nature, 375, 666-670.

Keeling, R.F., Piper, S.C., Bollenbacher, A.F., Walker, J.S., 2009. Atmospheric CO_2 records from sites in the SIO air sampling network. Trends: A Compendium of Data on Global Change. Oak Ridge, Tenn., U.S.A: Carbon Dioxide Information Analysis Center, Oak Ridge National Laboratory, U.S. Department of Energy, doi:10.3334/CDIAC/atg.035.

Langenfelds, R.L., Francey, R.J., Pak, B.C., Steele, L.P., Lloyd, J., Trudinger, C.M., Allison, C.E., 2002. Interannual growth rate variations of atmospheric CO_2 and its δ13C, H_2, CH_4, and CO between 1992 and 1999 linked to biomass burning. Global Biogeochem. Cycles, 16, 1048. doi:10.1029/2001GB001466.

Langner, A., Siegert, F., 2009. Spatiotemporal fire occurrence in Borneo over a period of 10 years. Glob. Change Biol., 15, 48-62.

Liang, S., Fang, H., Chen, M., Shuey, C.J., Walthall, C., Daughtry, C., Morisette, J., Schaaf, C., Strahler, A., 2002. Validating MODIS land surface reflectance and albedo products: Methods and preliminary results. Remote Sens. Environ., 83, 149-162.

Lucht, W., Lewis, P., 2000. Theoretical noise sensitivity of BRDF and albedo retrieval from the EOS-MODIS and MISR sensors with respect to angular sampling. Int. J. Remote Sens., 21, 81-98.

Marlier, M.E., DeFries, R.S., Voulgarakis, A., Kinney, P.L., Randerson, J.T., Shindell, D.T., Chen, Y., Faluvegi, G., 2013. El Niño and health risks from landscape fire emissions in Southeast Asia. Nature Clim. Change, 3, 131-136.

Miettinen, J., Shi, C., Liew, S.C., 2011. Deforestation rates in insular Southeast Asia between 2000 and 2010. Glob. Change Biol., 17, 2261-2270.

Myneni, R.B., Keeling, C.D., Tucker, C.J., Asrar, G., Nemani, R.R., 1997. Increased plant growth in the northern high latitudes from 1981-1991. Nature, 386, 698-702.

Myneni, R.B., Knyazikhin, Y., Privette, J.L., Glassy, J., 2002. Global products of vegetation leaf area and fraction absorbed PAR from year one of MODIS data. Remote Sens. Environ., 83, 214-231.

Page, S.E., Siegert, F., Rieley, J.O., Boehm, H-D.V., Jaya, A., Limin, S., 2002. The amount of carbon released from peat and forest fires in Indonesia in 1997. Nature, 420, 61-65.

Parton, W.J., Scurlock, J.M.O., Ojima, D.S., Gilmanov, T.G., Scholes, R.J., Schimel, D.S., Kirchner, T., Menaut, J.C., Seastedt, T., Moya, G.E., Kamnalrut, A., Kinyamario, J.I., 1993. Observations and modeling of biomass and soil organic matter dynamics for the grassland biome worldwide. Global Biogeochem. Cycles, 7, 785-809.

Randerson, J.T., Chen, Y., van der Werf, G.R., Rogers, B.M., Morton, D.C., 2012. Global burned area and biomass burning emissions from small fires. J. Geophys. Res., 117, G04012, doi:10.1029/2012JG002128.

Roy, D.P., Boschetti, L., Justice, C.O., Ju, J., 2008. The Collection 5 MODIS burned area product – global evaluation by comparison with the MODIS active fire product. Remote Sens., Environ., 112, 3690-3707.

Roy, D.P., Jin, Y., Lewis, P.E., Justice, C.O., 2005. Prototyping a global algorithm for systematic fire-affected area mapping using MODIS time series data. Remote Sens., Environ., 97, 137-162.

Saatchi, S.S., Harris, N.L., Brown, S., Lefsky, M., Mitchard, E.T.A., Salas, W., Zutta, B.R., Buermann, W., Lewis, S.L., Hagen, S., Petrova, S., White, L., Silman, M., Morel A., 2011. Benchmark map of forest carbon stocks in tropical regions across three continents. PNAS, 108, 9899-9904.

Sasai, T., Ichii, K., Yamaguchi, Y., Nemani, R.R., 2005. Simulating terrestrial carbon fluxes using the new biosphere model BEAMS: Biosphere model integrating Eco-physiological And Mechanistic approaches using Satellite data. J. Geophys. Res., 110, G02014, doi:10.1029/2005JG000045.

Sasai, T., Okamoto, K., Hiyama, T., Yamaguchi, Y., 2007. Comparing terrestrial carbon fluxes from the scale of a flux tower to the global scale. Ecol. Model., 208, 135-144.

Sasai, T., Saigusa, N., Nasahara, K.N., Ito, A., Hashimoto, H., Nemani, R.R., Hirata, R., Ichii, K., Takagi, K., Saitoh, T.M., Ohta, T., Murakami, K., Yamaguchi, Y., Oikawa, T., 2011. Satellite-driven estimation of terrestrial carbon flux over Far East Asia with 1-km grid resolution. Remote Sens. Environ., 115, 1758-1771.

Sasai, T., Nakai, S., Setoyama, Y., Ono, K., Kato, S., Mano, M., Kazutaka, M., Miyata, A., Saigusa, N., Nemani, R.R., Nasahara, K.N., 2012. Analysis of the spatial variation in the net ecosystem production of rice paddy fields using the diagnostic biosphere model, BEAMS. Ecol. Model., 247, 175-189.

Saxton, K.E., Rawls, W.J., Romberger, J.S., Papendick, R.I., 1986. Estimating generalized soil-water characteristics from texture. Soil Sci. Soc. Am. J., 50, 1031-1036.

Seiler, W., Crutzen, P.J., 1980. Estimates of the gross and net fluxes of carbon between

the biosphere and the atmosphere from biomass burning. Clim. Chang., 2, 207-247.

Setoyama, Y., Sasai, T., 2013. Analyzing decadal net ecosystem production control factors and the effects of recent climate events in Japan. J. Geophys. Res., 118, 337-351.

Siegert, F., Ruecker, G., Hinrichs, A., Hoffmann, A.A., 2001. Increased damage from fires in logged forests during droughts caused by El Niño. Nature, 414, 437-440.

Smith, T.M., Reynolds, R.W., 2003. Extended reconstruction of global sea surface temperature based on COADS data (1854-1997). J. Clim., 16, 1495-1510.

Taylor, D., 2010. Biomass burning, humans and climate change in Southeast Asia. Biodiversity Conserv.,19, 1025-1042.

Tian, H., Melillo, J.M., Kicklighter, D.W., Pan, S., Liu, J., McGuire, A.D., Moore, B., 2003. Regional carbon dynamics in monsoon Asia and its implications for the global carbon cycle. Global Planet. Change, 37, 201-217.

Tosca, M.G., Randerson, J.T., Zender, C.S., Nelson, D.L., Diner, D.J., Logan J.A., 2011. Dynamics of fire plumes and smoke clouds associated with peat and deforestation fires in Indonesia. J. Geophys. Res., 116, D08207, doi:10.1029/2010JD015148.

Vadrevu, K.P., Ellicott, E., Giglio, L., Badarinath, K.V.S., Vermote, E., Justice, C., Lau, W.K.M., 2012. Vegetation fires in the himalayan region - Aerosol load, black carbon emissions and smoke plume heights. Atmos. Environ., 47, 241-251.

van der Werf, G.R., Dempewolf, J., Trigg, S.N., Randerson, J.T., Kasibhatla, P.S., Giglio, L., Murdiyarso, D., Peters, W., Morton, D.C., Collatz, G.J., Dolman, A.J., DeFries, R.S., 2008. Climate regulation of fire emissions and deforestation in equatorial Asia. PNAS, 105, 20350-20355.

van der Werf, G.R., Randerson, J.T., Collatz, G.J., Giglio, L., 2003. Carbon emissions from fires in tropical and subtropical ecosystems. Global Change Biol., 9, 547-562.

van der Werf, G.R., Randerson, J.T., Collatz, G.J., Giglio, L., Kasibhatla, P.S., Arellano Jr. A.F., Olsen, S.C., Kasischke E.S., 2004. Continental-scale partitioning of fire emissions during the 1997 to 2001 El Niño/La Niña period. Science, 303, 73-76.

van der Werf, G.R., Randerson, J.T., Giglio, L., Collatz, G.J., Mu, M., Kasibhatla, P.S., Morton, D.C., DeFries, R.S., Jin, Y., van Leeuwen, T.T., 2010. Global fire emissions and the contribution of deforestation, savanna, forest, agricultural, and peat fires (1997-2009). Atmos. Chem. Phys., 10, 11707-11735.

van der Werf, G.R., Randerson, J.T., Giglio, L., Collatz, G.J., Kasibhatla, P.S., Arellano Jr. A.F., 2006. Interannual variability in global biomass burning emissions from 1997 to 2004. Atmos. Chem. Phys., 6, 3423-3441.

Wan, Z., Zhang, Y., Zhang, Y.Q., Li, Z.L., 2002. Validation of the land-surface temperature products retrieved from Moderate Resolution Imaging Spectroradiometer data. Remote Sens. Environ., 83, 163-180.

Wang, S., Zhou, L., Chen, J., Ju, W., Feng, X., Wu, W., 2011. Relationship between net primary productivity and stand age for several forest types and their influence on China's carbon balance. J. Environ. Manage., 92, 1651-1662.

Chapter 4

A high-resolution emissions inventory for open biomass burning in Southeast Asia during 2001-2010 and their global warming potential

Abstract: Biomass burning emissions from forest fires, agricultural waste burning and peatland combustion release large amounts of greenhouse gases (e.g., SO_2, NO_x, CO, NMVOC, NH_3, BC, OC, CH_4, CO_2, and N_2O), which has significant impact on the terrestrial ecosystem productivity, global atmospheric chemistry and climate change. High resolutions of spatial and temporal distribution in biomass burning emissions are fundamental inputs of atmospheric transport model and climate prediction. With the help of the recently released satellite product, satellite and observation data based biomass density and spatio-temporal variable combustion factors, this study developed a new high-resolution and multi-year emissions inventory for open biomass burning in Southeast Asia during the period of 2001-2010, and evaluated their global warming potentials. The 1 km high resolution emission grid showed its advantage in quantifying small sized fire emissions which were frequently misinterpreted by the coarse grid data due to their smoothed large pixels. The average annual biomass burning emissions in SEA during 2001-2010 were SO_2 (262 Gg), NO_x (1,013 Gg), CO (51,838 Gg), NMVOV (3,529 Gg), NH_3 (437 Gg), BC (302 Gg), OC (2,278 Gg), CH_4 (3,526 Gg), CO_2 (761,949 Gg), N_2O (96 Gg), respectively. The results showed that high emissions of biomass burning were mainly concentrated in Myanmar, Cambodia, and Indonesia, which accounted for approximately 60% of the total biomass burning emissions. And forest burning emissions was found to be the dominant contributor to the total emissions among all land types. The spatial pattern of biomass burning emissions were mainly

attributable to the burned area, which also showed consistent pattern with biomass burning emissions. In addition, we found that biomass burning emissions exhibited similar trends from 2001 to 2010 with strong interannual and intraannual variability. Three high emission years were observed in 2004, 2007, and 2010, respectively, which were attributed to the three peaks of corresponding burned areas in 2003, 2007, and 2010, respectively. The intraannual trend showed that biomass burning emissions in Jan-Mar was the highest all year around, with another small peak in Oct. The total net global warming potential estimated from Southeast Asia biomass burning emissions during 2001-2010 was around 792 (20 year horizon) and 775 (100 year horizon) Tg CO_2 equivalent, which contributed to 8.6% and 10.5% for both time horizons to the globe.

Key words: Biomass burning emissions, finer resolution, global warming potential, Southeast Asia

4.1 Introduction

Biomass burning due to forest fires and agricultural waste burning has been well recognized as an important source of greenhouse gases (GHGs) emissions (Andreae and Merlet, 2001; Chang and Song, 2010; Qin and Xie, 2011), and has significant impact on global atmospheric chemistry and climate change (Zhang et al., 2008; Vadrevu et al., 2011). These released emissions and their long distance transports contribute significantly to the uncertainty in simulating climate change and global warming (Kasischke et al., 2005; Langmann et al., 2009). Moreover, they also affect both the local and regional air quality and pose serious threat to human health and environment (Chang et al., 2013; Marlier et al., 2013).

As one of the vulnerable regions that are susceptible to fires, Southeast Asia (SEA) has been experiencing fast deforestation (Miettinen et al., 2011), slash-and-burn shifting cultivation (Jones, 2006), peatland burning for oil palm plantations (Koh et al., 2011), etc., and all these phenomena are closely related to fires, which

often cause serious burning of biomass. However, different regions have different fire types due to different anthropogenic activities (van der Werf et al., 2010). The large burned areas from fires in Myanmar, Thailand, Laos and Cambodia are usually attributed to the slash-and-burn agricultural practices and land clearing activities, especially during the periodic droughts from January to April annually (van der Werf et al., 2006). While, in Indonesia, Malaysia and Papua New Guinea, fires have received much attention for a variety of reasons, particularly in peatland burning for oil palm plantation and forest conversions, with much high emissions of GHGs during the dry season of August-October (Carlson et al., 2013). Overall, the regular slash-and-burn agricultural practices is the dominant contributor to the biomass burning emissions, which usually lead to large areas of deforestation and extensive combustion of forest biomass with large emissions of GHGs into the atmosphere, and heavy smokes and hazes as well. For example, during the period of 2000-2006, forest fire associated biomass burning in tropical Asia resulted in approximately 58 Tg CO_2 emissions annually (Chang and Song, 2010). Furthermore, in SEA, crop residue burning is a commonly used agricultural management practice as an inexpensive, effective, and quick method to remove excess residue to facilitate planning (Kanabkaew and Kim Oanh, 2011), control pests and weeds (Jones, 2006), and produce ash fertilization (Taylor, 2010). The extensive burning of crop residue is also a large emitter of GHGs. An estimated 250 Tg of crop residues were burned in Asia in 2000 (Streets et al., 2003). And the emissions of CO_2 released from crop residue burning can reach up to 34 Tg $year^{-1}$ in tropical Asia (Chang and Song, 2010). Besides, the most important feature of biomass burning in SEA is the extensive combustion of peatland in South Sumatra and South Kalimantan of Indonesian for the conversion into oil palm plantations during drought period (Field et al., 2009; Carlson et al., 2012). The recently most severe and devastating 1997/98 El Niño event reported that a total range of 0.8-2.6 Pg carbon were emitted from the fire induced peatland burning (Page et al., 2002), which is equivalent to approximately 40% of global fossil fuel emissions during that time (van der Werf et al., 2008).

Numerous studies have been conducted to improve the estimate the trace gases

from biomass burning emissions. Earlier studies quantified the biomass burning emissions with characteristics of land type oriented (e.g., cropland (Gadde et al., 2009; Kanabkaew and Kim Oanh, 2011), peatland (Page et al., 2002; Tosca et al., 2011), and forest (Song et al., 2010)), or country oriented (e.g., Thailand (Zhang et al., 2008), Indonesia (Field and Shen, 2008; Permadi and Kim Oanh, 2013), China (Yan et al., 2006; Song et al., 2009; Qin and Xie, 2011)), or specific year oriented (e.g., 1997/98 El Niño (Page et al., 2002), 2010 haze (Salinas et al., 2013)). They used the measurements data in some typical study plot or statistical data as available fuel with country/province based biomass (Yan et al., 2006; Song et al., 2010; Zhao et al., 2011) or land type based biomass density (Permadi and Kim Oanh, 2013), which mean the available fuels in some area or some land type were usually used to represent the whole area or land type. Such representation usually cannot reflect the spatial variations and heterogeneities of biomass within the area or land type because it varies significantly with the type of vegetation and geographical location. Recently, a detailed estimate of biomass burning emissions from all kinds of land types in tropical Asia was developed by Chang and Song (2010), burned area and active fire products derived from satellite provide spatially and temporally explicit estimates of biomass burning emissions and are useful tools for quantifying country-level trace gas emissions. However, the employed MCD45A1 burned area product showed its limitation in detecting burned area of SEA tropical peatland due to tropical cloud, haze and smokes (Giglio et al., 2010). Still, some other studies calculated the gaseous and aerosol emissions from biomass burning of Asia in 2000, but the one year short period of emissions cannot capture the interannual variation and also cannot reflect the recently updated emission characteristics annually. More recently, the Global Fire Emission Database 3 (GFED3) estimates the spatial and temporal patterns of global fire-induced biomass burning emissions at monthly intervals from 1997 to present (van der Werf et al., 2010), but it has a coarse resolution of 0.5°. Comparing with other large continents, for example, Amazon, Africa, Siberia and Australia, the fire size in SEA is relatively smaller (Randerson et al., 2012), since the overwhelming majority of fires are set by humans in very small

plot scale with the aim of perfecting their own lands or deforestation for lands. And such coarse grid data with 0.5° usually misses the small sized fires in SEA and misinterprets the spatial variations in biomass burning emissions due to its large smoothed pixels.

Therefore, a high resolution and multi-year emissions inventory for biomass burning in Southeast Asia terrestrial ecosystem during recently is more preferred, which will provide an overall assessment of the potential effects and the relevant information for formulation of appropriate mitigation measures for these Southeast Asian developing countries. The objective of this study was to develop a high resolution biomass burning emissions inventory covering all land types in Southeast Asia during the period of 2001-2010. We employed the newly released burned area product MCD64A1, satellite and observation data based biomass density, and spatio-temporal variable combustion factors to estimate the biomass burning emissions at high spatial resolution of 1 km. Besides, we also evaluated the effects of all the trace gases emissions to the global warming potentials. The trace gases emissions included carbon dioxide (CO_2), carbon monoxide (CO), methane (CH_4), Non-Methane Volatile Organic Compounds (NMVOC), black carbon (BC), organic carbon (OC), nitrogen oxides (NO_x), ammonia (NH_3), nitrous oxide (N_2O), and sulfur dioxide (SO_2).

4.2 Method and data source

Biomass burning emission from open fires was usually calculated by the burned area, available fuels, combustion factor and emissions factor, which was described by Seiler and Crutzen (1980) with the following equation:

$$\text{Emissions} = \sum_{i=1}^{11}(B \times F \times CF \times EF) \quad (1)$$

where B denotes an important parameter of burned area (m^2), F means the available fuels for combustion during biomass burning (kg m^{-2}), CF is combustion factor, which is defined as the fraction of combusted fuel to the total amount (-), and EF indicates emissions factors for species, conveying the amount of mass of species per mass of dry matter burned (g kg^{-1}), and i is land cover types.

4.2.1 Burned area and fire counts

Burned area data were derived from the monthly MODIS 500-m direct broadcast burned area product (MCD64A1) (http://modis-fire.umd.edu/) which was used to estimate the entire area that was burned in SEA from 2001-2010. MCD64A1 is a MODIS satellite-derived product that uses surface reflectance, daily active fire, and land cover products to delineate burned areas and burn cells are tagged with approximate burn data (Giglio et al., 2009). And MCD64A1 has a spatial resolution of 500 m and temporal resolution of a month, and the day of burning and a temporal uncertainty range of the burn date are noted for every pixel. MCD64A1 took peatland into consideration and estimated the burned area from human drained peatland into other kind of economic crops with large fires occurrence (Giglio et al., 2010). Firstly, we extracted the approximate Julian day of burning and their images from the downloaded monthly hierarchical data format MCD64A1 burned area product, then the images were converted to geographical coordinates and overlaid with national GIS land (Permadi and Kim Oanh, 2013). Finally, the monthly and annual burned areas were generated after resampling from the original 500 m binary map into 1 km percentage grid map.

MODIS active fire products (MOD14A2 and MYD14A2) - MODIS Thermal Anomalies/Fire 8-Day 1 km L3 global products from satellite Terra and Aqua were also selected from 2001 to 2010. Products were downloaded from NASA Land Processes Distributed Active Archive Center (LP-DAAC) anonymous FTP server (ftp://e4ftl01u.esc.nasa.gov/). We transformed the MODIS hierarchical data format files into GEOTIFF format with the help of MODIS Reprojection Tool (MRT v4.1). For MOD14A2 and MYD14A2, we considered all pixels class higher than or equal to 7 as fire pixel (class 7: low-confidence fire, class 8: nominal-confidence fire, class 9: high-confidence fire). We calculated fire density as the number of pixels that got fire within given areas (the whole study area, and each country, and the various land-cover and landform units) and fire frequency as the return interval of fire (i.e., the number of years a pixel got fire relatively to the number of observed years).

We derived the land cover map for the year 2005 from the 'Glob Cover' dataset with a resolution of 300 m (http://www.iscgm.org/cgi-bin/). The dataset with original

Land Cover Classification System (LCCS) was then reclassified into 4 broad categories of vegetation susceptible to fires in SEA (forest, shrubland, cropland and peatland) (Fig. 4.1). World Wildlife Fund terrestrial ecoregions map of peatland was used to provide the distribution of peat soil for the estimation of burned peatland underground, which was primarily located in Peninsular Malaysia, southern Borneo, eastern Sumatra and Papua New Guinea (Fig. 4.1). MCD64A1 burned area product and MOD14A2/MYD14A2 active fire product were overlaid with the land cover map and the burned area and active fires of each land type were determined for each country (within the administrative boundary).

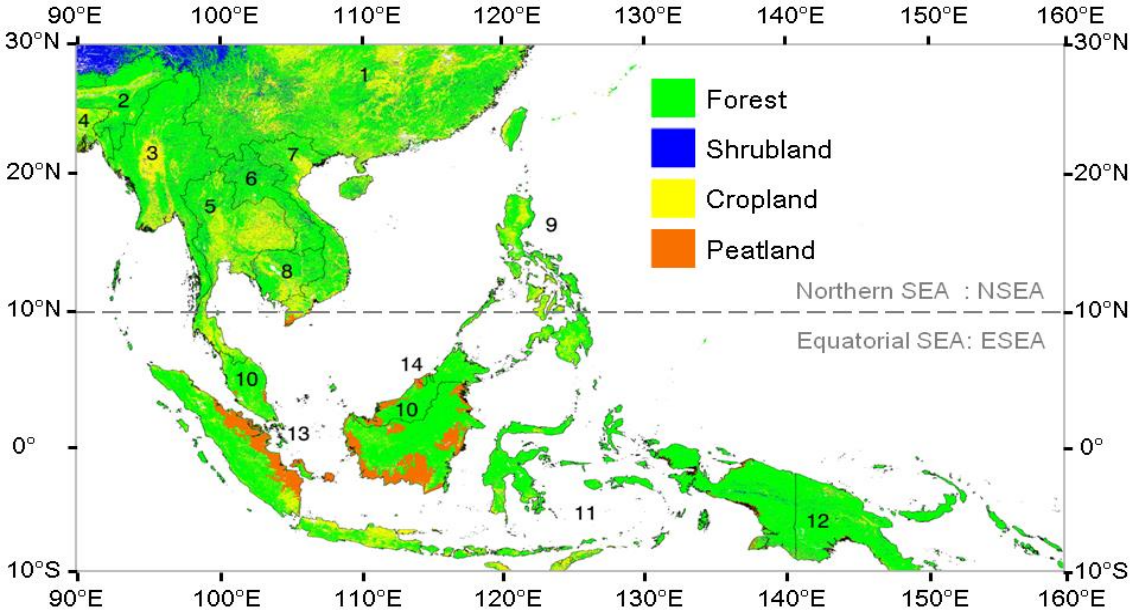

Fig. 4.1 Land cover maps of Southeast Asia (SEA),1-China; 2-India; 3-Myanmar; 4-Bangladesh; 5-Thailand; 6-Laos; 7-Vietnam; 8-Cambodia; 9-Philippines; 10-Malaysia; 11-Indonesia; 12-Papua New Guinea; 13-Singapore; 14-Brunei. SEA was divided into the Northern SEA (NSEA) and Equatorial SEA (ESEA). The spatial distribution of peat forest in SEA was extracted from World Wildlife Fund terrestrial ecoregions map (1999-2000; Tosca et al., 2011).

4.2.2 Available fuels

4.2.2.1 Forest and shrubland

Most studies cited statistical data as available fuel with country or province-specific aboveground biomass density (Chang and Song, 2010) or land type-specific

aboveground biomass density (McCarty et al., 2012) (for administrative territory based or land type based), which means the available fuels in the area or land type were used to represent the whole area or land type. The quality of such fuel datasets depends greatly on the class schemes of ecoregions and the representatives of fuel values. They usually cannot reflect the spatial variations and heterogeneities of biomass density. But actually the available fuel loads usually vary dramatically with the type of vegetation and geographical location from pixel to pixel due to the heterogeneous land surface properties (temperature, precipitation, elevation, soil texture, land type, etc.). Here, we introduced the aboveground biomass (AGB) and belowground biomass (BGB) from the study of Saatchi et al. (2011), which employed data from multiple satellites as well as thousands of ground plots to estimate the carbon stored in AGB and BGB and to map the spatial variations of biomass across three tropical continents. The AGB and BGB was mapped circus 2000 at 1 km spatial resolution. The distribution of AGB was highly heterogeneous in SEA, ranging from 500 g m^{-2} to 45000 g m^{-2} (mean: 17200 g m^{-2}) and the total AGB was 130.4 Pg. For forest and shrubland, the AGB will be consumed during fires, while for peatland, BGB will also be used for burn because of the rich soil organic matters.

4.2.2.2 Coarse woody debris and litter fall

Earlier studies showed that coarse woody debris (CWD) and litter fall were potentially significant carbon stores in forested ecosystems, but they are generally overlooked in the estimation of burned biomass (Matthews, 1997; Liu et al., 2003). In this study, we used the living tree biomass data to estimate the CWD pool based on the ratio of CWD to live tree biomass reported by Harmon and Hua (1991). They suggested that for tropical rain forests, the ratio was approximately 5%, while for subtropical, temperate, and boreal forests shrublands, and grasslands, the ratio was among the range of 20% to 25% (Matthews, 1997). We used the average total litter fall densities in Asian tropical forests compiled by Liu et al. (2003).

4.2.2.3 Crop residues

Crop residues, including residues from corn, wheat, rice, cotton, legumes, coarse cereals, rape, or peanut are often burned as fertilization in the field to ease

preparation for the next year. The emissions from crop residue burning were found to be significant source of GHGs and carbonaceous emissions, including emissions that negatively impact air quality (McCarty, 2011). In general, the amount of dry-matter crop residue burned in open fields was calculated from crop production, the residue-to-production ratios, and the percentage of dry-matter residue that was burned in the field (Yevich and Logan, 2003). In this study, the crop residues burning covering four broad categories of crop types (maize, sugarcane, rice, and wheat) in each country were provided from Food and Agriculture Organization (FAO) Statistics. The burned crop residues for each country in SEA crop production data were gathered from FAO Statistical Yearbook (http://faostat.fao.org) from 2001 to 2010. The amount of field-burned crop residues was estimated by multiplying the total annual crop production data, crop specific residue-to-production ratios, dry matter-to-crop residue ratio, and the fraction of dry matter residues that are burned in the field.

Actually, the amount of crop residues burned in fields in SEA are often missed and could not be reflected accurately in burned area products (MCD64A1) due to their small sizes, but they could be located by MODIS fire counts data (van der Werf et al., 2006; Huang et al., 2011). Here, we selected MOD14A2 and MYD14A2 products to determine the open fire counts and spatial distribution on a 1 km grid (Giglio, 2010). And only open fires in land cover classes defined as "crop" (also at 1 km resolution) was identified as crops burning in the fields. Based on the fire counts in each kind of cropland in each pixel, we allocated the amount of crop residues burning accordingly by using the FAO statistics of each kind of crop residue burning in each country of SEA. Since some part of China falls into the study area, firstly, we quantified the crop residues burnings in each of the province by using the proportion of crop residue burnings in each province of the whole China (Gao et al., 2002; Huang et al., 2011), and then allocated them into each fire pixel according to fire counts by using the following equation.

$$E_i = \frac{FC_i}{FC_k} \times E_k \quad (2)$$

where E_i is the crop residue burning in i pixel, FC_i is the fire counts in i pixel, FC_k is the total fire counts in country/province k and E_k is the total estimated crop residue burning in the field in country/province k.

4.2.2.4 Peatland

The tropical peatland burning in SEA, especially in Sumatra and Kalimantan, is a large fraction of biomass burning emission, which comes from the extensive burning of soil organic matter in drained peatland (Carlson et al., 2012). Recent research has also stressed that Indonesia peatland combustion is the major source of biomass burning in tropical SEA (Page et al., 2002; Carlson et al., 2012). In Indonesia, peat clearing for oil palm plantations goes on practically all year, particularly during the dry season of August-October in drought years. These peatland fires tend to burn continuously for months with large quantities of carbon releasing into the atmosphere (Page et al., 2002). Indeed, more than 90% of the transboundary haze in ESEA is linked to peatland fires (Tosca et al., 2011) and numerous studies have shown that the haze in these regions was primarily attributable to smoldering peat fires in Sumatra and Kalimantan (Page et al., 2002; Marlier et al., 2013). Recent studies have proposed that the combustion of belowground biomass may be an important source of emissions in tropical regions (Page et al., 2002). Indeed, large fires that burn for a long time can penetrate the soil to a depth of 30 cm (van der Werf et al., 2006), and can burn even deeper according to Page et al. (2002). Therefore, except to AGB burning during fires, we also used the spatially mapped peatland BGB with 1 km resolution as fuels for combustion during peat fires. However, since relatively little information currently exists on the depth or thickness of burning in SEA, quantifying the emissions resulting from the combustion of soil organic matter of peatland is difficult (van der Werf et al., 2006). Here, we assumed that a fire consumed almost 50% of the BGB in peatland (van der Werf et al., 2006; Shi et al., 2014). And this assumption is very similar with the results from Chang and Song (2010), which used the mean peat dry bulk density of 100 kg m^{-3} and average carbon concentration of 60% with average peat burn depth of 51 cm in SEA.

4.2.3 Combustion factor

Combustion Factor (CF) is the fraction of biomass actually consumed in a fire as determined by fuel type and moisture condition. It varies greatly among different biomass of different fuel types. In forest and shrubland region, fuel moisture was taken into account when estimating CF for forest and shrubland. We determine fuel moisture conditions according to the time series of MODIS Vegetation Index, which are related to moisture category factors for estimating the combustion factors and emissions factors.

In this study, we employed the Vegetation Condition Index (VCI) as a surrogate to reflect the fuel moisture conditions required for calculating the combustion factors and emission factors. The weekly VCI provided in the NOAA AVHRR (National Oceanic and Atmospheric Administration-Advanced Very High Resolution Radiometer) product has been demonstrated to be effective in monitoring drought information for various environments (Kogan, 1995; Zhang et al., 2008). This parameter is derived from the Normalized Difference Vegetation Index (NDVI) (Kogan, 1995, 1997). In this study, we obtained monthly VCI values from 2001 to 2010, which are produced from MODIS (MOD13A3) monthly NDVI datasets at a spatial resolution of 1 km:

$$\mathrm{VCI} = 100 \times \frac{\mathrm{NDVI_t} - \mathrm{NDVI_{min}}}{\mathrm{NDVI_{max}} - \mathrm{NDVI_{min}}} \quad (3)$$

where $NDVI_t$ is the NDVI of time t, and $NDVI_{min}$ and $NDVI_{max}$ are the minimum and maximum of NDVI, respectively, in the corresponding month from 2001 to 2010. Then, we equally divided the VCI values, which range from 0 to 100, into six different categories, representing fuel moisture conditions of very dry, dry, moderate, moist, wet, and very wet, respectively (Zhang et al., 2008). The monthly variation in moisture conditions is used to associate with fuel moisture category factors (mcf), which are discussed as follows.

The CF is a function of fuel type and moisture category and usually is calculated from the following model (Anderson et al., 2004):

$$\mathrm{CF_i} = (1 - \mathrm{e}^{-1})^{\mathrm{mcf}} \quad (4)$$

where CF_i denotes the fraction of fuel loading consumed for fuel type i which is forest (canopy), shrub, and litter, separately; and mcf is the moisture category factor. The mcf value in each fuel type is determined using the fuel moisture condition derived from MODIS VCI data (Table 4.1), which increases from dry to wet fuel conditions.

Table 4.1 Moisture category factor (mcf) (From Anderson et al., 2004).

Moisture condition	Canopy	Shrub	Duff	CWD
Very dry	0.33	0.25	0.33	0.08
Dry	0.5	0.33	0.5	0.12
Moderate	1	0.5	1	0.15
Moist	2	1	2	0.22
Wet	4	2	4	0.31
Very wet	5	4	5	0.75

As a result, CF_i varies with the monthly MODIS VCI. While for CWD, the CF is calculated using the following formula (Anderson et al., 2004):

$$CF_{CWD} = 0.6 \times (0.31 + (0.03 \times (0.31 - mcf))) \quad (5)$$

Based on the above equation, time series and spatial variable CF maps were generated.

4.2.4 Emission factor

Emission factor (EF) is a signal of accompanying trace gases during burning, which have been measured for multiple species in laboratories, and in airborne and ground-based field studies for different biomes (Yokelson et al., 2008). In this study, the compiled EF data measured in each biomass types in Asian countries were collected. For forest and shrubland, the EF values were determined from representative Indonesian fires (Permadi and Kim Oanh, 2013) and tropical Asian fires (Chang and Song, 2010; Song et al., 2010), while for crop residue burning, the EF values measured for the sources in Thailand and Indonesia were used (Kanabkaew and Kim Oanh, 2011; Permadi and Kim Oanh, 2013). For EFs from agricultural fires not included in the study by Kanabkaew and Kim Oanh (2011) and Permadi and Kim Oanh (2013), the values from fires in South China were applied.

For peatland, the EFs are not readily available in the literature. Thus, we drew most of EFs from van der Werf et al. (2010) under the deforestation fire category except for four species (CO, NH_3, CO_2, CH_4) which were derived from the locally measured peat soil in Kalimantan of Indonesia by Christian et al. (2003). The selected EFs for all species from different biomes used in this study were summarized in Table 4.2.

Table 4.2 Selected emission factors for each kind of land type in g species per kg dry matter burned.

Species	Emission factors (g/kg)						
	Forest	Shrubland	Crop residues				Peatland
			Maize	Sugar	Rice	Wheat	
SO_2	0.57	0.35	0.44[a]	0.22[a]	0.18[a]	0.85[c]	0.71[d]
NO_x	1.6	3.9	4.3[a]	2.6[a]	2.28[a]	3.3[c]	2.26[d]
CO	104	65	114.7[a]	34.7[a]	93[a]	60[c]	210[d]
NMVOC	8.1	3.4	10[a]	2.2[a]	7.0[a]	7.5[c]	7.0[d]
NH_3	0.76	0.49	0.68[a]	1.0[a]	4.1[a]	0.37[c]	2.55[d]
BC	0.66	0.48	0.78[b]	0.82[b]	0.52[b]	0.52[b]	0.57[d]
OC	5.2	3.4	2.25[a]	3.3[a]	2.99[a]	3.9[b]	4.3[d]
CH_4	6.8	2.3	4.4[a]	0.4[a]	9.59[a]	3.4[c]	20.8[d]
CO_2	1580	1613	2327[a]	1130[a]	1177[a]	1470[c]	1703[d]
N_2O	0.20	0.21	0.14[c]	0.07[e]	0.07[e]	0.07[c]	0.22[d]

a: from Kanabkaew and Kim Oanh (2011) for crop residue burning in Thailand,

b: from Cao et al., (2008) for BC emission factor of crop residues in China.

c: from Li et al. (2007) for open burning of wheat and maize straw in China.

d: from Christian et al. (2003) for biomass burning in Indonesia.

e: from Andreae and Merlet (2001).

All the other data were from Permadi and Kim Oanh (2013) for biomass burning in Indonesia.

4.3 Results and discussions

4.3.1 Spatial distributions and variations

Overall, the average annual MCD64A1 burned area for the period of 2001-2010 in SEA was 6.8×10^4 km^2 year^{-1}. Spatial distribution showed that large burned areas were concentrated in east Myanmar, north Thailand, east Cambodia, north Laos, south Sumatra and Kalimantan of Indonesia, and south Papua New Guinea (Fig. 4.2).

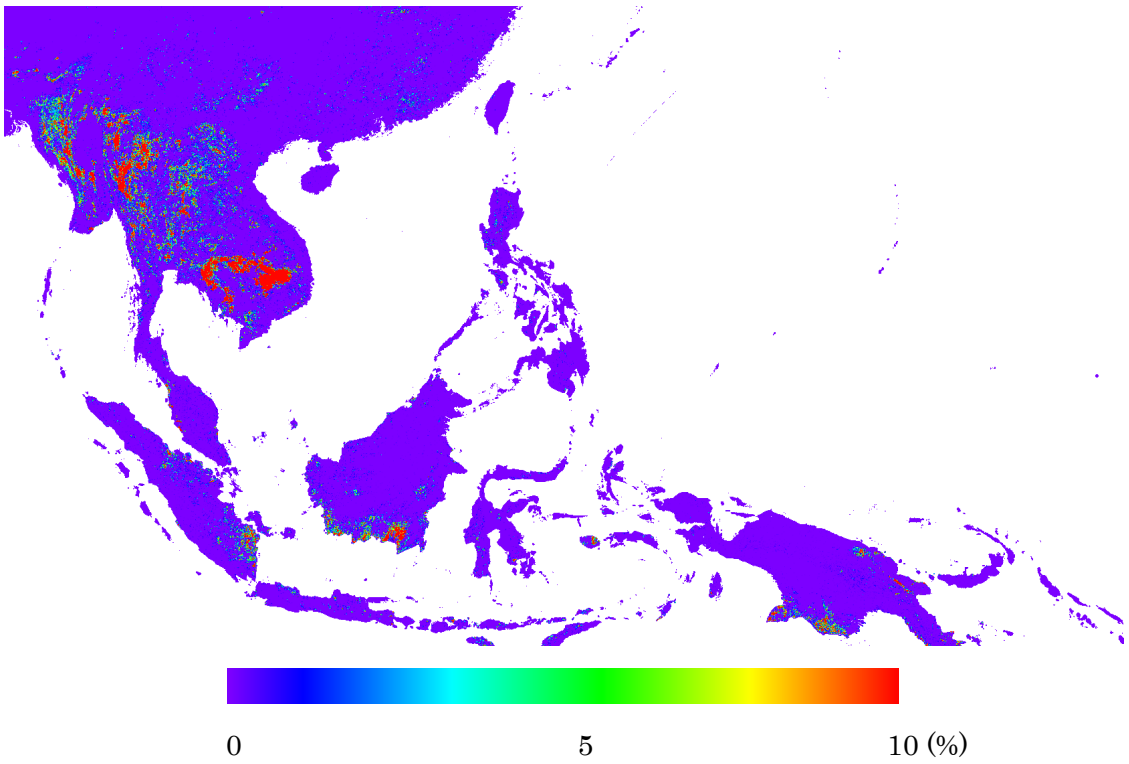

Fig. 4.2 Percentage of the average annual burned area with 1 km grid in SEA during 2001-2010.

Among the four broad categories of land types, the primary vegetation class burned was forest, which accounted for 70% (4.7×10^4 km^2 year^{-1}) of the total burned area. The average annual burned areas in shrubland and cropland were 0.4×10^4 (6%) and 1.2×10^4 (17%) km^2 year^{-1}, respectively. In addition, the burned area observed in the peatland area was 0.5×10^4 km^2 year^{-1}, almost all of which was in Indonesia. Although Indonesia was an important burning region in Asia, the burned area only accounted for about 7% of the total amount. The large area of burned forest can be attributable to numerous fire related slash-and-burn agricultural practices and land clearing, especially during particularly drought seasons (Shi et al., 2014). Besides,

we found that the burned area varied greatly from country to country. The burned area in Cambodia is the largest contributor to the total burned areas (31.9%), followed by Myanmar (25.7%), Indonesia (12.3%), Thailand (11.9%), Laos (4.7%), Vietnam (4.3%), South China (4.3%), Papua New Guinea (3.5%), Malaysia (1.0%) and Philippines (0.4%), respectively.

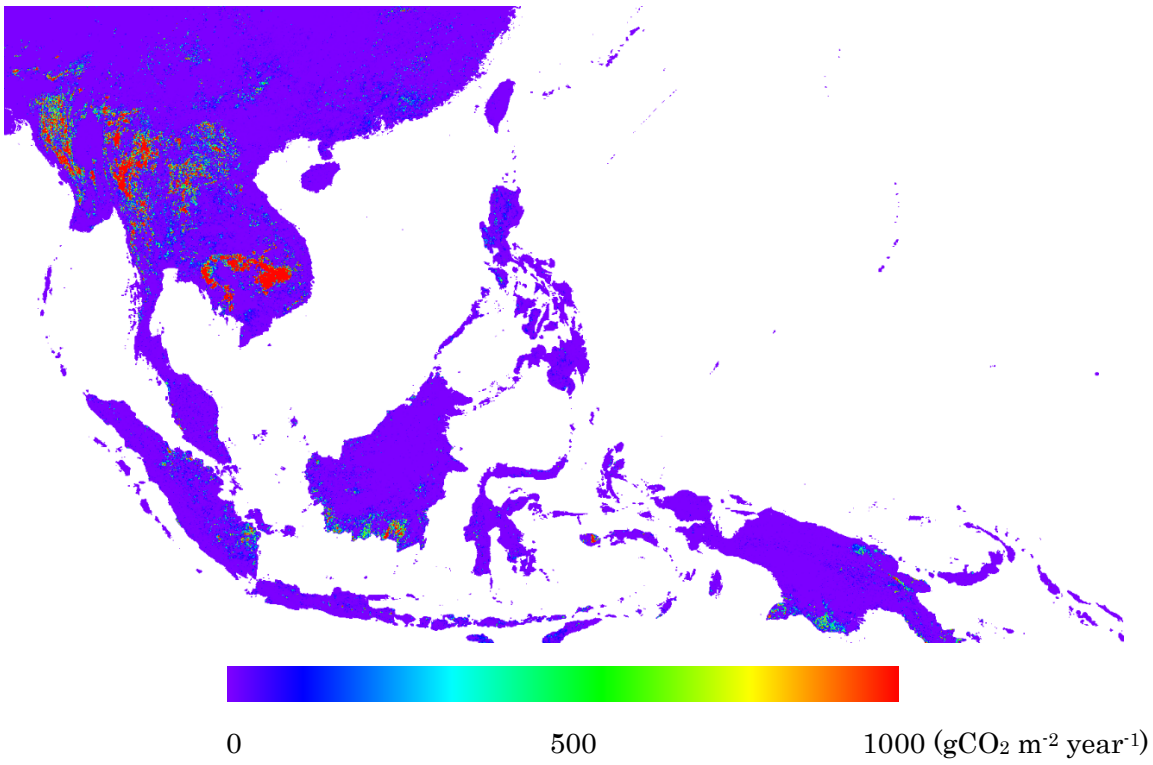

Fig. 4.3 Averaged annual CO_2 emissions from biomass burning with 1 km grid in SEA during 2001-2010.

The average annual open biomass burning emissions for each species (SO_2, NO_x, CO, NMVOC, NH_3, BC, OC, CH_4, CO_2, and N_2O) in SEA during 2001-2010 were quantified with 1 km spatial resolution. Firstly, we found that the biomass burning emissions in SEA presented consistent spatial patterns with burned areas. Then, the emissions of all species presented similar spatial distributions even though their magnitudes differ greatly. Taking CO_2 as an example, in general, the CO_2 emissions could be observed throughout the mostly SEA (Fig. 4.3). Moderate differences were observed in NSEA where relatively large amounts of emissions from fires were emitted from eastern and western Myanmar, north Thailand, eastern Cambodia,

and northern Laos. In ESEA, the emissions were high in south Sumatra and south Kalimantan of Indonesia, and relatively low in Papua New Guinea. The distribution of CO_2 emissions throughout the ESEA indicated that most CO_2 emissions were from the burning of peatland in Indonesia (Fig. 4.1). SEA fires were primarily caused by humans starting small fires for clearing their own lands, which produced fire scars with a speckled pattern. The estimated biomass burning emissions by employing MCD64A1 product with fine spatial resolutions were more effective at capturing the effects of small sized fires in certain plots. For example, the coarse grid data of GFED3, which had a relatively low spatial resolution, was frequently misinterpreted in small sized fires because of its smoothed large pixel (Fig. 4.4).

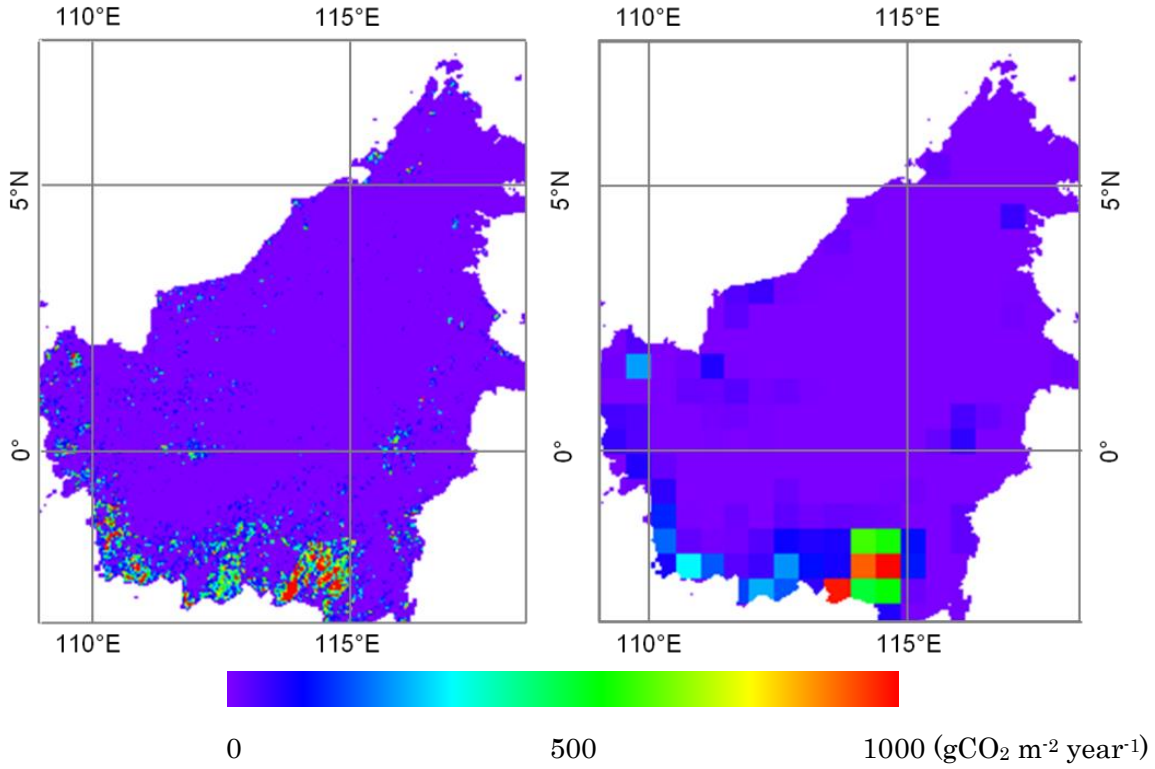

Fig. 4.4 Comparison of CO_2 emissions from biomass burning between (a) this study with 1 km grid and (b) GFED3 with 0.5° grid in Kalimantan of Indonesia ranging from 8° N to 4° S and 109-119° E during the period of 2001-2010.

More specifically, we quantified the average annual SO_2, NO_x, CO, NMVOC, NH_3, BC, OC, CH_4, CO_2, and N_2O from biomass burning emissions during the period of 2001-2010 in SEA (Table 4.3). And the contributions of annual biomass burning

Table 4.3 Summary of average annual biomass burning emissions during 2001-2010 for each land type in SEA. (Unit: Gg = 10^9 g)

Species	Vegetation Type								
	Forest	Shrub	CWD &Litter	Crop residues				Peatland	Total
				Maize	Sugar	Rice	Wheat		
SO_2	195.5	14.2	11.0	6.4	0.3	0.7	2.5	31.2	261.8
NO_x	548.8	157.8	122.2	62.1	3.7	9.5	9.7	99.3	1013.2
CO	35674.3	2630.4	2037.0	1656.8	49.7	387.4	177.1	9225.5	51838.2
NMVOC	2778.5	137.6	106.6	144.4	3.2	29.2	22.1	307.5	3529.0
NH_3	260.7	19.8	15.4	9.8	1.4	17.1	1.1	112.0	437.3
BC	226.4	19.4	15.0	11.3	1.2	2.2	1.5	25.0	302.0
OC	1783.7	137.6	106.6	32.5	4.7	12.5	11.5	188.9	2278.0
CH_4	2332.5	93.1	72.1	63.6	0.6	40.0	10.0	913.8	3525.6
CO_2	541974.8	65273.3	35413.1	33613.5	1618.2	4903.4	4338.0	74814.5	761948.6
N_2O	68.6	8.5	6.6	2.0	0.1	0.3	0.2	9.7	96.0

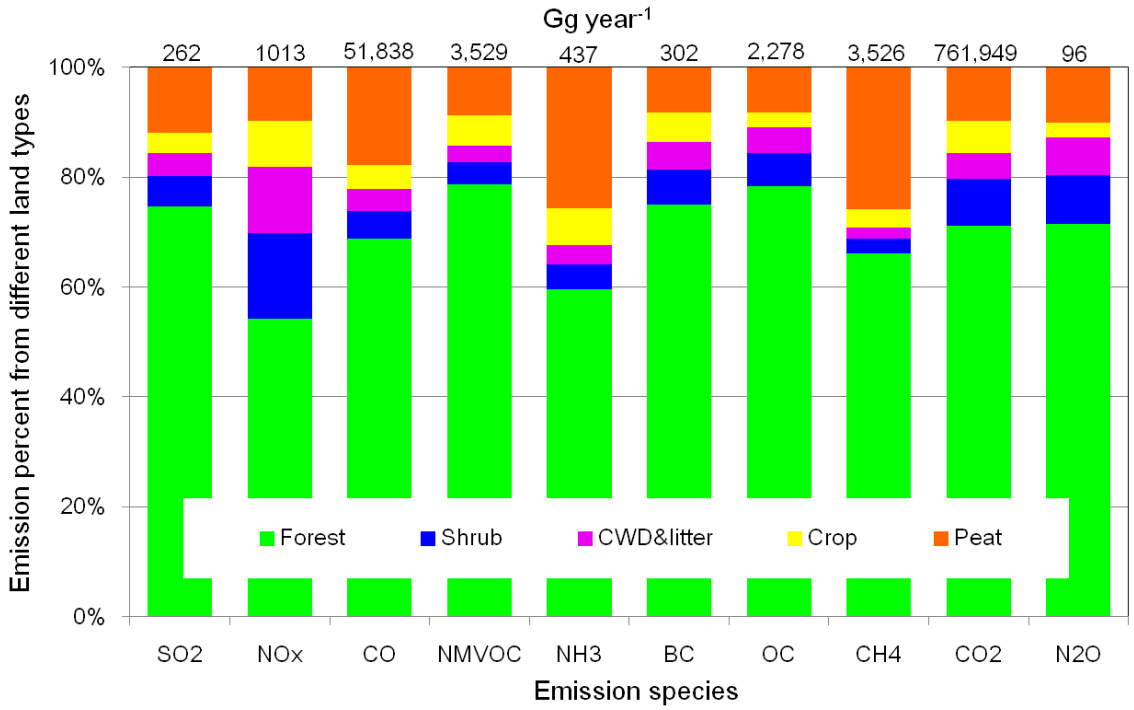

Fig. 4.5 Percentage of average annual emission species from biomass burning for each land in SEA during the period of 2001-2010.

emissions from each land type to the total were graphed for all GHGs (Fig. 4.5). The results showed that emissions from forest biomass burning is the biggest contributor to the total emissions (69.8% on average) for all kinds of GHGs, followed by peatland combustion (13.6%), shrubland (6.7%), CWD and litter (5.0%), and field burning of crop residues (4.9%). But for different emission species, the contribution of each land type to the total amount varied moderately.

Forest fire was the dominant fire type and the highest biomass burning emissions of each species was also observed in forest. In total, the overwhelming largest contributor of forest biomass burning emissions emitted about 54-79% of the total amounts of GHGs. We use burned areas and CO_2 emissions for 2001-2010 as a representative example. In general, the spatial distribution of the annual emissions of CO_2 from forest biomass burning showed that the high emissions in NSEA were seen concentrated in Cambodia (due to primary and secondary forest fires), north Thailand (due to forest fires and land clearing), west Myanmar (due to shrubland fires). There were also the grids with high emission scattered in Laos. While in ESEA, the highest emissions were found in the border line of south Sumatra and south Kalimantan, which appeared to be closely linked to peatland fires. Another area also with the same highest emission was detected in the south Papua New Guinea. All the large emissions appeared to be consistent with the burned area mapping of MCD64A1 showing more extensive burning in west Myanmar, north Thailand, east Cambodia, south Sumatra, south Kalimantan and south Papua New Guinea. Forests experienced relatively largest burned area of average 4.7×10^4 km^2 $year^{-1}$ (which contributed 70% to the total burned area) with a result of largest emissions of CO_2 with 542.0 Tg (71% of the total emissions). It means that the large amount of CO_2 emissions from forest was mainly attributable to its large burned areas. Moreover, the reason for the largest emissions in forests can be explained that the forests in SEA exhibit much higher biomass densities than shrubland, CWD and litter, and cropland. The explosive population in SEA poses a large demand on more cropland for crop production, which will cause the increased slash-and-burn cultivation by deforestation, resulting in large amounts of burned area accordingly.

By contrast, biomass burning emissions from shrubland, CWD and litter, crop residue burning, peatland only accounted for a small fraction of total levels (approximately 21-46% totally). The relationship between burned areas and land use classification is necessarily consistent with that between biomass burning emissions and land use types. In cropland, relatively high emissions from crop residue burning were seen in Thailand, Myanmar, and Laos which are well known major agricultural areas in SEA. After harvest, the crop residues were usually burned for land clearing and fertilizers. Moderate emissions were also observed in South China (e.g., Guangdong, Guangxi, Guizhou, etc.) even though strict rules and regulation on prohibiting crop residue burning in field, but in some remote rural areas, burning crop residues is still a very common phenomenon. Peatland burning emission was found to be the second largest emitter among the four major categories of land types, especially for NH_3 and CH_4 emissions, even though its burned area was smaller than forest and shrubland. The burned peatland accounted for 0.5×10^4 km^2 $year^{-1}$, which contributed only 7% of the total burned areas. However, its contribution to the total emissions can reach up to a range of 8-26% among all emission species. This was

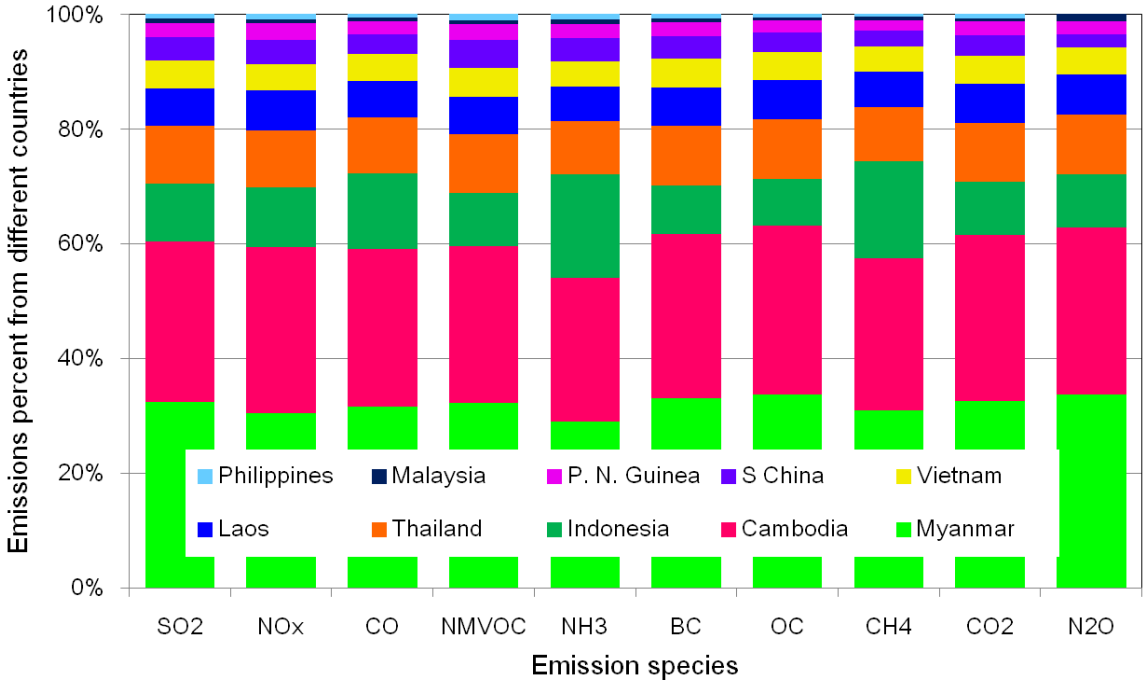

Fig. 4.6 Percentage of average annual emission species from biomass burning for each country in SEA during the period of 2001-2010.

attributed to peatland having a relatively higher density of biomass than forest on average. High emissions were located in the south Sumatra, south Kalimantan and south Papua New Guinea.

The spatial distribution of biomass burning emissions is also similar to that of the burned areas. In SEA, the largest burned areas were observed in Cambodia with 2.17×10^4 km^2 burned annually. Other major countries with highest emissions contributions included Myanmar (1.75×10^4 km^2), Indonesia (0.84×10^4 km^2), Thailand (0.81×10^4 km^2), Laos (0.32×10^4 km^2), Vietnam (0.29×10^4 km^2), South China (0.29×10^4 km^2), Papua New Guinea (0.24×10^4 km^2), Malaysia (0.07×10^4 km^2) and Philippines (0.03×10^4 km^2), respectively. The biomass burning emissions is mainly determined by its burned areas. However, Myanmar was also found to be the largest contributor to all species from biomass burning emissions in SEA, followed by Cambodia, Indonesia, Thailand, Laos, Vietnam, South China, Papua New Guinea, Malaysia and Philippines, respectively (Fig. 4.6). This was attributed to the higher biomass density in Myanmar compared with lower one in Cambodia. As a way of example, the largest emitter of Myanmar produced an average of 226 Tg $year^{-1}$ of CO_2 from biomass burning emission for the period 2001-2010, accounting for 30% of the total CO_2 emissions. Other big contributors includes Cambodia, Indonesia, Thailand, Laos, Vietnam, South China, Papua New Guinea, Malaysia and Philippines, which released an average of 199, 135, 71, 47, 34, 25, 17, 4, 4 Tg $year^{-1}$ of CO_2 from biomass burning emissions, accounting for 26%, 18%, 9%, 6%, 4%, 3%, 2%, 1%, 1% of the total CO_2 released.

In SEA, the major drivers of deforestation are frequently linked to anthropogenic activities, such as slash-and-burn agriculture and shifting cultivation, logging of natural forests in NSEA, and the establishment of oil palm plantation and industrial timber estates in ESEA (Carlson et al., 2013). The largest burned area in Cambodia, Thailand, Myanmar and Laos in NSEA are usually attributable to slash-and-burn agricultural practices and land clearing activities, especially during dry weather conditions (Page et al., 2002). While in Indonesia and Malaysia of ESEA, extensive peatland are drained and burned for planting more oil palm plantations by fires,

resulting in large burned areas and high emissions.

4.3.2 Temporal variations

Annual biomass burning emissions of all species in SEA fluctuated variably from 2001 to 2010. Taking the interannual variability of CO_2 as an example as well, it is clearly seen that the burned areas, burned biomass, and CO_2 emissions all presented consistent temporal trends with three obvious peaks of emissions in 2004, 2007 and 2010, respectively (Fig. 4.7). The CO_2 emissions in 2004 are by far the highest (1,143.0 Tg), followed by 2007 (1,074.0 Tg) and 2010 (1,063.1 Tg), respectively. The amounts of CO_2 emissions in the three peak years was almost twice or three times larger than that in other years. Similarly, the three years exhibited the greatest amounts of burned areas in MCD64A1 products with 11.1×10^4 km^2 in 2004, 8.8×10^4 km^2 in 2007 and 8.6×10^4 km^2 in 2010, respectively (Fig. 4.2). This indicates that total burned area is one of the most important factors in determining biomass burning emissions. The remaining values for burned area from largest to smallest are 7.4×10^4 km^2 (2006), 6.8×10^4 km^2 (2009), 6.1×10^4 km^2 (2002), 5.6×10^4 km^2 (2005), 5.6×10^4 km^2 (2003), 4.5×10^4 km^2 (2008), 3.4×10^4 km^2 (2001). Annual total CO_2 emissions are ranked from highest to lowest as follows: 1,143.0 Tg (2004), 1,074.0 Tg (2007), 1,063.1 Tg (2010), 840.1 Tg (2009), 788.7 Tg (2006), 627.2 Tg (2005), 601.2 Tg (2002), 568.8 Tg (2003), 549.7 Tg (2008), and 363.6 Tg (2001), respectively. Biomass density is another important parameter for determining biomass burning emissions. The burned biomass, including biomass density, CWD and litter, crop residues and peatland, showed consistent pattern with burned area. It conveyed that extensive fires usually can combust extensive biomass. And the burned biomasses in SEA were strongly dependent on burned areas. Therefore, the available biomass was not the limiting factor of biomass burning emissions and burned areas actually played a decisive role in characterizing the spatial and temporal patterns of biomass burning emissions.

Among all land types, the overwhelmingly dominant contributor of forest displayed three peaks on biomass burning emissions and burned areas, which showed consistent temporal variations with the total emissions and burned areas. It

indicated that the temporal variation of biomass burning emissions in SEA was strongly controlled by the variability of emissions in forest. In addition, we noticed that the CO_2 emissions from peatland showed different interannual trends with total CO_2 emissions and forest CO_2 emissions. The small peaks of peatland occurred in 2002, 2004, 2006 and 2009, respectively. During these years, the severe and persist droughts induced by ENSO phenomenon extended the burning of drained peatland in Indonesia, which resulted in large quantities of CO_2 emissions in these four years (Shi et al., 2014). Although peatland had relatively higher biomass density than other land types, the smaller burned areas determined that its biomass burning emissions cannot be larger than that of forests. Biomass burning emissions from shrubland, CWD and litter, and crop residues actually took a minor proportion to the total amount. These was not only due of their small burned areas, but also might because of their low biomass density.

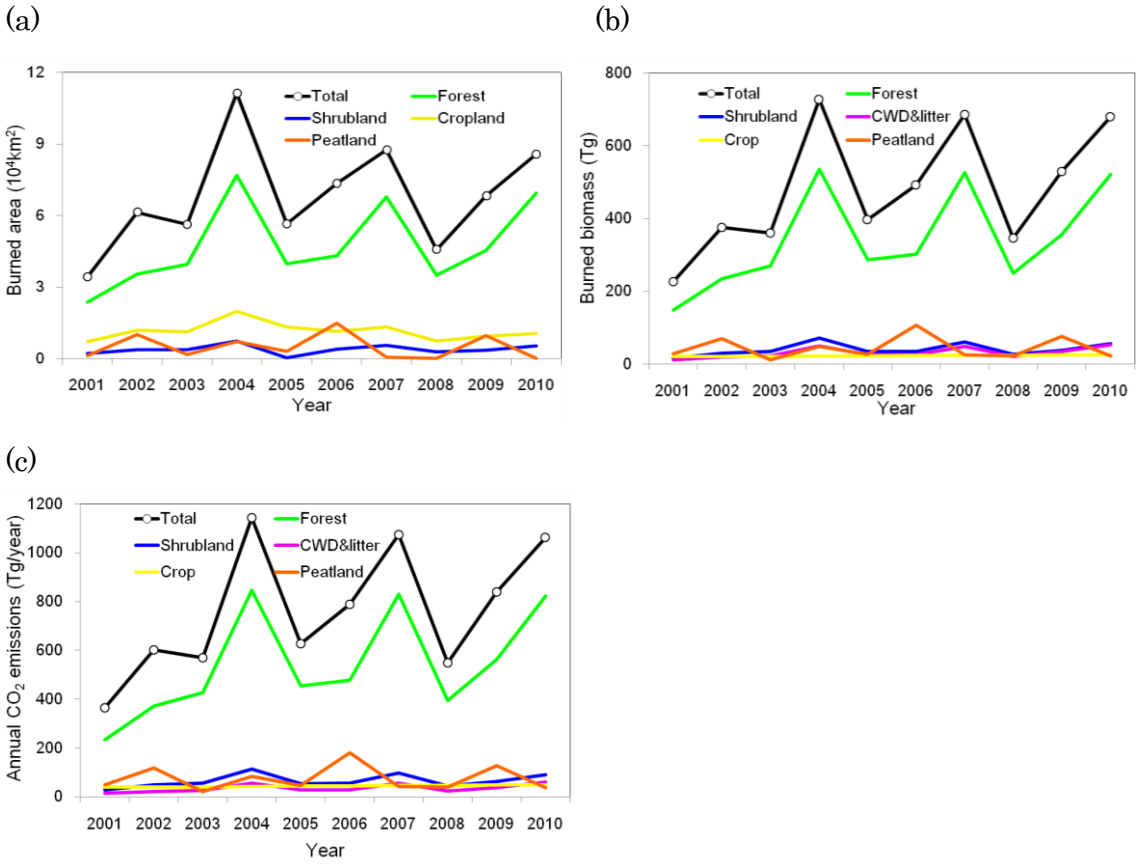

Fig. 4.7 Interannual variations of (a) burned area, (b) burned biomass and (c) CO_2 emissions from biomass burning in SEA and the amounts from each land type.

Biomass burning emissions also presented obvious intraannual variations with dramatic difference within one year (Fig. 4.8). At the same time, we found that the burned area and burned biomass both also displayed consistent temporal trends with the corresponding CO_2 emissions. The large peak in burned area was during the period of annual January-March, which is the typical fire season for the primary contributors, i.e., Myanmar, Thailand, and Cambodia. Intraannual variations in CO_2 emissions revealed that they were highest during January-March when relatively dry weather prevailed (Field et al., 2009). The dry season in NSEA generally lasts from January through March when relatively little precipitation falls (Taylor, 2010) and the potential for burning areas to clear and renew farmland and rangeland before the spring growing season is highest. Local farmers usually prepare fields by cutting down the accessible forest and short vegetation, which they then allow to dry

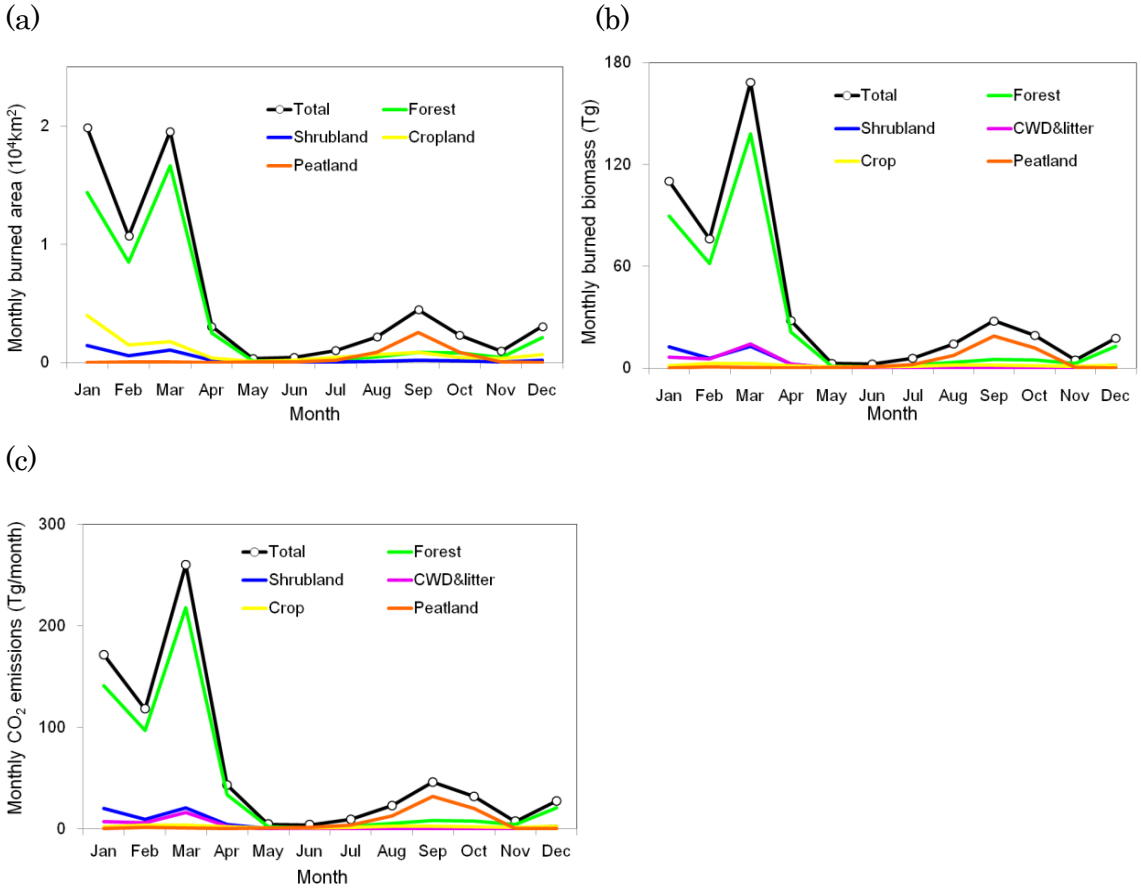

Fig. 4.8 Intraannual variations of (a) burned area, (b) burned biomass and (c) CO_2 emissions from biomass burning in SEA and the amounts from each land type.

until immediately before the rainiest part of the year to ensure an effective burn (Taylor, 2010). Consequently, values in CO_2 emissions and burned area are typically high during the dry period (January-March). Another peak month occurred in September-October, when Indonesia and Malaysia regions saw extensive burning practices in peatland. The ESEA biomass burning emissions exhibit considerable intraannual variability due to a coupling between El Niño-induced drought and anthropogenic land use changes (Field et al., 2009). Humans set fire to accessible areas of forest, increasing the fire occurrence of the drained peatland for palm oil plantations. In Indonesia, fire is primarily used to clear vegetation waste and is closely associated with deforestation and agricultural expansion (Siegert et al., 2001; Duncan et al., 2003). Indeed, the main causes of forest fires are the traditional farmers and plantation owners who clear their land to plant commercial tree crops (palm oil trees) (Jones, 2006). Drought acts as a trigger for fire occurrence, but it is humans who primarily ignite the fires either intentionally or unintentionally through practices such as slash-and-burn agriculture, or draining peatland and deforesting areas to establish oil palm plantations.

4.3.3 Comparison with other studies

Many studies have estimated the open fire emissions from biomass burning in SEA for recent years. Here, the widely available data source of GFED3, a dataset of all emissions of trace gases from biomass burning emissions, was selected to make a comparison with our study (Table 4.4). Since China partly falls into our study area of SEA, therefore, the statistics data for comparison excluded the emissions from China. Generally, our estimations were comparable with GFED3 even though some underestimations. This is because FAO statistics can only provide four broad categories of the crop residue burnings in each country of SEA, but actually, some countries also have other kind of agriculture, e.g., soybean, potato, groundnuts and cotton in Thailand. This can explain the disparity between the two results. Among all species, NH_3 and CH_4 presented 42% and 22% underestimations compared with GFED3. Although our study showed that CO was underestimated by 5,045 Gg, it only accounted for approximately 10% of the GFED3 CO emissions. However, for

CO_2 emissions, our results showed good agreement with the GFED3 estimation with only less than 1% (2,640 Gg) overestimation.

Moreover, forest biomass burning emissions of SEA in 2005 from other datasets were also collected to make a comparison (Table 4.5). Even though there were some differences among the five categories of emissions, our study showed more consistent with GFED3 with closer estimates of emissions from all species. And emissions from Song et al. (2010) showed too much underestimation compared with other four datasets.

Table 4.4 Averaged annual biomass burning emissions of SEA during 2001-2010 (Unit: Gg = 10^9g).

Total emissions	SO_2	NO_x	CO	NMVOC	NH_3	BC	OC	CH_4	CO_2	N_2O
GFED3	280	962	51620	2757	676	230	1834	4024	684600	84
This study	238	906	46575	3195	392	274	2089	3158	687240	87

Table 4.5 Forest biomass burning emissions of SEA in 2005 (Unit: Gg = 10^9g).

Forest emissions	SO_2	NO_x	CO	NMVOC	NH_3	BC	OC	CH_4	CO_2	N_2O
EDGAR	93	301	16612	1319	174	--	--	1107	851861	33
Song et al. (2010)	20	41	2764	223	120	14	126	170	39916	--
CGRER	134	737	24672	4602	309	156	1291	1607	373710	--
GFED3	157	525	20640	1473	259	124	1038	1243	358600	46
This study	158	442	28748	2239	210	182	1437	1880	436744	55

4.3.4 Emission uncertainties

Biomass burning emissions were determined by burned area, fuel loads, combustion factors and emissions factors. Therefore, emission uncertainty is associated with these parameters. The MCD64A1 burned area product is at a medium resolution and has been validated to be reliable (Shi et al., 2014). The combustion factor was calculated from empirical formulae. Thus, the uncertainties in this study mainly come from fuel loads and emission factor. According to Saatchi

et al. (2011), the fuel load was within an uncertainty range of about ±50% around the mean value. In addition, Hoelzemann et al. (2004) indicated that the typical uncertainty of the emission factor was in the order of 20-30%. Then, we ran 20000 Monte Carlo simulations to estimate the range of biomass burning emissions with a 90% confidence interval. The estimated emission ranges were 182-312 Gg SO_2 $year^{-1}$, 826-1,238 Gg NO_x $year^{-1}$, 461,95-68,214 Gg CO $year^{-1}$, 2,846-4,102 Gg NMVOV $year^{-1}$, 314-508 Gg NH_3 $year^{-1}$, 234-360 Gg BC $year^{-1}$, 1,834-3,027 Gg OC $year^{-1}$, 2,836-4,216 Gg CH_4 $year^{-1}$, 641,285-861,839 Gg CO_2 $year^{-1}$, 68-152 Gg N_2O $year^{-1}$, respectively.

4.3.5 Global Warming Potential (GWP)

The concept of global warming potential (GWP) has been developed in order to evaluate the comprehensive greenhouse effect. It determines the relative radiative forcing effect of a given emissions mass of a species compared to CO_2, integrated over a chosen time horizon. According to the IPCC Fourth Assessment Report (IPCC, 2007), the GWP generally has three temporal scales which are 20-year, 100-year and 500-year. Here, we chose 20-year and 100-year GWP. And related studies suggested that biomass burning contributed to global warming (IPCC, 2007; Jiang et al., 2010). But the total GWPs amount might be diverse and vary greatly in different regions. We assessed GWP of common greenhouse gases (GHGs) and other short-lived climate forcers emitted from biomass burning in SEA by using CO_2-equvalent emissions reported in previous studies as presented in Table S1. For the short-lived species (SO_2, BC, NO_x, CO, and OC), GWP values generally depend on the geographical location of the emissions (Fuglestvedt et al., 2010), therefore, the regional available GWP (Asia/SEA) values were used firstly.

GWP of GHGs and short-lived climate forcers released from SEA biomass burning during 2001-2010 relative to CO_2 is presented in Table 4.6. The assessment includes both the GWP of warming agents (i.e. CO_2, CH_4, NO_x, CO, BC with positive forcing) and cooling agents (SO_2 and OC with negative forcing). The total GWP of warming agents estimated from the annual SEA open biomass burning during 2001-2010 was around 2,037 (20 year horizon) and 1,120 (100 year horizon) Tg CO_2

Table 4.6 Contribution of SEA biomass open burning to the global biomass open burning GWP.

Species	This study (SEA), Gg year^{-1}			Global estimate, Gg year^{-1}		
	Emissions	CO_2 equivalent (20 years)	CO_2 equivalent (100 years)	Emissionsa	CO_2 equivalent (20 years)	CO_2 equivalent (100 years)
Global warming agents						
CO_2	761,949	761,949	761,949	6,529,200	6,529,200	6,529,200
CH_4	3,526	253,872	88,150	17,668	1,272,096	441,700
N_2O	96	27,744	14,688	849	245,361	129,897
BC	302	513,400	144,960	2,032	3,251,200	934,720
NO_x	1,013	43,559	-28,364	9,458	179,702	-104,038
CO	51,838	373,234	119,227	332,510	1,995,060	665,020
NMVOC	4,529	63,406	20,381	19,966	279,524	89,847
Sub total 1		2,037,164	1,120,991		13,752,143	8,686,346
Global cooling agents						
SO_2	262	-14,934	-4,192	2,244	-314,160	-89,760
OC	2,278	-1,230,120	-341,700	17,694	-4,246,560	-1,220,886
Sub total 2		-1,245,054	-345,892		-4,560,720	-1,310,646
Total net GWP		792,110	775,099		9,191,423	7,375,700

a. Global mean annual open biomass burning emissions during 2001-2010 were taken from GFED3, http://www.falw.vu/~gwerf/GFED/GFED3/tables/.

equivalents while the net GWP was 792 (20 year horizon) and 775 (100 year horizon) Tg CO_2 equivalents. Note that GWP for BC alone is around 513 (20 year horizon) and 145 (100 year horizon) Tg CO_2 equivalents, i.e. 12.9-25.2% of the total positive forcing, which is the second most important warming agent after CO_2 (20 year horizon). OC, the dominant negative forcing agent, has overwhelming cooling effects on GWP with 1230 (20 year horizon) and 341 (100 year horizon) Tg CO_2 equivalents. The GWP of global open biomass burning estimated using the data extracted from GFED3 for 2001-2010 was around 9,191 (20 year horizon) and 7,375 (100 year horizon) Tg CO_2 equivalents. And SEA accounted for a substantial portion of the GWP. The contribution from the SEA open biomass burning was about 8.6% and

10.5% of the global value for both time horizons.

4.4 Conclusions

In this study, high spatial resolution and multi-year inventories of open biomass burning emissions in Southeast Asia during the period of 2001-2010 were developed. With the help of the recently released satellite product, satellite and observation data based biomass density and spatio-temporal variable combustion factors, we estimated the biomass burning emissions of all species from each land type and each country. Comparing with the 0.5° coarse grid dataset, our study with 1 km high spatial resolution has advantages in capturing more small sized fires and their biomass burning emissions, which were frequently misinterpreted by the smoothed coarse data.

For the satellite burned area product, the burned areas were predominantly concentrated in forest, followed by shrubland, cropland, and then peatland. Large burned areas were detected in Cambodia (30%), Myanmar and Indonesia. The average annual biomass burning emissions in SEA during 2001-2010 were SO_2 (262 Gg $year^{-1}$), NO_x (1,013 Gg $year^{-1}$), CO (51,838 Gg $year^{-1}$), NMVOV (3,529 Gg $year^{-1}$), NH_3 (437 Gg $year^{-1}$), BC (302 Gg $year^{-1}$), OC (2,278 Gg $year^{-1}$), CH_4 (3,526 Gg $year^{-1}$), CO_2 (761,949 Gg $year^{-1}$), N_2O (96 Gg $year^{-1}$), respectively. Of which, the overwhelming majority of biomass burning emissions was found in forest. Also, Cambodia, Myanmar, and Indonesia were the main three contributors to total biomass burning emissions. In addition, we found that all species from biomass burning emissions exhibited similar trends from 2001 to 2010 with strong interannual variability. Three high emission years were observed in 2004, 2007, and 2010, respectively. The peaks of emissions were attributed to the three peaks of corresponding burned areas in 2003, 2007, and 2010, respectively. The main reason was that during the drought season of these years, local residents explored more agricultural land by deforestation for crop production. The commonly used method is by fires. The intraannual trend showed that biomass burning emissions in Jan-Mar was the highest all year around, with another small peak in Oct. The large amounts of

biomass burning emissions released into the atmosphere can have deep implications to the climate conditions and global warming potential. The total net global warming potential estimated from Southeast Asia biomass burning emissions during 2001-2010 was around 792 (20 year horizon) and 775 (100 year horizon) Tg CO_2 equivalent, which contributed to 8.6% and 10.5% for both time horizons to the globe.

Our high-resolution and multi-years emissions inventory for open biomass burning provided a step forward for the air quality forecasting and regional chemical transport model, which will improve our understanding on the interactions of ecosystem biogeochemical cycles and climate change. This emission inventory should be further improved by incorporating the biomass burning in other sectors. In particular, the emissions from fuelwood and other kinds of crop residues will be considered in the future analysis to reflect the recent changes in the emissions sources. Measurement of emission factor from each land type or biomes in this area should be conducted in the following study.

References

Anderson, G.K., Sandberg, D.V., Norheim, R.A., 2004. Fire Emission Production Simulator (FEPS) User's Guide (version 1.0). http://www.fs.fed.us/pnw/fera/publications/fulltext/FEPS_User_Guide.pdf

Andreae, M.O., Merlet, P., 2001. Emission of trace gases and aerosols from biomass burning. Global Biogeochem. Cycles., 15, 955-966.

Cao, G., Zhang, X., Wang, Y., Zheng, F., 2008. Estimation of emissions from field burning of crop straw in China. Chin. Sci. Bull., 53, 784-790.

Carlson, K.M., Curran, L.M., Asner, G.P., Pittman, A.M., Trigg, S.N., Adeney, J.M., 2013. Carbon emissions from forest conversion by Kalimantan oil palm plantations. Nature Clim. Change, 3, 283-287.

Carlson, K.M., Curran, L.M., Ratnasari, D., Pittman, A.M., Soares-Filho, B.S., Asner, G.P., Trigg, S.N., Gaveau, D.A., Lawrence, D., Rodrigues, H.O., 2012. Committed carbon emissions, deforestation, and community land conversion from oil palm

plantation expansion in West Kalimantan, Indonesia. PNAS., 109, 7559-7564.

Chang, D., Song, Y., 2010. Estimates of biomass burning emissions in tropical Asia based on satellite-derived data. Atmos. Chem. Phys., 10, 2335-2351.

Chang, S.S., Lee, W.J., Wang, L.C., Lin, N.H., Chang-Chien, G.P., 2013. Influence of the Southeast Asian biomass burnings on the atmospheric persistent organic pollutants observed at near source and receptor site. Atmos. Environ., 78, 184-194.

Christian, T.J., Kleiss, B., Yokelson, R.J., Holzinger, R., Crutzen, P.J., Hao, W.M., Saharjo, B.H., Ward, D.E., 2003. Comprehensive laboratory measurements of biomass-burning emissions: 1. Emissions from Indonesian, African, and other fuels. J. Geophys. Res., 108, 4719. doi:10.1029/2003JD003704.

Duncan, B.N., Martin, R.V., Staudt, A.C., Yevich, R., Logan, J.A., 2003. Interannual and seasonal variability of biomass burning emissions constrained by satellite observations. J. Geophys. Res., 108, 4100. doi:10.1029/2002JD002378.

Field, R.D., Shen, S.S.P., 2008. Predictability of carbon emissions from biomass burning in Indonesia from 1997 to 2006. J. Geophys. Res., 113, G04024, doi:10.1029/2008JG000694.

Field, R.D., van der Werf, G.R., Shen, S.S.P., 2009. Human amplification of drought-induced biomass burning in Indonesia since 1960. Nature Geosci., 2, 185-188.

Fuglestvedt, J.S., Shine, K.P., Berntsen, T., Cook, J., Lee, D.S., Stenke, A., Skeie, R.B., Velders, G.J.M., Waitz, I.A., 2010. Transport impacts on atmosphere and climate: metrics. Atmos. Environ., 44, 4648-4677.

Gadde, B., Bonnet, S., Menke, C., Garivait, S., 2009. Air pollution emissions from rice straw open field burning in India, Thailand and the Philippines. Environ. Pollut., 157, 1554-1558.

Gao, X., Ma, W., Ma, C., Zhang, F., Wang, Y., 2002. Analysis on the current status of utilization of crop straw in China. J. Huazhong Agri. Univ., 21, 242-247.

Giglio, L., 2010. MODIS Collection 5 Active Fire Product User's Guide Version 2.4,

Science System and Applications, Inc.: University of Maryland, Department of Geography, MD.

Giglio, L., Loboda, T., Roy, D.P., Quayle, B., Justice, C.O., 2009. An active-fire based burned area mapping algorithm for the MODIS sensor. Remote Sens. Environ., 113, 408-420.

Giglio, L., Randerson, J.T., van der Werf, G.R., Kasibhatla, P.S., Collatz, G.J., Morton, D.C., DeFries, R.S., 2010. Assessing variability and long-term trends in burned area by merging multiple satellite fire products. Biogeosciences, 7, 1171-1186.

Harmon, M.E., Hua, C., 1991. Coarse woody debris dynamics in two old-growth ecosystems. BioScience, 41, 604-610.

Hoelzemann, J.J., Schultz, M.G., Brasseur, G.P., Granier, C., 2004. Global wildland fire emission model (GWEM): evaluating the use of global area burnt satellite data. J. Geophys. Res., 109, D14S04. doi:10.1029/2003JD003666.

Huang, X., Li, M., Friedli, H.R., Song, Y., Chang, D., Zhu, L., 2011. Mercury emissions from biomass burning in China. Environ. Sci. Technol., 45, 9442-9448.

IPCC, 2007. Climate change 2007: Synthesis report. http://www.ipcc.ch/pdf/assessment-report/ar4/syr/ar4_syr.pdf

Jiang, C., Yu, G., Fang, H., Cao, G., Li, Y., 2010. Short-term effect of increasing nitrogen deposition on CO2, CH4, and N2O fluxes in an alpine meadow on the Qinghai-Tibetan Plateau, China. Atmos. Environ., 44, 2920-2926.

Jones, D.S., 2006. ASEAN and transboundary haze pollution in Southeast Asia. Asia Eur. J., 4, 431-446.

Kanabkaew, T., Kim Oanh, N.T., 2011. Development of spatial and temporal emissions inventory for crop residue field burning. Environ. Model. Assess., 16, 453-464.

Kasischke, E.S., Hyer, E.J., Novelli, P.C., Bruhwiler, L.P., French, N.H.F., Sukhinin, A.I., Hewson, J.H., Stocks, B.J., 2005. Influences of boreal fire emissions on Northern Hemisphere atmospheric carbon and carbon monoxide. Global Biogeochem. Cycles,

19, GB1012, doi:10.1029/2004GB002300.

Kogan, F.N., 1995. Application of vegetation index and brightness temperature for drought detection. Adv. Space Res., 15, 91-100.

Kogan, F.N., 1997. Global drought watch from space. Bull. Am. Meteorol. Soc., 78, 621-636.

Koh, L.P., Miettinen, J., Liew, S.C., Ghazoul, J., 2011. Remotely sensed evidence of tropical peatland conversion to oil palm. PNAS, 108, 5127-5132.

Langmann, B., Duncan, B., Textor, C., Trentmann, J., van der Werf, G.R., 2009. Vegetation fire emissions and their impact on air pollution and climate. Atmos. Environ., 43, 107-116.

Li, X., Wang, S., Duan L., Hao, J., Li, C., Chen, Y., Yang, L., 2007. Particulate and Trace Gas Emissions from Open Burning of Wheat Straw and Corn Stover in China. Environ. Sci. Technol., 41, 6052-6058.

Liu, C., Hannu, I., Bjorn, B., Wemer, K., Yang, Y., Ma, X., Carl, J.W., 2003. Aboveground litterfall in Eurasian forests. J. For. Res., 14, 27-34.

Marlier, M.E., DeFries, R.S., Voulgarakis, A., Kinney, P.L., Randerson, J.T., Shindell, D.T., Chen, Y., Faluvegi, G., 2013. El Niño and health risks from landscape fire emissions in Southeast Asia. Nature Clim. Change, 3, 131-136.

Matthews, E., 1997. Global litter production, pools, and turnover times: estimates from measurements and regression models. J. Geophys. Res., 102, 18771-18800.

McCarty, J.L., 2011. Remote sensing-based estimates of annual and seasonal emissions from crop residue burning in the contiguous United States. J. Air Waste Manage. Assoc., 61, 22-34.

McCarty, J.L., Ellicott, E.A., Romanenkov, V., Rukhovitch, D., Koroleva, P., 2012. Multi-year black carbon emissions from cropland burning in the Russian Federation. Atmos. Environ., 63, 223-238.

Miettinen, J., Shi, C., Liew, S.C., 2011. Deforestation rates in insular Southeast Asia

between 2000 and 2010. Global Change Biol., 17, 2261-2270.

Page, S.E., Siegert, F., Rieley, J.O., Boehm, H-D.V., Jaya, A., Limin, S., 2002. The amount of carbon released from peat and forest fires in Indonesia in 1997. Nature, 420, 61-65.

Permadi, D.A., Kim Oanh, N.T., 2013. Assessment of biomass open burning emissions in Indonesia and potential climate forcing impact. Atmos. Environ., 2013, 78, 250-258.

Qin, Y., Xie, S.D., 2011. Historical estimation of carbonaceous aerosol emissions from biomass open burning in China for the period 1990-2005. Environ. Pollut., 159, 3316-3323.

Randerson, J.T., Chen, Y., van der Werf, G.R., Rogers, B.M., Morton, D.C., 2012. Global burned area and biomass burning emissions from small fires. J. Geophys. Res., 117, G04012, doi:10.1029/2012JG002128.

Saatchi, S.S., Harris, N.L., Brown, S., Lefsky, M., Mitchard, E.T.A., Salas, W., Zutta, B.R., Buermann, W., Lewis, S.L., Hagen, S., Petrova, S., White, L., Silman, M., Morel A., 2011. Benchmark map of forest carbon stocks in tropical regions across three continents. PNAS, 108, 9899-9904.

Salinas, S.V., Chew, B.N., Miettinen, J., Campbell, J.R., Welton, E.J., Reid, J.S., Yu, L.E., Liew, S.C., 2013. Physical and optical characteristics of the October 2010 haze event over Singapore: A photometric and lidar analysis. Atmos. Res., 122, 555-570.

Seiler, W., Crutzen, P.J., 1980. Estimates of gross and net fluxes of carbon between the biosphere and the atmosphere from biomass burning. Clim. Change, 2, 207-247.

Shi, Y., Sasai, T., Yamaguchi, Y., 2014. Spatio-temporal evaluation of carbon emissions from biomass burning in Southeast Asia during the period 2001-2010. Ecol. Model., 272, 98-115.

Siegert, F., Ruecker, G., Hinrichs, A., Hoffmann, A.A., 2001. Increased damage from fires in logged forests during droughts caused by El Niño. Nature, 414, 437-440.

Song, Y., Liu, B., Miao, W., Chang, D., and Zhang, Y., 2009. Spatiotemporal variation in

nonagricultural open fire emissions in China from 2000 to 2007. Global Biogeochem. Cycles, 23, GB2008. doi: 10.1029/2008GB003344.

Song, Y., Chang, D., Liu, B., Miao, W., Zhu, L., Zhang, Y., 2010. A new emission inventory for nonagricultural open fires in Asia from 2000 to 2009. Environ. Res. Lett., 5, 014014. doi:10.1088/1748-9326/5/1/014014.

Streets, D.G., Yarber, K.F., Woo, J.H., Carmichael, G.R., 2003. Biomass burning in Asia: Annual and seasonal estimates and atmospheric emissions. Global Biogeochem. Cycles, 17, 1099. doi: 10.1029/2003GB002040.

Taylor, D., 2010. Biomass burning, humans and climate change in Southeast Asia. Biodivers. Conserv., 19, 1025-1042.

Tosca, M.G., Randerson, J.T., Zender, C.S., Nelson, D.L., Diner, D.J., Logan J.A., 2011. Dynamics of fire plumes and smoke clouds associated with peat and deforestation fires in Indonesia. J. Geophys. Res., 116, D08207, doi:10.1029/2010JD015148.

Vadrevu, K.P., Ellicott, E., Badarinath, K.V.S., Vermote, E., 2011. MODIS derived fire characteristics and aerosol optical depth variations during the agricultural residue burning season, north India. Environ. Pollut., 159, 1560-1569.

van der Werf, G.R., Dempewolf, J., Trigg, S.N., Randerson, J.T., Kasibhatla, P.S., Giglio, L., Murdiyarso, D., Peters, W., Morton, D.C., Collatz, G.J., Dolman, A.J., DeFries, R.S., 2008. Climate regulation of fire emissions and deforestation in equatorial Asia. PNAS, 105, 20350-20355.

van der Werf, G.R., Randerson, J.T., Giglio, L., Collatz, G.J., Kasibhatla, P.S., Arellano Jr. A.F., 2006. Interannual variability in global biomass burning emissions from 1997 to 2004. Atmos. Chem. Phys., 6, 3423-3441.

van der Werf, G.R., Randerson, J.T., Giglio, L., Collatz, G.J., Mu, M., Kasibhatla, P.S., Morton, D.C., DeFries, R.S., Jin, Y., van Leeuwen, T.T., 2010. Global fire emissions and the contribution of deforestation, savanna, forest, agricultural, and peat fires (1997-2009). Atmos. Chem. Phys., 10, 11707-11735.

Yevich, R., Logan, J.A., 2003. An assessment of biofuel use and burning of agricultural

waste in the developing world. Global Biogeochem. Cycles, 17, 1095. doi:10.1029/2002GB001952.

Yan, X., Ohara, T., Akimoto, H., 2006. Bottom-up estimate of biomass burning in mainland China. Atmos. Environ., 40, 5262-5273.

Zhang, X., Kondragunta, S., Schmidt, C., Kogan, F., 2008. Near real time monitoring of biomass burning particulate emissions ($PM_{2.5}$) across contiguous United States using multiple satellite instruments. Atmos. Environ., 42, 6959-6972.

Zhao, Y., Nielsen, C.P., Lei, Y., McElroy, M.B., Hao, J., 2011. Quantifying the uncertainties of a bottom-up emissions inventory of anthropogenic atmospheric pollutants in China. Atmos. Chem. Phys., 11, 2295-2308.

Supporting Information

Table S1 GWP of different forcing agents.

Radiative forcing agents (Gases/Aerosols)	GWP	
	20 year time horizons	100 year time horizons
CO_2	1	1
CH_4[a]	72	25
N_2O[a]	289	153
NO_x	19[b], 43[c]	-11[b], -28[c]
NMVOC	14	4.5
CO	6, 7.2[f]	2, 2.3[f]
BC (Black Carbon)	1600[h], 1700[i]	460[h], 480[i]
OC (Organic Carbon)	-240[h], -540[g]	-69[h], -150[g]
SO_2	-57[i], -140[h]	-16[i], -40[h]

Source: values compiled from various sources in Permadi and Kim Oanh, (2013); Fuglestvedt et al. (2010) and

[a]Forster et al. (2007). Global GWP, for CH4 indirect effect is included.

[b]Wild et al. (2001). Global GWP.

[c]Naik et al. (2007). Regional GWP reported for tropical region.

[d]Collins et al. (2002). Global GWP.

[e]Derwent et al. (2008). Global GWP.

[f]Berntsen et al. (2006). Regional GWP reported for Asia.

[g]Naik et al. (2005). Regional GWP reported for Southeast Asia based on the experiment with a focus on biomass burning emissions.

[h]Schulz et al. (2006). Global GWP, values were derived from multi-models mean value. OC was reported to have higher uncertainty of around 51%.

[i]Koch et al. (2007). Regional GWP reported for Southeast Asia.

Reference for Supporting Information

Berntsen, T., Fuglestvedt, J., Myhre, G., Stordal, F., Berglen, T.F., 2006. Abatement of greenhouse gases: does location matter? Clim. Change, 74, 377-411.

Collins, W.J., Derwent, R.G., Johnson, C.E., Stevenson, D.S., 2002. The oxidation of organic compounds in the troposphere and their global warming potentials potentials. Clim. Change, 52, 453-479.

Derwent, R.G., Stevenson, D.S., Doherty, R.M., Collins, W.J., Sanderson, M.G., Johnson, C.E., 2008. Radiative forcing from surface NOx emissions: spatial and seasonal variations. Clim. Change, 88, 385-401.

Forster, P., Ramaswamy, V., Artaxo, P., Berntsen, T., Betts, R., Fahey, D.W., Haywood, J., Lean, J., Lowe, D.C., Myhre, G., Nganga, J., Prinn, R., Raga, G., Schulz, M., Van Dorland, R., 2007a. Changes in atmospheric constituents and in radiative forcing. In: Solomon, S., et al. (Eds.), Climate Change, 2007: the Physical Science Basis. Contribution of Working Group I to the Fourth Assessment Report of the Intergovernmental Panel on Climate Change. Cambridge University Press, Cambridge.

Fuglestvedt, J.S., Shine, K.P., Berntsen, T., Cook, J., Lee, D.S., Stenke, A., Skeie, R.B., Velders, G.J.M., Waitz, I.A., 2010. Transport impacts on atmosphere and climate: metrics. Atmos. Environ., 44, 4648-4677.

Koch, D., Bond, T.C., Streets, D., Unger, N., van der Werf, G.R., 2007. Global impacts of aerosols from particular source regions and sectors. J. Geophys. Res., 112, D02205.

Naik, V., Mauzerall, D.L., Horowitz, L.W., Schwarzkopf, M.D., Ramaswamy, V., Oppenheimer, M., 2005. Net radiative forcing due to changes in regional emissions of tropospheric ozone precursors. J. Geophys. Res., 110, D24306.

Naik, V., Mauzerall, D.L., Horowitz, L.W., Schwarzkopf, M.D., Ramaswamy, V., Oppenheimer, M., 2007. On the sensitivity of radiative forcing from biomass burning aerosols and ozone to emission location. Geophys. Res Lett., 34, L03818.

Permadi, D.A., Kim Oanh, N.T., 2013. Assessment of biomass open burning emissions in Indonesia and potential climate forcing impact. Atmos. Environ., 2013, 78, 250-258.

Schulz, M., Textor, C., Kinne, S., Balkanski, Y., Bauer, S., Berntsen, T., Berglen, T., Boucher, O., Dentener, F., Guibert, S., Isaksen, I.S.A., Iversen, T., Koch, D., Kirkevåg, A., Liu, X., Montanaro, V., Myhre, G., Penner, J.E., Pitari, G., Reddy, S., Seland, Ø., Stier, P., Takemura, T., 2006. Radiative forcing by aerosols as derived from the AeroCom present-day and pre-industrial simulations. Atmos. Chem. Phys., 6, 5225-5246.

Wild, O., Prather, M.J., Akimoto, H., 2001. Indirect long-term global radiative cooling from NOx emissions. Geophys. Res. Lett., 28, 1719-1722.

Chapter 5

Conclusions and recommendations

5.1 Summary of the research

Fire and biomass burning are unique disturbances on ecosystem processes and dynamics. Their direct release of ecosystem carbon that are stored in large terrestrial pools (live vegetation, dead vegetation, litter, organic soil) have deep implication to the ecosystem productivity and stability. At the same time, the resultant elevated concentrations of trace gases (e.g., carbon monoxide, methane) and aerosol particles in the atmosphere also have significant effects on global atmospheric chemistry and climate change in various regions of the world, causing serious air pollutions as well.

Throughout Southeast Asia nearly all fires open burning is used for disposal of crop waste/residue, preparation of agricultural fields, maintenance of open understory, stimulation of grass growth, forest clearing and conversion to cultivated lands. The fire size are relative small. However, most inventories on global biomass burning emissions have a coarse spatial resolution of 0.5° currently. Since the overwhelming majority of fires in Southeast Asia are set by humans in very small plot scale with the aim of perfecting their own lands or deforestation for lands. Consequently, the data at a spatial resolution of 0.5° are not considered to be well suited to representing fire-induced biomass burning emissions at regional or continental scales. Thus, in order to accurately estimate the carbon budgets of terrestrial ecosystems in Southeast Asia, detailed examinations of the spatiotemporal variations in biomass burning emissions from fires at fine level of resolution are urgently required. Still, spatial and temporal distribution in biomass burning emissions are fundamental inputs of atmospheric transport model and climate prediction. Therefore, a high resolution and multi-year emissions inventory for biomass burning in Southeast Asia terrestrial ecosystem during recently is more preferred, which will provide an

overall assessment of the potential effects and the relevant information for formulation of appropriate mitigation measures for these Southeast Asian developing countries.

Fire induced biomass burning emissions are commonly calculated as the product of burned area, fuel loads, and combustion completeness, integrated over the time and space scale of interest. With the help of the recently released satellite product, terrestrial biosphere model based biomass density and spatio-temporal variable combustion factors and site-specific emission factors, this study estimated the fire carbon emissions from biomass burning in Southeast Asia during the year 2001-2010. We made three simulations by using different burned area products and the same biomass density, and made a comparison with the GFED3. The difference among the three emissions showed that they depended solely on burned areas, which is a key parameter in biomass burning emissions. Then, we evaluated the spatial variations and temporal dynamics of fire carbon emissions in Southeast Asia from 2001 to 2010 at spatial resolution of 5 km and monthly time step by integrating some human activity index and climate indices.

Besides, with the help of the recently released satellite product, satellite and observation data based biomass density and spatio-temporal variable combustion factors, our study also developed a new high-resolution and multi-year emissions inventory for open biomass burning on SO_2, NO_x, CO, NMVOC, NH_3, BC, OC, CH_4, CO_2, and N_2O in Southeast Asia during the period of 2001-2010. The biomass burning emissions from different fuel types and different countries vary greatly, and we calculated all trace gases emissions from each land cover in each country, and evaluated their global warming potentials and contributions to the globe.

5.2 Conclusions

In this study, fire carbon emissions from biomass burning in SEA were estimated for ten fire years from 2001 to 2010 at spatial resolution of 5 km. The methods used recently released satellite products and a physical process-based biosphere model (BEAMS) with embedded carbon emission. The high spatial resolution was effective for detecting small scale fires and carbon emissions that are usually lost in data with

a coarser resolution. Briefly,

(1). Burned areas were predominantly concentrated in Myanmar, northern Thailand, eastern Cambodia, and northern Laos, with marked differences in Sumatra and Kalimantan of Indonesia where peatland is extensively distributed.

(2). Through comparing different burned area products, we found that the burned area datasets from MCD64A1, MCD45A1 and GFED3 (Global Fire Emission Database) showed consistent temporal variation from 2001 to 2010 with average annual burned areas measuring 68104, 50933 and 61263 km^2 $year^{-1}$, respectively.

(3). Fire carbon emissions estimated in the three simulations (BEAMS/MCD64A1, BEAMS/MCD45A1-Peat and BEAMS/GFED) by using the three burned area products exhibited similar spatial patterns with respect to burned area, with average annual fire carbon emissions of 232.6, 214.1 and 228.8 TgC, respectively, of which, in our current study the best result among the three estimations was BEAMS/MCD45A1-Peat, which was close to that obtained by GFED3 with 210.7 TgC.

(4). The largest emitter of fire carbon emission was Indonesia, followed by Myanmar, Cambodia and Thailand. Marked increases in ESEA fire carbon emissions were observed during the dry years of 2002, 2004, 2006 and 2009, when BEAMS/MCD45A1-Peat displayed same trend.

(5). Aerosol Optical Depth (AOD) values showed good consistency with both fire CE and Multivariate ENSO (El Niño Southern Oscillation) Index values during 2001 to 2010, likely because of the deep peat soil burning under the influence of the El Niño phenomenon and Indian Ocean Dipole pattern in combination with anthropogenic disturbance through deforestation for palm oil plantation production.

The 1 km high spatial resolution and multi-year inventories of open biomass burning emissions in Southeast Asia during the period of 2001-2010 were also developed. The results showed that

(6). The burned areas were predominantly concentrated in forest, followed by shrubland, cropland, and then peatland. Large burned areas were detected in Cambodia (30%), Myanmar and Indonesia.

(7). The average annual biomass burning emissions in SEA during 2001-2010 were SO_2 (262 Gg $year^{-1}$), NO_x (1,013 Gg $year^{-1}$), CO (51,838 Gg $year^{-1}$), NMVOV (3,529 Gg $year^{-1}$), NH_3 (437 Gg $year^{-1}$), BC (302 Gg $year^{-1}$), OC (2,278 Gg $year^{-1}$), CH_4 (3,526 Gg $year^{-1}$), CO_2 (761,949 Gg $year^{-1}$), N_2O (96 Gg $year^{-1}$), respectively.

(8). Of which, the overwhelming majority of biomass burning emissions was found in forest. Also, Cambodia, Myanmar, and Indonesia were the main three contributors to total biomass burning emissions.

(9). In addition, we found that all species from biomass burning emissions exhibited similar trends from 2001 to 2010 with strong interannual variability. Three high emission years were observed in 2004, 2007, and 2010, respectively.

(10). The total net global warming potential estimated from Southeast Asia biomass burning emissions during 2001-2010 was around 792 (20 year horizon) and 775 (100 year horizon) Tg CO_2 equivalent, which contributed to 8.6% and 10.5% for both time horizons to the globe.

5.3 Suggestions for future research

Biomass burning emissions in SEA has gained more and more attention, meanwhile, considerable efforts have been made in emission estimation over the recent years. It is believed that biomass burning activity is a main source of atmospheric aerosols and trace gases (e.g. carbon dioxide (CO_2), methane (CH_4), carbon monoxide (CO), nitrogen oxides (NO_x), formaldehyde (HCHO), nonmethane hydrocarbon (NMHC), and methyl chloride (CH_3Cl)) (Andreae and Merlet, 2001). More recently, biomass burning is on the rise over SEA, due to both natural and anthropogenic activities. Depending on the types of vegetation, biomass burning may additionally contribute to the loading of atmospheric black carbon, enhancing the atmospheric heating processes. Biomass burning over Southeast Asia and Indo-China may be an important factor in the formation of the bright cloud and rain band spanning Southeast Asia and southern China in April-May associated with the pre-Meiyu frontal weather system.

Aerosols from biomass burning also impact regional and global energy cycle, by directly perturbing the energy balance of the atmosphere-earth surface system, and

by affecting the microphysics of cloud and rain formation. The responses of the regional water cycle to aerosol forcing are strongly dependent on the aerosol chemical and physical properties, concentration, composition and distribution (both horizontal and vertical), as well as the ambient atmospheric dynamical state. Generally, aerosols, such as sulfate, that reflect sunlight, cool the earth surface, increase stability, and thereby reduce convection, and rainfall locally. On the other hand, aerosols that absorb solar radiation, such as dust and black carbon, not only cool the surface, but also heat the atmosphere, and thus are more capable in producing dynamical feedback. A number of recent studies have identified the important role of absorbing aerosols (dust and black carbon) from long-range transport and local emission in spurring hydro-climate feedback processes in the Asian monsoon regions, resulting in strong modulation of the Asian monsoon rainfall (Lau et al., 2009).

Here, we propose a highly interdisciplinary research project to investigate the possible impacts of aerosols from biomass burning on the weather and climate systems of the Southeast Asian monsoon regions. Six coordinated research tasks are proposed (Lau et al., 2009; 2013).

Task 1-3 are observations-based task with focus on

1) Spatial and temporal distribution of biomass burning sources, characteristics and composition of biomass aerosols, particularly the emission of trace gases;

2) Use of satellite data to build the correlation among aerosol-cloud-precipitation and explore their interactions; and

3) Use of in-situ monitoring and field campaign data to investigate properties of aerosols and trace gases.

Task 4-6 are modeling based tasks, making full use of results from the Task 1-3 to provide inputs for emission sources, plume height in defining the forcing functions, and validations for the models. The modeling based tasks are focused respectively on

4) GCM modeling of biomass burning aerosol transport and impacts including both direct and indirect effects on Southeast Asian monsoon;

5) High-resolution regional modeling of trace gases emissions from biomass

burning on “elevated heat pump” effects by deep convection over Himalaya’s complex terrain, and on aerosol-cloud-precipitation interactions for pre-Meiyu rainband over southern China;

6) Experiments to study interactive effects of biomass burning aerosols on Asian monsoon climate, hydrological cycle and vegetation dynamics.

We expect to deliver a comprehensive understanding of the characteristics of biomass burning emissions, and their impacts on the climate, vegetation and hydrological cycle of Southeast Asia.

References

Andreae, M.O., Merlet, P., 2001. Emission of trace gases and aerosols from biomass burning. Global Biogeochem. Cycle, 15(4), 955-966.

Lau, K.M., Kim M.K., Sud, Y.C., Walker, G.K., 2009. A GCM study of the response of the atmospheric water cycle of West Africa and the Atlantic to Saharan dust radiative forcing. Ann. Geophys., 27, 4023-4037.

Lau, K.M., Wu, H.T., Kim, K.M., 2013. A canonical response of precipitation characteristics to global warming from CMIP5 models, Geophys. Res. Lett., 40, 3163-3169.

Appendix

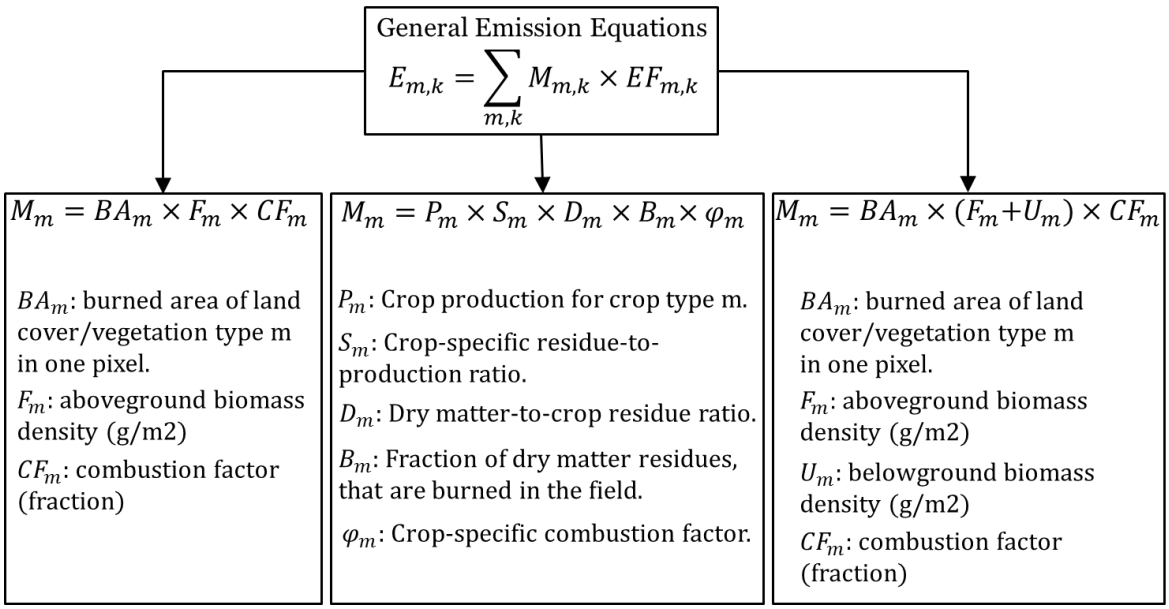

Fig. S1. Overall framework of estimation methodology.

Note:

$E_{m,k}$ = emissions (kg/yr) for fuel type m (type of biomass burned) and land type k (forest, shrubland, crop residue, peatland).

$M_{m,k}$ = the amount of biomass burned (kg/yr).

$EF_{m,k}$ = the emission factor (-).

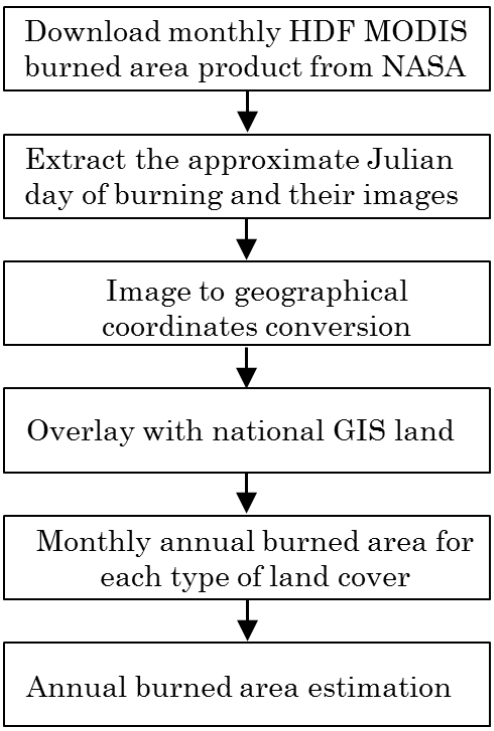

Fig. S2. Steps for estimation of burned area of forest fire (Permadi and Kim Oanh, 2013). Note: HDF (hierarchical data format)